Master's thesis

NTNU
Norwegian University of Science and Technology
Faculty of Engineering
Department of Energy and Process Engineering

Simen Are Madsen

Liquid Hydrogen Flow Operation for Maritime Usage

From Tank to Fuel Cell

Master's thesis in Mechanical Engineering
Supervisor: Federico Zenith
June 2020

NTNU
Kunnskap for en bedre verden

1 Abstract

The goal of this paper is to describe liquid-hydrogen flow operations for maritime applications. This was done by studying the Topeka base-to-base liquid hydrogen cargo vessel concept. We described the project, then followed the flow of hydrogen. First, from the tank on land, then through the bunkering process to the vessel fuel tank. Onboard, we reviewed step by step the hydrogen's journey from the main tank to the conditioning tank, through the evaporator and heat exchanger, and into the fuel cell. We also described the broader aspects of the ship as a full energy system by discussing the propulsion and power demand. Finally, we examined the possibility of increasing the capacity of the battery pack to combine land-power and hydrogen into a plug-in hybrid propulsion set-up to optimize the ship as a zero-emission vessel.

The methodology was to combine the information provided by the industrial players involved with the relevant engineering theory and then aggregate the results into a full system description. The project participants were mainly engineering companies focusing on naval architecture and cryogen gas technology and shipping companies focusing on owning and operating the tonnage on the water. We took the data that was shared with us and examined it from a theoretical perspective, describing the fundamentals behind the choices. These descriptions and discussions were cumulated into a paper that follows the flow of fuel through the system, as a response to the energy demand created by a given vessel velocity on the ocean.

The conclusion was that it is fully feasible to design and build a ship that can support a regular and predictable timetable sailing along the coast, powered by hydrogen in its liquid form. Based on our assessment, we deem it conceivable to operate a bunkering structure that can supply adequate fuel for the route. The hydrogen flow processes onboard can be performed with today's technology. The decision to combine the cooling cycle of the fuel cells and the heating cycle of the cryogen fuel is possible from an energy balance point-of-view. It became apparent that the higher pressure used on the hydrogen into the cell, the more energy is consumed by the air compression. We determined that by increasing the battery capacity and scale it to the available electrical grid power capacity on the ports of call, a plug-in hybrid system could improve fuel economics and reliability.

2 Sammendrag

Denne oppgaven har som målsetning å beskrive strømningsprosesser til hydrogen innenfor maritime bruksområder. Denne problemstillingen ble løst ved å studere Topeka konseptet som består av base-til-base lasteskip som benytter flytende hydrogen som drivstoff. Vi beskrev først selve konseptet før vi fulgte flyten av hydrogen. Flyten starter i lagringstanken lokalisert ved kaianlegget, hvor bunkringsprosessen finner sted. Etter hydrogenet er bunkret på skipets drivstofftank så beskrev vi skritt for skritt hydrogenets reise fra hovedtanken, via forberedelsestankene, gjennom fordamperen og varmeveksleren og inn i brenselscellen. Vi har også diskutert noen bredere aspekt rundt konseptet ved å se på hele skipet som et helhetlig system hvor vi eksaminerte fremdrift og kraftetterspørselen. Avslutningsvis så utforsket vi mulighetene for å øke batterienes kapasitet og kombinere dette med land-strøm fra havnene til å oppnå et plug-in hybrid fremdriftssystem. Dette ble utført for å kunne optimalisere skipet som et nullutslipps fartøy.

Metodikken vi benyttet oss av i denne oppgaven var å kombinere den informasjonen vi fikk av de industrielle aktørene som er involvert med relevant teknisk teori. Disse delbeskrivelsene ble satt sammen til en helhetlig beskrivelse. De deltakende bedriftene driver hovedsakelig innen skipsdesign, gassteknologi og rederivirksomhet. Vi tok dataene som ble delt med oss og utforsket det fra et teoretisk perspektiv hvor vi utforsket fundamentale aspekter bak design valgene. Disse diskusjonene ble sammensatt til en oppgave som følger hydrogen strømmen gjennom systemet, som en direkte respons på energibehovet som oppstår fra en gitt skips hastighet.

Resultatet vi kom frem til viser at det er mulig å designe og bygge et skip som kan opprettholde en regulær og forutsigbar rutetabell langs kysten, drevet av flytende hydrogen. Basert på vår analyse så anser vi det vi det som overkommelig å drifte en bunkringsstruktur som kan tilby tilstrekkelig med drivstoff for ruten. Selve hydrogen strømningsprosessene om bord kan utføres med dagens teknologi. Design valget ved å kombinere kjølesystemet til brenselscellene med varmeveksleren til hydrogenet viste seg mulig fra et energibalanse-perspektiv. Utregninger viste tydelig at desto høyere trykk på hydrogenet inn i cellen, desto mer energi vil konsumeres av luft kompressorene. Vi kom frem til at ved å øke batterikapasiteten og skalere den etter den tilgjengelige landstrømmen ved havnene så er det gjennomførbart å oppnå en plug-in hybrid løsning. Dette vil øke drivstofføkonomien og forbedre påliteligheten til systemet.

3 Contents

3.1 Abbreviations

AFC – Alkaline Fuel Cell

bara – Bar absolute

barg – Bar gauge

BCC – Body-Centered Cubic

BCE – Before Common Era

BKK – Bergens halvøens Kommunale Kraftselskap

BO – Boil-off

BOG – Boil-off Gas

BoL – Beginning of Life

CAPEX – Capital Expenditures

CCS – Carbon Capture and Storage

CH2 – Compressed hydrogen gas

DNV GL – Det Norske Veritas & Germanischer Lloyd

DP – Dynamic Positioning

EMSA – European Maritime Safety Agency

EoL – End of Life

EoS – Equation of State

FC – Fuel Cell

FCC – Face Centered Cubic

GH2 – Gaseous hydrogen

GHG – Green House Gases

GHG – Green House Gases

HRSG – Heat Recovery Steam Generator

HX – Heat Exchanger

ICE – Internal Combustion Engine

IMO – International Maritime Organization

LH2 – Liquid hydrogen

LHV – Lower Heating Value

LIB – Lithium-Ion Battery

LNG – Liquefied Natural Gas

LOA – Length Overall

LPV – Lattice Pressure Vessel

MCFC – Molten Carbonate Fuel Cell

MEA – Membrane Electrode Assembly

NASA – National Aeronautics and Space Agency

NCE – Norwegian Innovation Cluster

NG – Natural Gas

nm – Nautical mile

NOK – Norwegian Kroner

NORCE – Norwegian Research Center

OER – Oxygen Excess Ratio

P/O – Para to Ortho hydrogen relationship

PAFC – Phosphoric Acid Fuel Cell

PEM – Proton Exchange Membrane/Polymer Electrolyte Membrane

Pr – Prandtl Number

Re – Reynold Number

Ro-Ro – Roll on Roll off

SI – System International

SMR – Steam Methane Reformation

SOFC – Solid Oxide Fuel Cell

SPM – Solid Polymer Membrane

TEU – Twenty-foot Equivalent Unit

UN – United Nations

3.2 Formulas

3.3 Tables

3.4 Figures

5 Introduction

Humans have always been attracted to water when forming societies and cities. Today, of the 15 largest cities in the world 14 are located close to the sea or an ocean (Location of Cities, 2017). This makes sense as ships have for ages been the most important form of transport for human civilizations. The first written accounts of waterborne vessels are dated to 4000 BCE (Stilwell, 2018). This predates the development of non-water-based motorized vehicles like trucks, trains and planes by nearly 6000 years (Muller, 1996). It is easy to get the impression of ships as a less important form of transport today when most people mainly interact with goods in stores or online, both of which are delivered by truck. The large passenger vessels are also not what they used to be now that planes connect the world in our modern globalized paradigm.

However, even as planes, trucks and railways connect most parts of the world, international shipping is still responsible for 90 % of world trade (Shipping and World Trade, 2020). This is important now when we face the challenge of global warming. Shipping is the most environmentally friendly way of transport when considering emissions per unit cargo per unit distance (Environmentally friendly sea transport, 2019) but still, the shipping industry was in 2012 responsible for 2.5 % of global GHG emissions (Third IMO study, 2014).

In an attempt to reverse the trend, the United Nations Development Program's sustainable development goal number 13 says: "Take urgent action to combat climate change and its impacts", where carbon emissions are attributed to most of the greenhouse effect (Sustainable Development Goals, 2015). As a direct response to this The International Maritime Organization, IMO, adopted a strategy in 2018 worded as: "…a reduction in total GHG emissions from international shipping which should peak as soon as possible and to reduce the total annual GHG emissions by at least 50 % by 2050 compared to 2008" (UN body adopts climate change strategy for shipping, 2018). As this target is based on the emission level in 2008 and as global shipping has been increasing since then, the target relative to today exceeds 50 %. The effective lifetime of most modern tonnage is in the range of 25 – 30 years (Life Cycle of a Ship, 2013). This implies that if we are to achieve the goal of IMO, the standard of ships built must soon adhere to the target of >50 % emissions reduction.

Nearly all of today's oceangoing fleet of vessels use either heavy fuel oil or marine gas oil as their primary fuel source (Latarche, 2017). All of these are hydrocarbons that are combusted and therefore emit carbon dioxide into the atmosphere. The carbon-based fuel must be replaced with an alternative energy source that can be produced in an environmentally friendly manner and also stored in quantities adequate for intercontinental voyages. The Norwegian national transportation network is at the forefront of achieving this by replacing more and more of its fleet of traditional diesel-driven ferries by greener battery-driven ones (Stensvold, 2017). As the electricity source is hydro-powered, this results in a solid shift in a green direction for the maritime sector (Kraftproduksjon, 2019). The issue here is that modern battery technology for effective usage by ship limits itself to routes mainly below 1 hour at sea (DNV GL, 2019a). To implement an environmentally friendly fuel for longer distances we need to find other alternatives. One of the more promising energy storage solutions today is hydrogen.

The usage of hydrogen in the maritime sector has been proposed many times over the last few decades, but without any fully commercial projects being realized yet. Many issues have presented themselves on this subject including, but not limited to, the price of fuel cell technology, the availability of infrastructure of hydrogen for bunkering, onboard storage systems and regulatory guidelines for the development and commercialization of the technology. Driven by the new IMO regulations and the general push in society towards a less carbon dependent world, the field of

hydrogen technology moves forward. The possibility of carbon taxation is especially positive for the more expensive, alternative fuels (Guarascio, 2019). The European Commission states specifically in its plan for the European Green Deal that: “The price of transport must reflect the impact it has on the environment and Health” (European Commission, 2019). This illustrates the momentum toward alternative green fuels. The Norwegian government has comparable targets for lowering emissions. Through the political platform of the Government referred to as the Granavolden Platform where the environmental goal is 90-95 % GHG reduction by 2050 (Granavolden-plattformen, 2019).

To achieve this target the administration utilizes many different tools like regulations or monetary support to induce a positive drive in the industries and companies popularly referred to as “AS Norge”. PILOT-E is a governmental funding scheme from ENOVA, Innovasjon Norge and Forskningsrådet. It is used as a tool to help with the initial development of concepts and technologies that are believed to have a positive impact on the environment. In the summer of 2019, they announced a grant for projects that could develop a full value chain of hydrogen as an energy carrier (PILOT-E, 2019).

In the fall of 2019, a consortium of companies responded to the PILOT-E announcement for economical support to develop, build and operate a liquid hydrogen value chain. The involved entities were Air Liquide, BKK, Equinor, NCE Maritime Cleantech, NORCE, Norled, NorSea Group, Viking Cruises and Wilhelmsen. All of them are involved in businesses where the question of low emission maritime fuel is of particular interest. In December of the same year, they received approval and were awarded NOK 33.5m (95 millioner til utslippsfrie løsninger, 2019). As mentioned, one of the obstacles to overcome has been infrastructure and cost. One of the key components in cost reduction is to produce and deliver large volumes. This has not been done before as the customer base does not yet exist and as long as there is no infrastructure for reliable bunkering, they will not likely materialize either. What this pilot and its participants intend to do is to design and build a full-scale national liquid hydrogen infrastructure in parallel with the development of vessels that can consume it. A fully integrated concept including the whole value chain has never been done before.

Norway has proven that battery-powered ferries are a viable option if the supply of green electricity is available and by 2022 it is estimated that over 70 Norwegian ferries will be electrical (Norled, 2019a). Norway can use its naturally given assets with both fully renewable hydropower, in addition to being the 2nd largest exporter of natural gas globally (Export of Oil and Gas, 2019). The hydrogen production will at first be based on electrolysis before steam methane reformation (SMR), in combination with carbon capture and storage (CCS) takes over to supply larger volumes. Another reason for Norway’s ability to be a front runner for the *hydrogenation* of the maritime industry is its broad usage of short-haul shipping domestically as testing of new technology might be easier on shorter trips.

The Stavanger based ferry operator Norled is at the forefront of the global development of hydrogen propelled vessels. The world's first hydrogen-powered ferry is planned to commence operations in the spring of 2021 and will be constructed by Westcon (Norled, 2019a). It will connect the roads between Hjelmeland, Skipavik and Nesvik in Rogaland on the western coast of Norway with a capacity of 299 passengers and 80 cars (Norled, 2019b). The Norwegian Public Roads Administration requires the vessel's energy consumption to be 50 % minimum based on hydrogen (Norled, 2019c).

The choice between hydrogen storage solutions for the project fell on a liquid form in a cryogenic state. The general background for this decision was the volumetric advantage of LH2 to CH2, 4 times

more hydrogen per cubic meter based on the most accessible technology, and 6-8 times longer bunkering time for CH2 (BKK, 2019).

The international shipping company Wilhelmsen will be involved in several parts of the pilot. One of which is to design and build a commercial base-to-base logistics system and vessel for the transport of goods between ports in Norway. This set-up has been named Topeka. The concept is having the Topeka ro-ro feeder for the transport of cargo between the industrial bases along the western coast of Norway, with a predetermined schedule for reliable and predictable transport. This will contribute to reaching the government target of moving cargo from the national road system on to ships for safety and environmental reasons (Mer gods fra vei til sjø og bane, 2017). As a testing ground for the usage of liquid hydrogen as fuel, this set up can be advantageous due to the proximity to natural gas production, predetermined traveling distances and a given set of necessary refueling locations owned and operated by the same company that provides the ships. Eliminating both the infrastructure issue and providing a long-term customer simultaneously provides a solid backbone for testing and commercialization of industrial-scale liquid hydrogen usage.

This master thesis is performed with support from Wilhelmsen and will address some issues regarding the conceptual Topeka base-to-base LH2 vessel (Throughout this paper this will be referred to in the form of “the/our vessel”, “the Topeka vessel” or “the base-to-base vessel”). Using liquid hydrogen as a fuel for a ship is a concept that has been discussed on multiple occasions, but excluding a few scientific projects is not yet done on a large scale (Stensvold, 2018). There are many technical challenges related to it. Bunkering in port, LH2 tanks onboard able to handle continuous movements in the ship structure, boil-off, continuous fuel supply from tank to fuel cell, safety valves and measurements, regasification of LH2, amongst other. The problems at hand could potentially result in many papers. The safety aspect is very important as well with fire and explosion hazards. Here, we will review the technical feasibility of the process but the safety discussion is an important element for future work.

This thesis will present a description of the flow operations of liquid hydrogen from a land-based tank and into the fuel cell on a maritime vessel. We base the paper on the Topeka vessel and will present the technical solutions chosen by the industrial players designing it. As the technology develops rapidly, there is a chance that the solutions presented here will not be used in the final design of the ship upon initiation of construction.

To describe the flow operation, we choose to divide the theme into several sub-questions to answer.

- How much power is needed to operate the vessel?
- How much hydrogen is needed to fuel the ship?
- Which conditions does the hydrogen have to be in for utilization in the fuel cell?
- How do we bring the fuel from land and onto the ship?
- How much energy does it take to bunker the vessel?
- How is the hydrogen extracted from the LH2 tank?
- How do we pressurize the hydrogen?
- How can we regasify the LH2?
- How will the GH2 be heated?
- Can we use the FC heat production to warm up the cryogenic GH2?
- What is the ortho/para conversion effect in the system?
- How much energy does it take to bring hydrogen from the tank condition and to FC conditions?
- How does the FC pressure affect air compression energy usage?

- How can batteries be included in the set-up?

It becomes apparent that this subject touches many different aspects of engineering from material science to thermo and fluid dynamics. This paper will combine engineering theory and utilize scientific publications with help from industrial players to answer these questions. In this thesis, we will present a theory part that will contain the problems to be examined, the theoretical aspects behind, and a discussion and conclusion on the effect. Towards the end of the paper, we have included a conclusion/summary part where we briefly will address the most important aspects that have been presented in the theory part and also aggregate the answers to the sub-questions.

Throughout the paper, both the SI system and the standard maritime system of units will be used. For all calculations, the SI units will be used as this is the international standard and simplifies the mathematics. Note that some data and results will be presented in knots and nautical miles. This will be done to make the results more relatable to the respective industry it tries to describe. The units used will be indicated and discussed wherever deemed necessary.

6 Theory

6.1 Basics of the ship

The vessel in question is a roll-on-roll-off short sea commercial transportation ship, also referred to as ro-ro. It is intended to have a reliable schedule with frequent stops at the most important ports and offshore bases along the western coast of Norway. By using a hydrogen propelled ship, the project offers large savings in emissions. This concept is named Topeka. In this part we will briefly examine the details on Topeka presented so far by the involved entities. Note that as this project is still in its planning and design phase, the details may evolve further and in the future deviate from the descriptions provided here.

Figure 1 The Topeka logo

6.1.1 Main characteristics of the vessel

All details presented here is gathered from LMG Marin and their project presentations dated to February 13th and March 3rd, 2020.

Characteristics of the vessel	
Length overall (LOA)	125 m
Breadth	24 m
Hull depth	8 m
Design draught	4.7 m
Gross tonnage	Approx. 5,000 tons
Trade area	Small coasting
Deck area	2,500 m^2
TEU capacity	119
Deck load capacity	2,000 tons
Main propulsion	2 x 1,600 kW
Bow thrusters	2 x 600 kW
LH2 storage	2 x 100 m^3
Battery capacity	1,600 kWh
Transit speed	12 kts

Table 1 Characteristics of the vessel

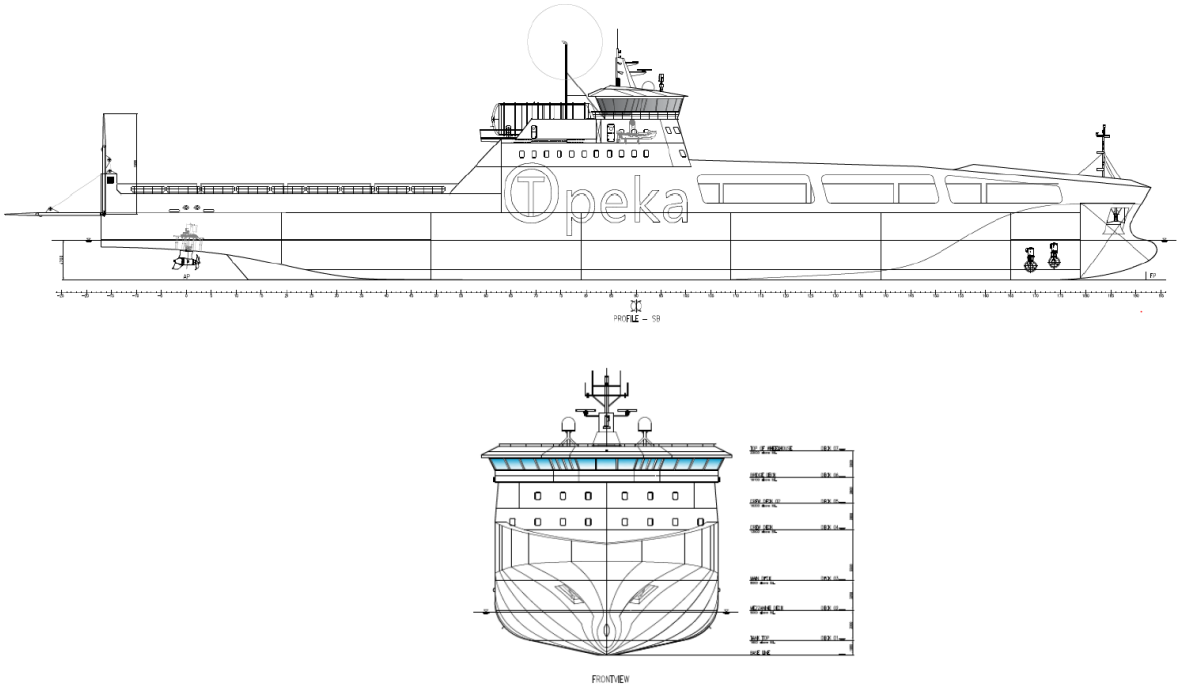

Figure 2 Technical drawing of the Topeka vessel by LMG

6.1.2 Description of route and service speed

The plan is to initiate a route between a few specific ports and offshore bases actively involved in the project. This is to ensure the necessary logistic network for fuel and a certain amount of cargo volume for the first phase. The mobility and scalability of a coastal transport service open for the opportunity to add other destinations for Topeka as demand rises and more ships are added to the fleet.

The initial and most important calls are made to these ports:

- Risavika
- Dusavika
- Karmsund
- Bergen
- CCB Ågotnes
- Mongstad

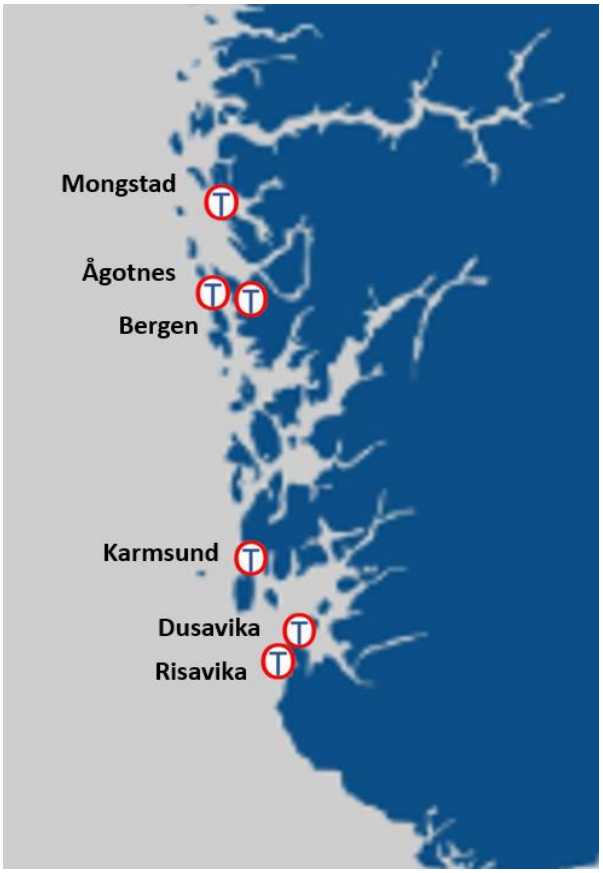

These are all important parts of the logistics network the Norwegian offshore oil sector is dependent on. A large part of the transport to and from these bases is not directed to and from the oil rigs but rather transfers between the bases. This is where Topeka can contribute to reducing the total environmental impact of Norway's most important industry.

Figure 3 Overview of area of operation

The specific timetable between these destinations is in the works by the project members. From a technical point of view, this is of importance as it will determine the necessary speed of the vessel, the resulting size of the drive train and the scale of fuel tanks given the different bunkering locations. We will assume that these parameters are given as the ones specified in the latest updated documentation from the consortium and we will not go into further detail on the routing table.

The service speed is the same as the transit speed set to 12 kts. This equates to 6.17 m/s when we use SI units. When a ship is between ports and in relatively open waters the velocity can be kept constant. Excluding the operations for maneuvering in and out of port, we assume a constant speed of 12 knots for the Topeka vessel. In this paper, we will present formulas describing different relationships where velocity is the variable factor. However, 12 knots will be defined as the standard reference condition.

$$V^{ref} = 12\ kts = 3.17\ m/s$$

Below we have presented a table provided by Wilhelmsen, of the split between the different operation modes and the respective energy consumption.

Operation modes						
	Acceleration	Retardation	In Quay	Maneuvering	Transit	**Total**
Time in each operation mode	0,8 %	0,8 %	14,8 %	1,6 %	81,9 %	**100 %**
Consumed energy in each operation mode	1,1 %	0,5 %	1,6 %	2,1 %	94,6 %	**100 %**

Table 2 Time in different operation modes

As observable from this table, the utilization of a constant reference speed equal to the transit speed will describe 94.6 % of the total energy consumption. We consider this as highly satisfactory and will use this definition.

6.1.3 Mechanical equipment

The vessel will have two propulsion systems. One for transit and one for maneuvering. The general propulsion will be driven by 2 pulling type fixed-pitch Azimuth thrusters with an individual power of 1.6 MW. The ship's total forward propulsion power of 3.2 MW is sufficient to produce a velocity greater than the reference service speed. The relationship between speed and power will be discussed in more detail in the next chapter. In addition to the two main propellers, the ship also has a set of two bow thrusters. These are fixed pitch tunnel type propellers with an individual power of 600 kW. Both propulsion systems will have a frequency-controlled electric drive.

6.2 Propulsion and power

In this subchapter, we will provide a brief discussion on ship propulsion and power consumption before we utilize some general principles of fluid mechanics to estimate the necessary hydrogen consumption for different speeds of our vessel.

Ships can be moved forward in many ways. For a long time, the wind was the most used form of ship propulsion as large sails pulled the ships across the oceans. Then came the steam engines and revolutionized the industry in the 19th century, first with paddles and later with propellers (Vance, 2018). As an important sector, technological development moved forward in the 20th century with the introduction of the internal combustion engine driven by petroleum-based fuels like diesel (Vance, 2018). This concept is in broad terms still the standard today. Advancement has been in the field of diesel-electric propulsion systems. This concept is based on having regular diesel engines connected to a generator rather than the propeller. Here the mechanical power is translated into electric power which is then passed on to electric engines driving the propellers. This can be advantageous for optimization of fuel economy, the better response of engine power, or the use of more complex engine set-ups like dynamic positioning systems (DP), amongst other (*Diesel-Electric Propulsion, 2020).*

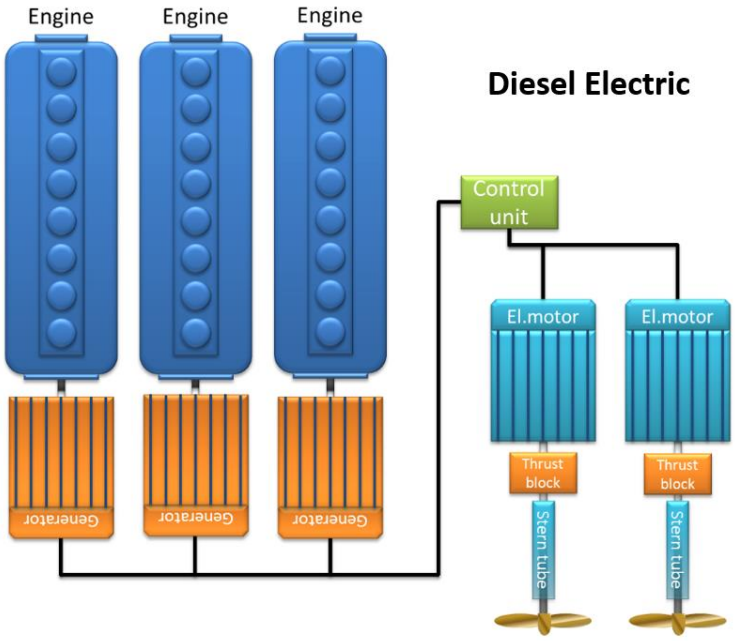

Figure 4 An illustration of a general diesel-electric setup. (Shippipedia, 2013)

This is relevant for us as it illustrates what needs to be adapted on modern vessels for an effective introduction of hydrogen-based propulsion. As we see from the illustration sourced from Shippipedia, the motors and propeller systems are only connected to the diesel engines by an electric wire. A simplified modification of this provides a set-up applicable to us.

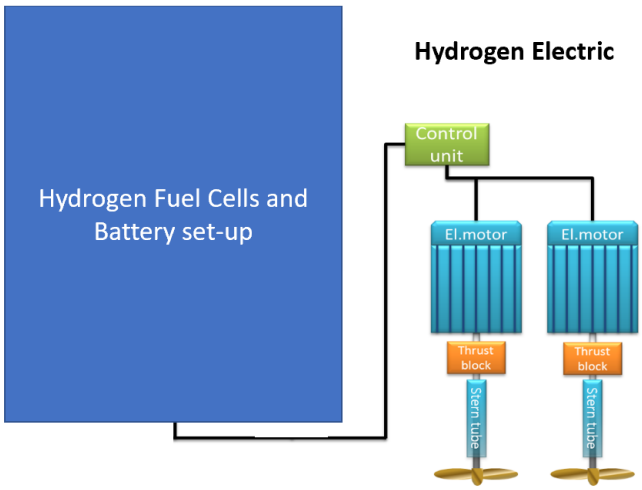

Figure 5 Conceptual illustration of a hydrogen electric propulsion system (Shippipedia, 2013)

We included this brief discussion to show that using hydrogen as a fuel for ships does not involve any fundamental changes to the general propulsion as we already have electric engines as one of the standard set-ups.

6.2.1 Resistance

6.2.1.1 Friction drag vs pressure drag

When a ship moves forward the engines must produce power to accelerate the mass of the vessel itself and to overcome the drag force of the fluid in the surface of the hull and superstructure. From Newton's second law of motion, we state that as long as the speed is constant (i.e. acceleration equals zero) the forces the propeller must overcome is the drag forces (Encyclopedia Britannica, 2020).

When a body moves through a fluid it will "feel" resistance against the motion, from the fluid. These forces exerted by the fluid are called drag. Drag forces can be separated into two different components based on the physical phenomena that describe them, friction drag and pressure drag. Also, we have wave resistance. When a fluid flows over a surface the no-slip condition and resulting boundary layer cause wall shear stress. This force is called the friction drag and is highly dependent on the viscosity of the fluid and increasing viscosity will increase friction (Cengal and Cimbala, 2010). The pressure drag is a product of diverging pressure in front of and behind a body. It is directly proportional to the frontal area of the object. This factor becomes significant when the flow is high enough for the fluid to not follow the curvature of the body – creating a separation point – resulting in low-pressure regions behind the object (Cengal and Cimbala, 2010). In naval architecture, the pressure drag is sometimes referred to as the "form drag". The forces can be expressed as:

$$F_D = C_D \frac{1}{2} \rho V^2 A$$

Equation 1 Drag force to velocity

$$F_D = Drag\ Force$$

$$C_D = Drag\ coefficient$$

$$\rho = Density\ of\ fluid$$

$$V = Velocity\ of\ fluid$$

$$A = Cross\ area\ of\ the\ body$$

Here we can denote the drag as the total drag or separate the two drag components. As the relationship between the two factors is the same as described in (1), we can create a combined drag coefficient by summing up the friction and pressure components.

$$C_D = C_{D,Friction} + C_{D,Pressure}$$

Equation 2 Drag coefficient

This paper will use the combined coefficient as there is no need for us to separate the components when the geometry of the vessel is assumed given. The drag coefficients for most geometries can be assumed constant for flows in the turbulent region (Cengal and Cimbala, 2010). To determine if we are in a turbulent or laminar flow region, we can use the dimensionless coefficient named the Reynolds number, R_e (Schlichting and Gersten, 2000).

Laminar region – $R_e < 5 \times 10^5$ < Transitioning region < $1 \times 10^6 < R_e$ – Turbulent region

$$R_e = \frac{\rho V L}{\mu}$$

Equation 3 Reynolds number

$$L = Length\ of\ flow - hull\ length$$

$$\mu = dynamic\ viscosity\ of\ fluid$$

In our case, the hull is 125 meters (LMG Marin AS, 2020). We assume the sea temperature to be 10 °C, resulting in a density of 1,027 kg/m^3 and dynamic viscosity of 0.00141 PaS (Properties of Seawater, 2005). Based on these parameters the turbulent transitioning will take place at speeds above 0.011 m/s, equal to 0.02 knots. It becomes apparent that laminar flow will have far fewer implications on drag than turbulent and from here on out we will assume the flow to only be turbulent and drag coefficients to be constant. As ½, the density of water and the hull area are all assumed constant we can combine them into one constant, K_D, resulting in:

$$F_D = K_D V^2$$

Equation 4 Simplified drag force to velocity

6.2.1.2 Wave resistance

A ship in motion on the water will cause disturbances on the surface. These phenomena are known as waves and as it demands energy it will present additional resistance to the motion of the ship. The wave resistance force has been described as (Havelock, 1909):

$$F_w = \frac{1}{4} K \rho V^4$$

Equation 5 Wave resistance to velocity

$$K = Hull\ specific\ constant$$

As the hull specific K, ¼ and the density of the seawater are assumed constant, we will combine them to K_W.

$$F_w = K_W V^4$$

Equation 6 Wave resistance to velocity, simplified

6.2.1.3 Air resistance

The part of the ship that's above water will also cause some resistance towards motion. In this case, the fluid in question is not water in liquid form but the air in gas form. Water is incompressible while air is compressible, and this can affect the drag and fluid properties. However, normal engineering practice assumes that air is incompressible for flow velocities below Mach 1 (NASA, 2014). At standard temperatures typically a velocity of below 400 km/h is deemed within this range and we can conclude that for a ship on the water the airflow can be assumed as incompressible (NASA, 2014). This implies that the same models can be used, and the drag force will be in the form of (1).

In general, there is a large discrepancy in drag from water vs air as both the density and viscosity are different. Imagine walking in the water on a shallow beach. Even though only parts of your legs are submerged in water it becomes much more difficult to maintain speed than outside of the water. This is also true for ships and resistance due to air is typically in the range of 4-6 % of total drag (Principles of Ship Performance) and we denote this additional drag as K_A. To simplify we will model air resistance by adding 5 %, the mean value.

6.2.2 Non-propulsion power

A ship will need power for other operations and procedures than direct propulsion. This includes the electrical systems, navigation, lighting and crew accommodation. This baseload can be denoted K_B. LMG informs that they assume this power necessity to be 200 kW. In the Sandia feasibility report of hydrogen fuel cell fast ferry SF-BREEZE it is assumed a power need of 120 kW for the ship (Pratt and Klebanoff, 2016). As the Topeka vessel is much larger than the SF-BREEZE this can seem sensible even though the fast ferry needs more energy for passenger accommodation.

6.2.3 Total power

The engines must overcome the total force on the ship, $F = (F_D + F_W)*1.05$, where the additional 5 % accounts for the air resistance. This power is the force times the velocity, i.e. Power = F*V. In addition to this, the power needs to account for the baseload. The total expression of power is, therefore:

$$Power = (K_W V^5 + K_D V^3) * (1 + K_A) + K_B$$

Equation 7 Velocity to power, theoretical

This expression provides a theoretical estimate for the power needed to maintain a given speed of the vessel.

6.2.4 Empirical power consumption

The real power consumption is given from empirical values based on experience and test of models in real water. For our vessel, the naval architects at LMG have provided a table of power consumption to speed.

TRANSIT incl. 15 % Sea Margin	
Speed	**Req. Prop power**
[kts]	**[kW]**
7.0	403
7.5	491
8.0	591
8.5	704
9.0	831
9.5	974
10.0	1 133
10.5	1 310
11.0	1 507
11.5	1 725
12.0	1 966
12.5	2 233
13.0	2 527
13.5	2 852
14.0	3 210
14.5	3 603
15.0	4 035

Table 3 Power requirements to velocity

In addition to this, the baseload, K_B, of 200 kW must be added. Based on the provided data and by using the polynomial regression tool in excel we found an empirical relationship between speed and power. The velocity input is changed from knots to meters per second for adaptation to the SI system.

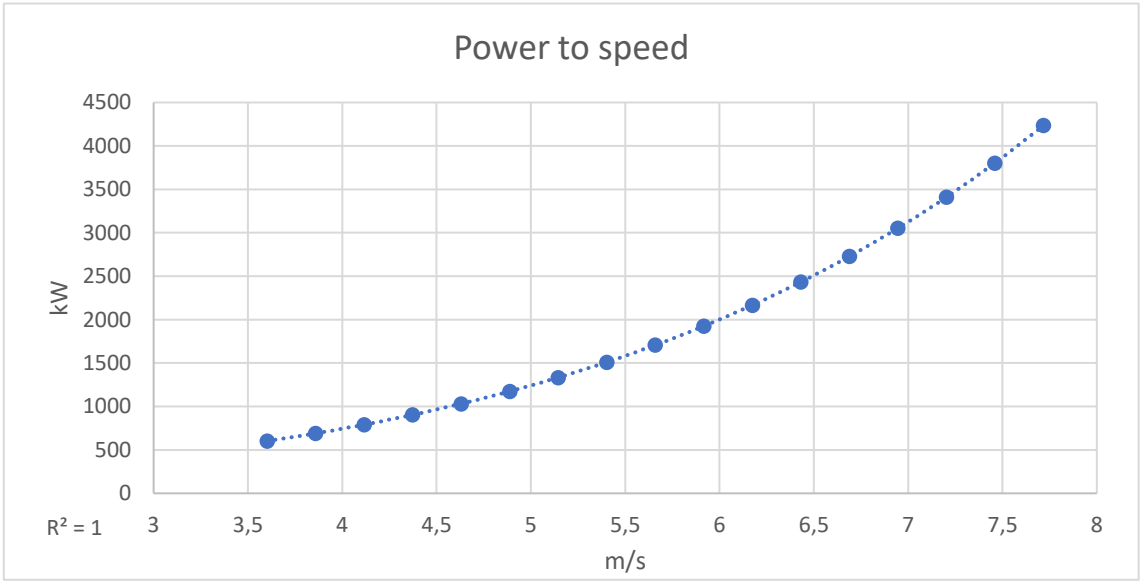

Figure 6 Power to speed plot

$$Power = 1.6422V^4 - 18.797V^3 + 164.83V^2 - 445.25V + 670.38$$

Equation 8 Velocity to power - empirical

This is the formula we will utilize from here on out to calculate the necessary power supply from the velocity in meters per second.

The reference velocity of 12 kts represents a total power demand of 2,166 kW.

$$Power^{ref} = 2{,}166\ kW$$

The hydrogen flow for a respective speed is not only given by the power need of the propulsion system but also the efficiency of the FC at the given load.

6.3 Fuel cells

In this subchapter, we will provide a brief discussion on the basics of fuel cells and list a few of the technology options. We will describe some of the characteristics when used in ships compared to traditional ICE systems. We will discuss the lifetime, the difference in efficiency experienced at different loads and present the required inlet conditions for our case. In the end, we present an analytical assessment of the empirical data for fuel consumption.

6.3.1 Theory

A fuel cell is a machine that can transform the chemical energy of some form of fuel into electricity by the use of an electrochemical reaction. The oxidizing agent most commonly used is oxygen. The fuel is often hydrogen and this is the case for us and the focus in this paper, but an FC can also be used with other chemicals like ethanol or ammonia (Holtebekk, 2018). As some of the energy is converted directly into electricity, the Carnot limit for thermal efficiency does not apply. The cell itself shares many similarities with a standard battery and has the same main components. The difference is that a fuel cell needs a continuous supply of fuel. The components are the electrodes where the anode supplies *electrons*, which are then absorbed by the cathode. These two are separated by an electrolyte enclosing the circuit by conducting ions (Schumm, 2018). The fact that the FC directly changes the electrochemical energy to electricity is the reason for the high efficiency of up to 60 %. Where a regular ICE combusts the fuel and utilizes the expanding gas to do the work only obtains an efficiency of < 40 %. The theoretical upper limit for fuel cell efficiency goes toward 100 % but with today's technology the range of 50 to 60 % is deemed as decent (Holtebekk, 2018). A very general reaction is presented below.

$$H_2(Fuel) + O_2(Oxidant) \rightarrow H_2O(Product) + W(Work/Electricity) + Q(Heat)$$

Equation 9 Fuel cell general reaction

Note that this equation is presented to represent the reaction conceptually and the stoichiometric coefficients are therefore not balanced. A correct chemical reaction for the PEM case will be presented later.

6.3.2 Fuel cell technologies

The most common method of categorizing different fuel cells is by their respective electrolyte. These can be solid or liquid and consist of various materials. We also separate between the high and low operating temperature and as we shall see, this will be of importance for the Topeka FC choice of a PEM system. As a PEM is defined from the beginning, we will not go into much detail on all of the different technologies but rather present some of the main factors. We start by describing some of the high-temperature fuel cells.

6.3.2.1 Phosphoric Acid Fuel Cell – PAFC

The PAFC uses phosphoric acid as the electrolyte connecting the electrodes. The concept and reactions are similar to the alkaline fuel cell that will be discussed later. This was one of the first cells to be commercialized. The operating temperature in the range of 200 °C leads to a higher tolerance for impurities and this makes it more suitable to include in an SMR set up than low-temperature cells (Tronstad, 2017). The electric efficiency from the cell itself is low at around 40 % but as the temperature is high it is possible to include a heat recovery steam cycle and hence increase the total system efficiency to up towards 80 % (Tronstad, 2017). The total power density of the system, however, is low and the warm-up time is in the range of several hours (Pratt, 2016). This concept is not suitable for a vessel of our type.

6.3.2.2 Molten Carbonate Fuel Cell – MCFC and Solid Oxide Fuel Cells – SOFC

Both of these technologies operate in the +500 °C range with the challenging start-up time that comes with these temperatures. The choice of fuel is flexible but there are no commercially available FCs for the use of pure hydrogen (Pratt, 2016). This eliminates them as alternatives for us and we will not go into further detail.

As the high temperature is challenging regarding start-up time and has a low power density as the high-efficiency operation is obtained in connection with an HRSG, we will now assess some low-temperature alternatives. As PEM is the concept we shall use, this is also the one where we will go into the most details.

6.3.2.3 Polymer Electrolyte Membrane – PEM

This is one of the more mature technologies for mobile applications. This is due to rapid start-up, high power density and fast response to a change in load. It is also the most commercially available and with a good track record (Pratt, 2016). The combination of these factors is the main reason for choosing it as the power-supply for the Topeka vessel.

A PEM fuel cell takes in hydrogen gas on one end, the anode or the negative side. Hydrogen atoms consist of 1 proton and 1 electron, and in its gaseous state, the atoms form hydrogen molecules by pairing up in H_2. On the other side of the cell, at the positive side or the cathode, oxygen enters. The hydrogen and oxygen "want" to react and form water. This implies that the molecules must split up to form new water molecules. The protons and the electrons in hydrogen split up on the surface of the electrode. This is driven by the Gibbs reaction where according to the laws of thermodynamics, a system will tend towards the state of lower energy and higher entropy (Khotseng, 2019). The two sides of the cell are separated by a special polymer membrane where only the protons can pass through, while the electrons go through an external circuit. The protons move to the other side of the membrane in the form of ions, more specifically H_3O^+, solved in the water (*Conversion and Storage of Energy*). The hydrogen side include a catalyst made of noble metals like platinum to increase the speed of the total process. To make the fuel cell work, the two sides are connected with an outer electric circuit where the electrons flow, generating the current. On the airside, the hydrogen's protons come through the electrolyte and react with oxygen and electrons, resulting in the formation of H_2O – water, the only physical byproduct of the DC electricity production. Below we will present the main reactions.

Anode reaction: $2H_2 \rightarrow 4H^+ + 4e^-$

Equation 10 PEM anode reaction

Cathode reaction: $O_2 + 4H^+ + 4e^- \rightarrow 2H_2O$

Equation 11 PEM cathode reaction

Total reaction: $2H_2 + O_2 \rightarrow 2H_2O$

Equation 12 PEM reaction

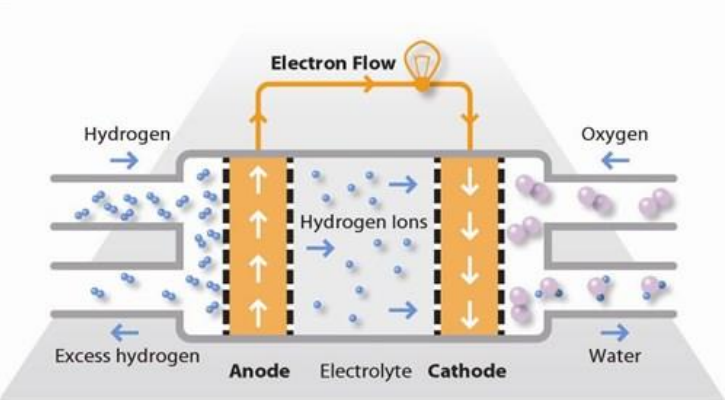

Figure 7 Conceptual illustration of a PEM-FC (FuelCellToday, 2020a)

The PEMFC has a low tolerance for impurities due to the materials used. This especially goes for the platinum regarding the compounds like carbon monoxide (CO) or sulfur (S) (FuelCellToday, 2020a). With the case of our Topeka vessel, the hydrogen source onboard is in the form of LH2. This is inherently pure, as the 20 K temperature does not allow for any other substances to mix with the hydrogen.

The name, Polymer Electrolyte Membrane is commonly shortened to PEM. This abbreviation is also used to refer to the Proton Exchange Membrane. This is the same technology but described by a name that emphasizes what the function of the membrane is, not the material. As the proton-conducting membrane is fabricated from a solid polymer, in contrast to the liquid electrolyte solution used in alkaline cells, these fuel cells are also referred to as Solid Polymer Electrolyte (SPE) in some literature (Godula-Jopek, 2015).

6.3.2.4 Alkaline Fuel Cell – AFC

The alkaline fuel cell is the oldest technology in the FC space. This was the chosen FC for the space missions in the 20th century. The cell is commonly designed with a cathode made with silver and an anode of nickel. These two are separated by an alkaline electrolyte, often KOH, potassium hydroxide (Tronstad, 2017). In the case of the PEM FC, H^+ moves between the anode and cathode. For AFC's it is OH^- that is the mobile ion.

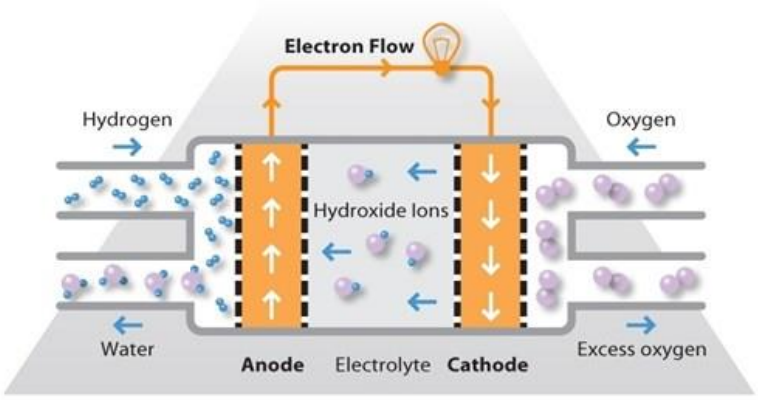

Figure 8 Conceptual illustration of an AFC (FuelCellToday, 2020b)

6.3.3 Other characteristics

The most important attribute of hydrogen-based fuel cell technology is the elimination of emissions of GHG, NO_x, SO_x and particulate matter. Note that this statement excludes the production of the hydrogen itself. Production by either renewable energy or by SMR, in combination with CCS, can ensure a complete environmentally friendly value chain and this is the long-term goal of the project (PILOT-E, 2019). As it is of limited technical importance for the Topeka vessel, we will not go into further detail on the source of hydrogen.

In contrast to the legacy diesel propelled vessel, the fuel here is non-toxic to both humans and the natural environment and disperses quickly in case of an unwanted spillage (Cadwallader, 1999).

With the legacy technology, there have been cases of waxing (freezing) of fuel at arctic temperatures. This is due to the temperature sensitivity of petroleum-based fuels (Gupta, 2016). This would not become an issue with the fuel supply of hydrogen as there is no chance of naturally occurring temperatures threatening to freeze GH2. The risk of extremely low temperatures can possess a risk towards the heating fluids used in the process and this issue is discussed further in the part for heat exchangers.

A fuel cell produces little to no noise or vibrations compared to traditional diesel engines (Chubbock, 2016). This has many potential benefits. These factors are of significance to the crew and passenger comfort and the International Maritime Organization in 2012 adopted regulations requiring ships to be constructed to adhere to the accordance of noise levels on board (*Ship noise*, 2020). This allows for less material being used on FC vessels for noise insulation and therefore can contribute to a reduction in weight and material cost of the ship and still exceed the comfort level experienced on legacy vessels. These considerations are not only of importance to the persons on board the vessel but also extend to marine wildlife. The effect of man-made underwater noise pollution is negative and this is especially a concern for marine mammals. This is why the IMO in 2014 implemented guidelines for commercial shipping companies for underwater noise reduction. However, the sound waves propagated through water are mostly created by propeller cavitation and not the engine itself so the total reduction in noise pollution from FC implementation is of lesser effect (*Ship noise,* 2020).

As established in the previous subchapter, the electric efficiency of the PEM cell is in the area of 50 to 60 %. This implies that 40 to 50 % of the available energy in the fuel is lost in the process. According to the laws of thermodynamics, the energy cannot disappear, but rather disperse as a lower-quality

form of energy. This "waste" energy from the electrochemical process is mainly in the form of heat (Mohamed, 2016). A simple concretization based on this statement is to assume the heat production to be of the order of magnitude of $1 - \eta_{electric}$ where $\eta_{electric}$ symbolizes the electric efficiency of the cell. This is a simplification but it provides a general assessment. As a low-temperature FC is chosen, the resulting heat energy is of low quality as it is not of a magnitude that can be used for further electricity production. It can, however, be used to heat the cryogenic fuel. This will be discussed in the part on heat exchangers.

A factor of importance when designing a power system connected to the propulsion set-up on a vessel is the dynamics of the power supply. Here, we will denote this as the ramp-up speed which describes the time it takes for the stacks to raise their power production in response to a change in load. The specific numbers will vary based on which manufacturer of cells is chosen but here we will discuss the characteristics provided by PowerCell. They inform that their stacks are developed for a ramp-up of above 100 A/s. This is a very high rate but reviewing the fuel cell itself only provides half of the picture. In a full system, it would rather be the fuel supply than the cell that will represent the limiting factor. PowerCell states that the total ramp-up from a system based on cryogenic storage has a total ramp-up speed that would compare to an electrical acceleration of 20 A/s. One of the reasons why this parameter is important is when scaling the battery pack. The combined system must be able to respond to any given realistic situation regarding the vessel. The battery pack will be discussed further in this paper in a separate subchapter.

6.3.4 Lifespan of FC

An uncertain factor when it comes to industrial fuel cells is the length of the useful life. Ballard states an estimated lifespan of around 25,000 hours. This number was discussed with a researcher from Prototech who stated that one could assume at least this lifespan with today's technology from PEM FC's for installation onboard ships. The true lifespan is still uncertain and the research is moving forward rapidly indicating a higher number in the near future. Prototech highlights that the load profile and the number of start-and-stops will impact the lifetime.

According to PowerCell, the dynamics of the load profile, i.e. how rapidly the load is changed, will lead to some degrading of the stack. However, they highlight the fact that it is start-and-stops that is responsible for the highest degradation.

Our set-up consists of battery packs on a vessel which will travel at a constant service speed for most of the time at sea. We will not try to determine any specific numbers around the start-and-stop frequency here but it can be stated that based on these facts, a ship seems like one of the more suitable modes of transport where hydrogen can play a role.

A different factor considering the lifespan of the FC is the change in efficiency. The available output from a stack falls with the number of hours in use (Bruijn, 2011). We will define two situations, Beginning of Life (BoL) and End of Life (EoL). The abbreviations will be used. The real power output from the cells and the change from beginning and to the end of its useful life will be heavily dependent on the manufacturer and we will use empirical numbers provided by Ballard, in this paper. These numbers are presented in the segment of fuel consumption.

After the useful lifespan of the cell, it must be replaced for the continuing of vessel operation. The PEM technology does not contain any toxic or hazardous materials that need to be accounted for during disposal and recycling. Ballard has a refurbishment program where used fuel cells are renewed with the reuse of the hardware and plates, replacing only the membrane electrode

assembly (MEA). They state a potential cost saving of a third and according to them, they manage to extract and recycle more than 95 % of the precious metals in the MEA (*Recycling PEM Fuel Cells,* 2017).

6.3.5 Inlet conditions of fuel

As the fuel cell functions with an aqueous solution between the electrodes, the limiting factors will be 0 °C on the low side. This to avoid any risk of freezing in the cell. On the upper side, the limit is in the area of 100 °C, i.e. normal boiling point to avoid boiling in the cell. According to correspondence with researchers from the fuel cell research company of Prototech the temperature at the inlet of the FC should be in the area of ambient conditions. The range of 0 to 60 °C is suggested. Due to higher molecular velocity at higher temperatures, increasing the temperature will increase the reaction kinetics. This is why the power output often improves for higher temperatures (Mohamed, 2016). It is of minor practical importance compared to the energy needed to heat the hydrogen and we, therefore, use a temperature in the lower part of the range but with a margin to the limit. We continue the calculations based on an inlet temperature of 10 °C or 283 Kelvin into the stacks. We will continue our calculations with this being the final temperature after the complete compression, evaporation and heating process.

The pressure of the hydrogen gas into the cell is also of relevance. An important factor in maintaining net-zero pressure on the membrane. This implies a similar pressure on both the hydrogen side and the airside to avoid mechanical stress on the polymer membrane. Compression is a cost in both CAPEX and energy and to obtain a high total efficiency of the set-up, the FC operates at a low to moderate overpressure. Different companies produce stacks with variability in demand for pressure internally in the cell.

In discussion with LMG Marine on the system pressure levels, an acceptable range into the stacks of 3.5 to 5 barg is stated. A pressure of 4 barg is assumed as our relevant inlet pressure as this is the target they design for.

6.3.6 Fuel consumption of FC

How much fuel the FC consumes is a function of the load. Empirical values are provided by Ballard for a 200 kW unit. These are the ones intended for the Topeka project. The idea is to bundle several units to a set-up that provides the required power which was calculated in (8). The load factor can be calculated easily by dividing the estimated power consumption by the total installed and available FC capacity. The data presented is given in grams of hydrogen per kWh produced energy.

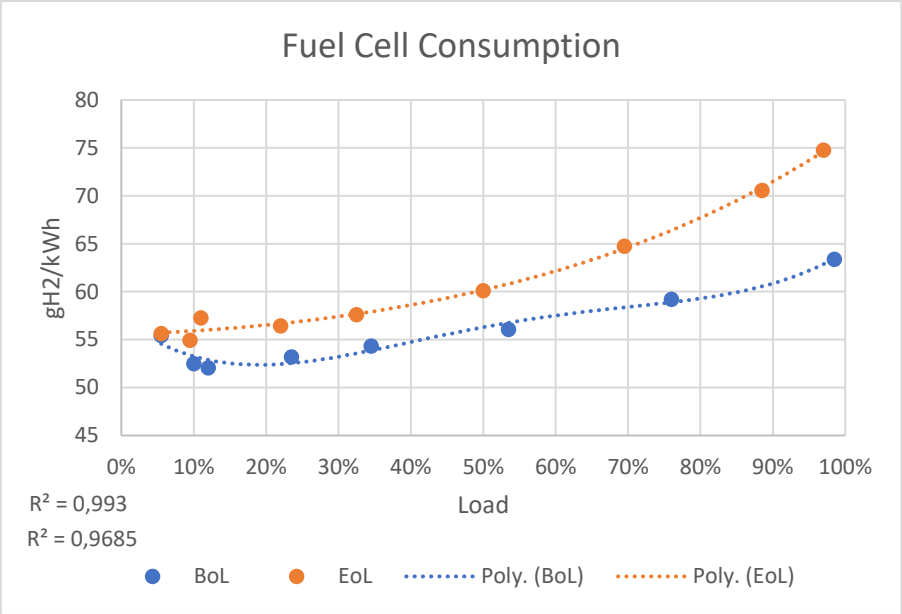

Figure 9 Plot of fuel cell consumption to load

Based on the data point provided by Ballard, we have used excel to do a polynomial regression to the fourth degree to approximate expressions that can be used analytically. We here denote the FC consumption as C. The x denotes the load.

$$C_{BoL} = 140.83x^4 - 310.55x^3 + 236.83x^2 - 60.215x + 57.214$$

Equation 13 Fuel cell consumption to load – BoL

$$C_{EoL} = 7.777x^4 - 3.803x^3 + 14.862x^2 + 1.688x + 55.605$$

Equation 14 Fuel cell consumption to load – EoL

The reference velocity of 12 kts and the reference power demand of 2,166 kW equates to the reference fuel cell consumption:

$$C_{BoL}^{ref} = 56.85\ gH_2/kWh \qquad C_{EoL}^{ref} = 60.94\ gH_2/kWh$$

One can observe that the two reference cases are in the area between 54 and 55 % of full FC load.

As these relationships represent the extreme cases of initiation of operation and the very end of the operational life we see the value of an approximation including the relevant service time. We do this by including a parameter β describing the "age" of the system as a number between 0 and 1 where they represent BoL and EoL conditions, respectively.

$$C(x,\beta) = \mathrm{C_{BoL}(x)} * (1-\beta) + \beta * \mathrm{C_{EoL}(x)}$$

Equation 15 Fuel cell consumption to load and age

The β will, in theory, represent the real age of the stacks as a ratio of its lifetime. Factors like how the load ratios have been practiced, temperatures and pressures, potential pollutants from the air and the number of start-and-stop cycles performed may play a role here. A simplification will be used in this paper, where we idealize the age parameter as a linear function only dependent on the hours in operation.

$$\beta = \frac{Hours\ in\ operation}{Total\ assumed\ lifetime}$$

An assumption here is dependent on the manufacturer of the specific stack. Here we assume 25,000 hours as stated in the lifetime discussion.

From a scientific point of view, it can be interesting to review the efficiency of the FC at different loads as well. This is done by dividing the LHV of hydrogen, 30.03 g/kWh on the consumption. Here we have similarly plotted them as for the consumption plot. One can observe that they are a direct inverse of each other.

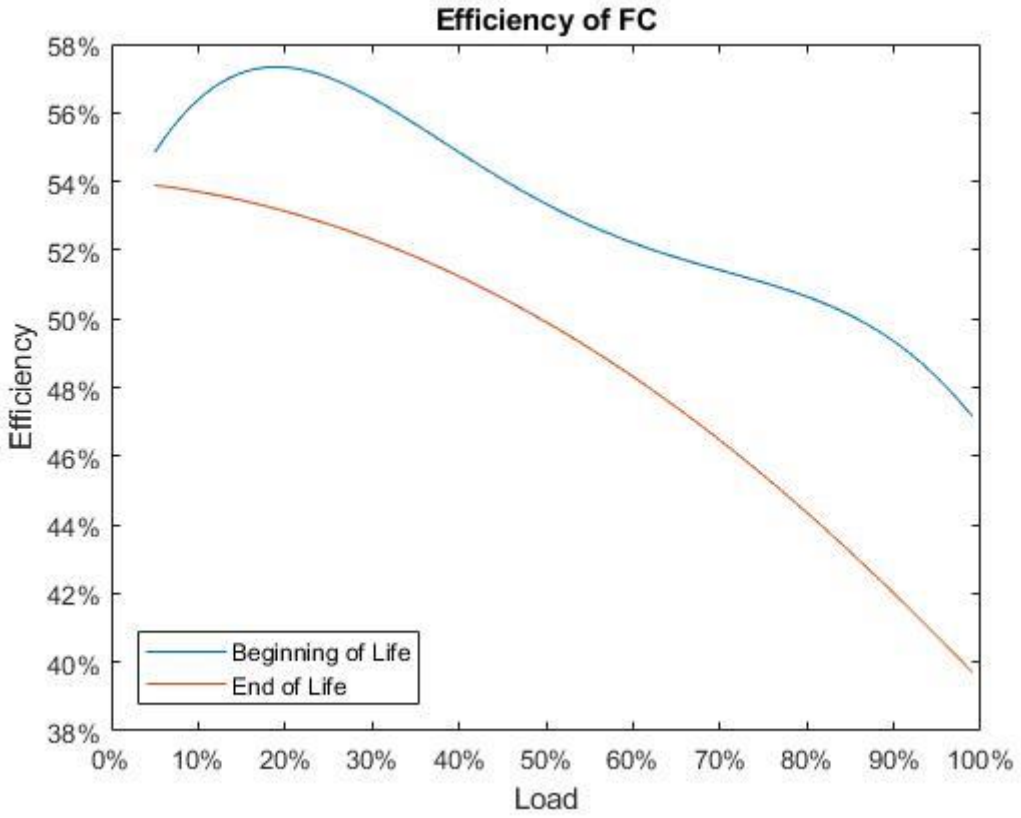

Figure 10 Plot of efficiency of fuel cell to load

The reference cases had loads of 54 and 55 %. The associated efficiencies are 52.8 and 49.1 %, respectively. We will take the average between these as a reference FC efficiency to use further.

$$\eta_{ref} = 51\ \%$$

This implies an available LHV of 61.14 MJ/kg.

We can assume that this data is independent of the total size of the set up as long as it consists of the same 200 kW units. In other words, the formulas are only dependent on load as a ratio. The total size is irrelevant.

Note that the efficiency of the cell goes up as the load goes down. This is especially interesting for our case of replacing legacy diesel engines with new hydrogen technology. For ICE the efficiency to load relationship diverges from hydrogen as the optimal load is much higher at 80 – 90 % and with a

curve that falls for lower loads (Khan, 2006). The delta in efficiency between different loads is also much larger for diesel ICE than the hydrogen equivalent.

6.3.7 Fuel consumption

In the respective subchapters, we have discussed how the flow of fuel is dependent on the power consumption of the vessel, again dependent on speed, and the efficiency of the FC, at the given load. Here we will combine those two relationships and use them to review the most efficient service speed regarding hydrogen per traveled nautical mile.

6.3.7.1 Mass flow

Mass flow equates to the flow of hydrogen in kg per second needed to produce the power to operate the vessel. In this part, we assume full energy supply from FC and exclude batteries from the calculations. This is a valid assumption as the batteries will not be of a size that can contribute over longer legs of travel at full service-speed. The batteries will be discussed further as a means to optimize efficiency and contribute during rapid changes in power consumption in its respective subchapter. The formula for mass flow is the total power consumption multiplied by the hydrogen consumption per power production.

$$\frac{\partial m}{\partial t} = \dot{m} = Power(V) * C(x)$$

Equation 16 Mass flow definition

$$x = \frac{Power(V)}{FC\ Capacity} = x(V)$$

Equation 17 Load on fuel cell to velocity

$$\dot{m}(V) = Power(V) * C(V)$$

Equation 18 Mass flow to velocity

We see that the flow rate for a given FC set-up is only dependent on the velocity of the vessel. As the consumption is related to the point of the life of the FC, we will model two cases, BoL and EoL. The true consumption will be somewhere between these limits but as of now, there is a lack of data on the progression of change in FC efficiency between these points. In (13) and (14) the consumption is provided in g/kWh. In our calculations, we will divide this number by 1000 to convert to kg and 3600 to convert to seconds to achieve SI units. Continuing with the assumption of an FC capacity of 4000 kW, we use Matlab to plot the curves of fuel flow to velocity.

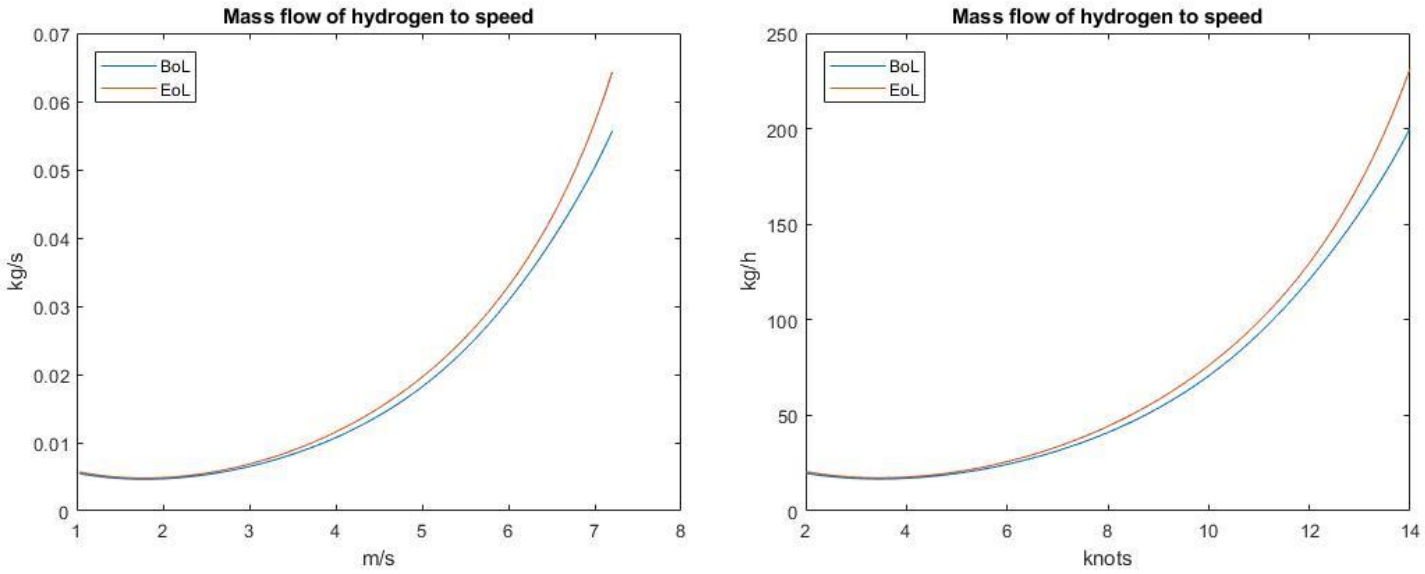

Figure 11 Plots of mass flow of hydrogen to speed

The reference mass flows are:

$$\dot{m}_{BoL}^{ref} = 121.50\ kgH_2/h \qquad \dot{m}_{EoL}^{ref} = 130.17\ kgH_2/h$$

Minimum fuel flow		Velocity	
Beginning of Life	**End of Life**	**Beginning of Life**	**End of Life**
4.64 g/s	4.81 g/s	1.79 m/s	1.79 m/s
16.71 kg/h	17.33 kg/h	3.48 kts	3.48 kts

Table 4 Minimum fuel flow and respective velocity

In the above table, the values for the most efficient velocity regarding hydrogen consumption per time is presented.

6.3.7.2 Mass flow per distance

As expected from the power to velocity curve, the hydrogen fuel consumption to speed is also of an exponential characteristic. When reviewing this system, it is also relevant to calculate the hydrogen consumption per distance traveled, in addition to per time. As the fuel flow per time rises with higher speed, so does the distance traveled per time. To obtain this chart, we must divide the fuel flow per time by the respective velocity.

$$\frac{fuel\ flux}{distance} = \frac{\dot{m}}{V} = \frac{Power(V) * C(V)}{V}$$

Equation 19 Fuel flow per distance

For a conversion to nautical miles, we multiply by a factor of 1,852 m/nm (Kjerstad, 2020).

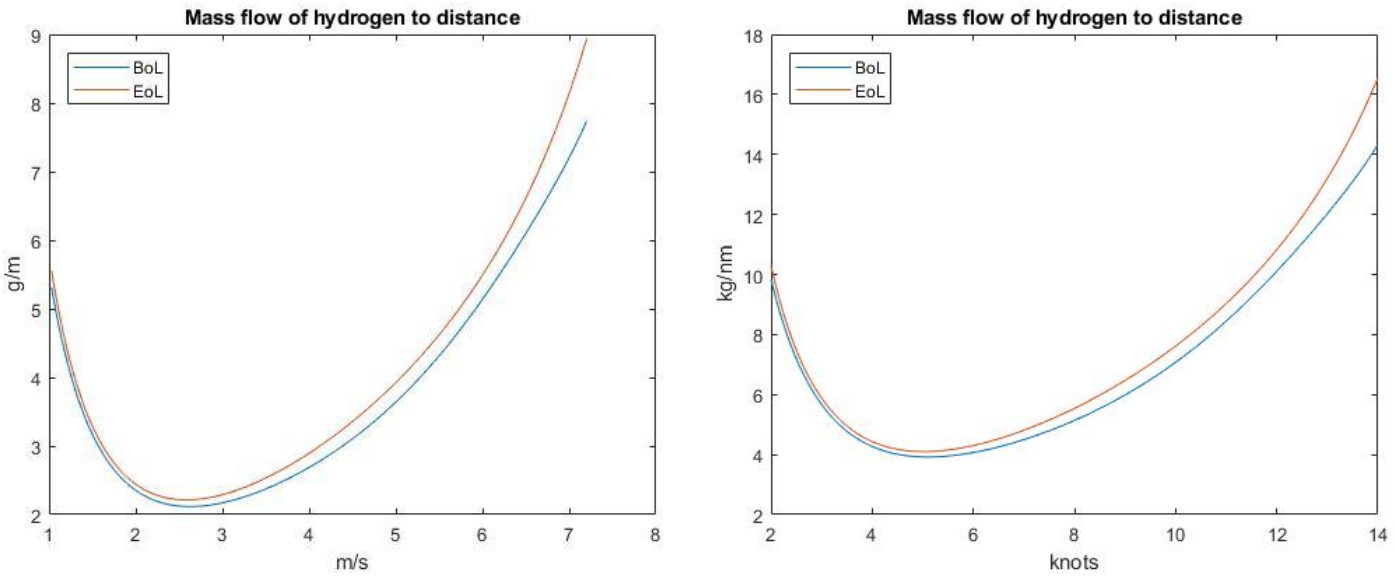

Figure 12 Mass flow of hydrogen to distance

Minimum fuel flow		Velocity	
Beginning of Life	**End of Life**	**Beginning of Life**	**End of Life**
2.12 g/m	2.21 g/m	2.63 m/s	2.59 m/s
8.60 kg/nm	8.91 kg/nm	5.11 kts	5.02 kts

Table 5 Minimum fuel flow to velocity

By accounting for the increase in distance traveled per time the optimal velocity is increased from 3.5 kts to 5.1 kts for initial conditions.

The reference fuel flows per distance are:

- BoL: 10.13 kg/nm
- EoL: 10.85 kg/nm

6.4 Fuel flow

With the necessary hydrogen fuel consumption known, we can review the process and calculate the energy needed for bringing the LH2 from the land-based tank and into the FC. In this segment, we will divide the process into four main procedures. First, the LH2 must be bunkered onto the vessel from land, afterward, the hydrogen needs to be compressed, then it must be evaporated to a gas before it is heated to be compatible with the FC inlet condition requirements.

All of these four will demand energy. This energy can be divided into two forms, electric and heat energy. What is meant by this and the reason for distinguishing between them is that the different procedures will utilize different energy types. The pressurization of the super cryogenic fluid will be done by electricity. The vaporization and warming of the gas will be done by heat energy through heat exchangers. As the FC produces both electricity and heat all of the procedures will be directly related to the stacks and their activity.

The bunkering will be driven by the pressurization of the land tank. It is connected to the vessel fuel tank by vacuum insulated pipes to maintain the liquid properties. After the Topeka vessel has left port and initiated FC electricity production, the general idea is that LH2 will flow from the large tank and into two smaller conditioning tanks where heat is added to build pressure. When the conditioning tank has reached the correct pressure it will release the hydrogen into a heat exchanger where a special heating fluid will bring heat from the FC and first vaporize the LH2 before it will be heated to the temperature necessary for the FC process. We will now go into detail on each of these processes.

6.4.1 Bunkering of LH2

The vessel will refuel at one or several ports. This implies the need for a bunkering set-up close to the quay at those locations. In this part, we will provide a general description of the concept and then perform the necessary calculations to obtain the pressure and energy needed to bunker the Topeka vessel.

6.4.1.1 General set up

The general outline of the concept is having a cryogen vacuum insulated tank on land. This is the LH2 storage tank supplying fuel for the vessel each time it calls the port. There will be a bunkering pipeline connecting the two tanks. This pipe can connect the land system into the side of the ship where internal pipes bring the hydrogen up to the fuel tank. Another alternative is to have the connection between the ship's system and the land system elevated at the height of the fuel tank. This reduces the need for a complex piping system onboard but as we then have a fuel pipeline and connection high above the ground, this can be undesirable from a safety perspective. As of this writing, the specific design choices for the connection concept has not yet been decided. As it is of less importance from a fluid mechanical perspective, we do not have to assume those design parameters to describe the system.

The fuel to be transferred between the tanks is at a temperature of -253 °C. At this temperature, it can pose several challenges to the material and therefore, with finding a pump system that is reliable over time and with a reasonable investment cost (Pritchard, 2010). The delivery method that will be designed is to use pressure build up in the land tank. This pressure will then force the fuel out and through the pipe, into the ship's fuel tank. The pipeline will be connected to the bottom of the onshore tank to maintain flow in the liquid phase. This is important as the tank will contain hydrogen in both gaseous and liquid form. For the ship's tank, the inlet will be at the top. There are several reasons for choosing this. From a safety aspect, it reduces the threat of a potential leak as only the gas phase will be in direct contact with it. The LH2 will enter the tank through spray nozzles. This allows the incoming hydrogen to cool down the vapor and can also be used for the initial tank cooldown. The same method is used for LNG carriers. In the LNG industry, it is also common with a separate top and bottom filling system. This is relevant for natural gas as the incoming LNG must be mixed with the heel as the two may be of different qualities, compositions and temperatures (ABS, 2015). This is not the case for LH2 and we assume only filling through the top.

The pressure driving the bunkering is produced by introducing heat into the land tank. This heat will evaporate a part of the hydrogen and as the gas cannot expand, it will build pressure. In addition to the initial pressure production, the heat ingress must also consider the outgoing flux of hydrogen to the ship. For every unit volume of LH2 going out, the same volume must be replaced by CH2. Below is a simplified conceptual illustration of the general bunkering set-up.

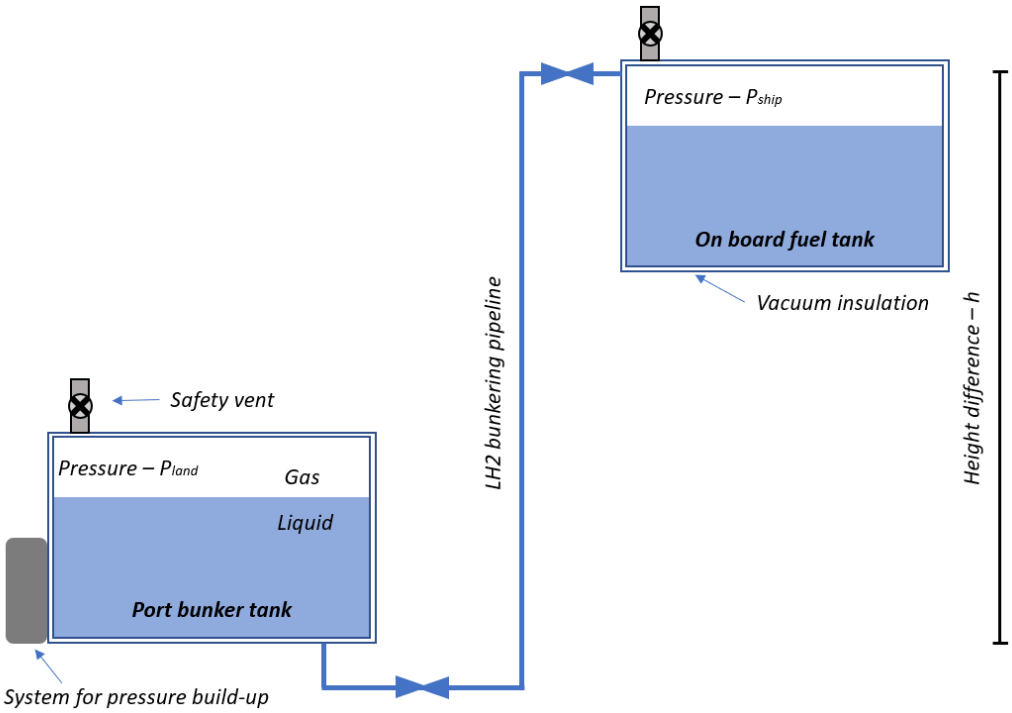

Figure 13 General concept of bunkering set-up

6.4.1.2 Calculations for the pressure

To calculate the necessary pressure production in the lower tank to obtain and maintain a steady and adequate bunkering speed we start with the general Bernoulli's equation along a streamline (Cengel, 2010).

$$P_1 + \frac{\rho V_1^2}{2} + \rho g z_1 = Constant$$

Equation 20 Bernoulli's equation for a streamline

This equation holds for steady and incompressible flow where frictional effects are excluded. The fluid in question is liquid para-hydrogen and we assume this to be incompressible. The gravity factor is included as we need to overcome the height difference between the tanks. The velocity component represents the speed of the fluid through the pipe. We assume the initial velocity to be zero and due to conservation of mass and incompressible flow, the velocity in the pipe is constant. The exclusion of frictional effects does not hold for a real engineering case and we have to add a pressure loss over the transport area to compensate for the friction. As we have an inlet, an outlet, bends and at least one union, we must also consider the minor losses from these flow disturbances. Finally, the pressure in the lower tank must overcome the pressure in the onboard ship tank. The expression for pressure ends up as:

$$P_{Land} = P_{Ship} + \Delta P_{friction} + \Delta P_{component} + \frac{\rho V_{pipe}^2}{2} + \rho g h$$

Equation 21 Pressure in the land tank (1)

The density of liquid hydrogen is 71.0 kg/m^3 (Godula-Jopek, 2015). The height is given by LMG Marine to be h = 13.8 m. The two factors that determine the velocity is the diameter of the pipe D

and the flow rate of fuel. The mass flow rate for the bunkering operation is given by LMG to be 60 kg/min or 1 kg/s. The resulting average velocity of the flow is the mass flux divided by the density and the cross area.

$$V = \frac{\dot{m}}{\rho A} = \frac{4\dot{m}}{\rho \pi D^2}$$

Equation 22 Flow velocity to the diameter and mass flow

We use this result in the full equation.

$$P_{Land} = P_{Ship} + \Delta P_{friction} + \Delta P_{component} + \frac{8\dot{m}^2}{\rho \pi^2 D^4} + \rho g h$$

Equation 23 Pressure in the land tank (2)

The expression for pressure-drop for fully developed circular internal flows is given as (Cengel, 2010):

$$\Delta P_{friction} = f \frac{L}{D} \frac{\rho V_{pipe}^2}{2} = f \frac{8 L \dot{m}^2}{\rho \pi^2 D^5}$$

Equation 24 Friction pressure drop

$$f = Darcy\ friction\ factor$$

To find the Darcy friction factor, we must first establish if the flow is turbulent or if it is laminar. We use the same approach as described in the propulsion chapter, i.e. we will assess the magnitude of the Reynolds number.

Laminar region – Re < 5 x 10^5 < Transitioning region < 1 x 10^6 < Re – Turbulent region

$$Re = \frac{\rho V L}{\mu} = \frac{4 L \dot{m}}{\mu \pi D^2}$$

Equation 25 Reynolds number to pipe diameter and mass flow

$$\mu = dynamic\ viscosity\ of\ fluid$$

The L represents the total length of the pipeline. As the bunkering system is yet to be designed in detail by the consortium, we assume it to be twice the height difference between the tanks.

$$L = 2h = 27.6\ m$$

The dynamic viscosity of para-hydrogen is 131.98*10^{-7} kg/(m s) at 1 bar and 109.69*10^{-7} kg/(m s) at 2 bar (McCarty, 1981c). By using the largest of the two viscosities and testing different diameters between 1 m and 1 cm we conclude that the flow will be in the turbulent region for every conceivable case. We use the Colebrook equation for establishing f (Cengel, 2010).

$$\frac{1}{\sqrt{f}} = -2.0 log\left(\frac{\varepsilon/D}{3.7} + \frac{2.51}{Re\sqrt{f}}\right) = -2.0 log\left(\frac{\varepsilon/D}{3.7} + \frac{2.51 \mu \pi D^2}{4 L \dot{m} \sqrt{f}}\right)$$

Equation 26 Colebrook equation for friction factor

$$\varepsilon = Roughness\ of\ pipe$$

The roughness of the pipe is a result of the material. We assume the pipeline's internal tubing is produced out of stainless steel. The roughness for the material is 0.015 mm (Absolute pipe roughness, 2011).

It is worth digressing from the friction factor to perform a brief discussion on the choice of material. There are two factors of importance here, hydrogen embrittlement and cryogen embrittlement. Hydrogen embrittlement is most common when dealing with hydrogen under pressure as the H_2 atoms can interact with the steel crystal lattice structure. The result of this is an enhanced probability of stress corrosion cracks (Brown, 2019). Brown states that metals with face-centered cubic lattices (FCC) are less susceptible to this issue than those of body-centered cubic's (BCC). The other challenge is due to the extremely low temperature. Most of the common steel types used for strength will lose a sizeable part of their toughness at temperatures below 100 K (Leachman, 2019). A material that maintains high strength at temperatures below 20 K is type 316 stainless steel (Ekin, 2006). This material contains a high nickel content and also consist of an FCC structure (Deegan, 2018). As this is a low-pressure environment the temperature is of more importance than the hydrogen itself but here, we see that there are types of stainless steel that can accommodate both these challenges and we deem our assumption to be acceptable.

We now move back to the equation describing the friction factor. This expression has to be solved numerically as there is no analytical solution for it. We will use Matlab for this calculation and as a first guess, we will use the approximation for the friction factor presented by S. E. Haaland in 1983.

$$\frac{1}{\sqrt{f}} = -1.8log\left(\frac{6.9}{Re} + \left(\frac{\varepsilon/D}{3.7}\right)^{1.11}\right) = -1.8log\left(\frac{6.9\mu\pi D^2}{4L\dot{m}} + \left(\frac{\varepsilon/D}{3.7}\right)^{1.11}\right)$$

Equation 27 Haaland equation for friction factor

Note that for both the equations (26) and (27) the logarithm is of base 10 and not the natural logarithm. The limit for deviations between two iterations is set to 10^{-8} in our script.

The losses in pressure from the components are often referred to as the minor losses as they for most pipes are of a smaller magnitude than the friction losses. In some cases, they can have a significant contribution to the total loss and that is the case if there are many bends and/or valves compared to the total length of the system. This might be the case here and therefore we will provide a discussion and include an assessment of the extent. The loss over a component is given as a loss coefficient K_L. Each component contributes to its own and the total loss of head over the system can be described as this sum (Cengel, 2010).

$$h_L = \sum_j K_{L,j} \frac{V_j^2}{2g}$$

Equation 28 Component head loss

The specific coefficient is very dependent on the geometry and production method of the component. In this paper, we make a few assumptions based on the generality of the set-up. Then we will use the tabulated values for loss coefficients of the components (Cengel, 2010). We will have an inlet from the tank to the pipe and assuming this is slightly rounded the loss amounts to 0.12. From the conceptual illustration, we observe three 90° bends. To provide a conservative estimate we add 2 more to 5 bends as a real set-up will contain 3 or more bends. Assuming a smooth bend, the coefficients are 0.3 each, summing up to 1.5. At the connection between the on-land pipeline and the boats, there must be some form of union. We add 0.08 to account for this. Finally, there is a loss from the exit region of the pipe and into the tank. As we have established a fully developed turbulent flow regime this is stated to be 1. Note that there is great uncertainty to each one of these assumptions and the company that will design the bunkering station must do a thorough analysis of each part supported with empirical data. The reason for the inclusion of these factors is that the

order of magnitude is assumed to be correct and the potential error of excluding the contribution leads to an under assessment of the needed pressure.

As the velocity of our pipe is constant, we can sum up the coefficients as $K_L = 2.7$.

The method we will use to incorporate this with the rest of the losses is by the equivalent length procedure. This makes it possible to describe the minor losses as a specific equivalent length of friction losses.

$$L_{equiv} = \frac{D}{f(D)} K_L$$

Equation 29 Length equivalent of component loss

The final equation describing the necessary pressure as a function of the diameter of the pipeline is presented below.

$$P_{Land} = P_{Ship} + f(D)\left[L + \frac{D}{f(D)} K_L\right]\frac{8\dot{m}^2}{\rho\pi^2 D^5} + \frac{8\dot{m}^2}{\rho\pi^2 D^4} + \rho g h$$

Equation 30 Pressure in the land tank (3)

A quick analysis shows that with a diameter of 0.06 meters and a friction factor in the area of 0.015 the equivalent length is in the area of 10.8 meters. For a long pipeline, this would not be of much significance but as our length is only 27.6 meters the minor losses represent almost 30 % of the total system pressure drop. Again, note that the largest uncertainty in the necessary pressure is attributed to the sum of component loss coefficients. The pressure in the onboard tank is assumed to be 1 barg. A discussion on this factor is presented in the LH2 tank subchapter later in the bunkering chapter.

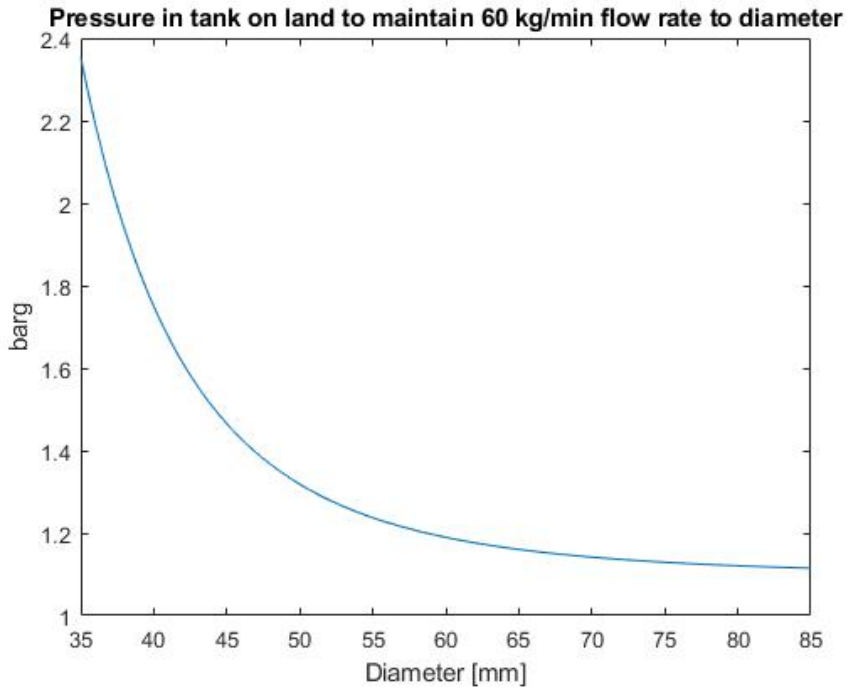

Figure 14 Pressure delta between land and vessel for bunkering to pipe diameter

We observe from this that as the diameter increases, the force needed to drive the flow through decreases and the limit goes towards the static gravity contribution at just shy of 0.1 bar, in addition to the ship's tank pressure of 1 barg.

The consortium has said that they assume the pipe to be designed with a diameter of 60 mm. We will use this as our reference case. The pressure this equates to is P = 1.2028 barg in the lower tank.

6.4.1.3 Calculations for the specific energy needed to maintain the flow

After the pressure needed has been built up it must be maintained throughout the bunkering process to sustain a steady flow rate. As mentioned, this implies that the LH2 volume leaving has to be replaced by a CH2 volume under the same pressure conditions.

We know the LH2 volume flow from the density and the bunkering rate.

$$Volume\ flow = \frac{\dot{m}}{\rho} = \frac{1\ {}^{kg}/_{s}}{71.0\ {}^{kg}/_{m^3}} = 0.014 \frac{m^3}{s}$$

Equation 31 Volume flow during bunkering

We now need to calculate the density of the gaseous hydrogen as this will replace the liquid flowing out of the tank.

6.4.1.3.1 Density of gaseous hydrogen

The density is a function of pressure and temperature and we will use the formulas and method presented in part 1.2.12 in *Selected Properties of Hydrogen* (McCarty, 1981b).

$$P = RT\rho(1 + B(T) * \rho + C(T) * \rho^2 + \cdots)$$

Equation 32 Equation of state for hydrogen

We only include the first two virial coefficients as this reduces complexity and is well within the accuracy deemed necessary in this paper. The virial coefficients B and C are dependent on temperature.

For temperatures above 100 Kelvin:

$$B(T) = \sum_{1}^{4} bi * {x_1}^{(2i-4)/4}$$

Equation 33 B factor of EoS above 100 kelvin

$$C(T) = c_1\sqrt{x_2} * (1 + c_2{x_2}^3) * (1 - \exp(1 - {x_2}^{-3}))$$

Equation 34 C factor of EoS above 100 kelvin

Where b, c and x are a series of coefficients. For temperatures below 100 Kelvin:

$$B(T) = \left(b_1 T + b_2 + \frac{b_3}{T} + \frac{b_4}{T^2}\right)/RT$$

Equation 35 B factor of EoS below 100 kelvin

The coefficients b in the virial coefficient B are constant in the range below 100 K. For C there are 3 temperature ranges below 100 K with different coefficients and/or expressions. For temperatures between 55 K and 100 K:

$$C(T) = a_1 \exp\left(\frac{a_2}{T}\right)\left(1 - exp\left(a_3\left(1 - \frac{T a_5}{a_4}\right)\right)\right)$$

Equation 36 C factor of EoS between 55 and 100 kelvin

With a single set of coefficients. For temperatures below 55 Kelvin:

$$C(T) = \left(c_1 T^2 + c_2 T + c_3 + \frac{c_4}{T} + \frac{c_5}{T^2} + \frac{c_6}{T^3}\right)/RT$$

Equation 37 C factor of EoS below 55 kelvin

For this range, we have two different sets of coefficients. One between the critical temperature of 32.957 K and 55 K and one below the critical temperature. All the mentioned coefficients have been found in chapter 1.2.13 in (McCarty, 1981b) and have been implemented in a Matlab function for calculations in this paper. They are presented in the table below.

Coefficients for the formulas						
Temperature above 100 Kelvin						
i	**1**	**2**	**3**	**4**	**5**	**6**
$\mathbf{b_i}$	42.464	-37.1172	-2.2982	3.0484	-	-
$\mathbf{c_i}$	1310.5	2.1486	-	-	-	-
$\mathbf{x_i}$	109.781/T	20.615/T	-	-	-	-
Temperatures below 100 Kelvin						
$\mathbf{b_i}$	1.9397741*10^3	-1.9279522*10^5	-2.2890051*10^6	1.1094088*10^7	-	-
Temperatures between 55 and 100 Kelvin						
$\mathbf{a_i}$	388.682	45.5	0.6	20.0	4.0	-
Temperatures between Tc and 55 Kelvin						
$\mathbf{c_i}$	$1.6971294*10^3$	$-5.0854223*10^5$	$6.7284118*10^7$	$-3.8045171*10^9$	$1.0789413*10^{11}$	$-1.1515642*10^{12}$
Temperatures below Tc						
$\mathbf{c_i}$	$1.0541776*10^5$	$-1.6597141*10^7$	$1.0431411*10^9$	$-3.2538718*10^{10}$	$5.1405848*10^{11}$	$-3.3123453*10^{12}$

Table 6 Coefficients for density calculations

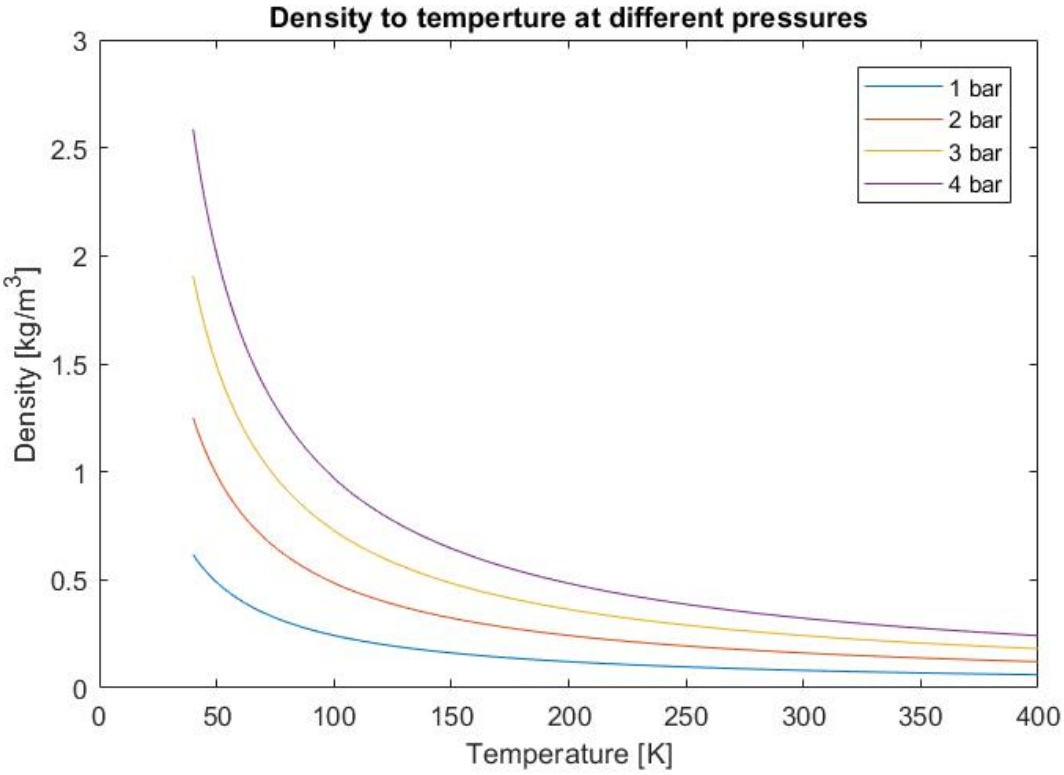

Figure 15 Density of hydrogen to temperature

This methodology and these formulas provide an accurate description of the EoS for densities up to about half of the critical density. This is the density obtained at the critical point and for hydrogen, this amounts to 31.05 kg/m^3 (NIST, 2018b). The implications is that our calculations have a reasonable degree of accuracy for combinations of pressure and temperatures resulting in densities up to 15.53 kg/m^3.

6.4.1.3.2 Specific energy for bunkering

$$\rho_{H2}^{gas}(2.2028\ bar, 22.8\ K) = 2.816\ \frac{kg}{m^3}$$

Note that the pressure we use is in absolute terms and not the gauge pressure as the relevant condition for the calculation is the "felt" pressure of the hydrogen and not the pressure we measure. The temperature used is the boiling point at 2 bar pressure (McCarty, 1981c) as this will be the temperature of the vapor. The evaporation rate is the product of the volume flow and the respective gas density.

$$\dot{m}_{evap} = Volume\ flow * \rho_{H2}^{gas} = 0.014 \frac{m^3}{s} * 2.816\ \frac{kg}{m^3} = 0.040 \frac{kg}{s}$$

Equation 38 Evaporation rate in the land tank during bunkering

The power or heat ingress Q needed to sustain this boiling throughout the bunkering is the product of the evaporation rate and the heat of vaporization. As discussed in the segment for regasification we used (Wakeham, 2011).

$$\Delta H_{L\to G} = T\Delta S_{L\to G} = T(S_G - S_L)$$

Equation 39 Latent heat of vaporization

The issue with this relationship is that the entropies of the liquid and gaseous hydrogen is dependent on the pressure. A table with values is presented below (McCarty, 1981c)

	1 bar	1.5 bar	2.0 bar	2.5 bar
Entropy – liq kJ/kgK	7.96	8.64	9.19	9.66
Entropy – gas kJ/kgK	30.00	28.84	28.00	27.32
Temperature K	20.27	21.67	22.81	23.75
$T^*(S_G - S_L) = H_{L\to G}$ kJ/kg	446.67	437.73	428.83	419.51

Table 7 Latent energy to pressure 1 - 2.5 bar

As we observe from the above table, the latent heat of vaporization decreases with pressure. To obtain a conservative estimate we will use the value for 2 bar as this will be marginally higher than for the reference case of 2.2028 bar.

$$Q = \Delta H_{L\to G}\dot{m}_{evap} = 428.83\frac{kJ}{kg} * 0.04\frac{kg}{s} = 17.00\ kW$$

Equation 40 Heat consumption during bunkering

The power needed for a bunkering process of 60 kg/min with a 60 mm pipe of stainless steel and a length of two times the height of 13.8 meters is 17.00 kW, assuming 1 bar gauge-pressure in the ships fuel tank and after the pressure has been built up.

This implies that a fueling procedure of 10 tons of LH2 will demand 47 kWh of energy. This is a theoretically calculated minimum energy usage and under real operation, there will be higher energy consumption. As the process on land will be powered by the national electrical grid, the power consumption relative to the fuel is not as relevant as the onboard processes. However, it can be mentioned that this energy demand is extremely low compared to the LHV of the fuel loaded to the ship. 10 tons of hydrogen amounts to 333.3 MWh or 7,000 times the demand.

If the pressure in the onboard tank is higher than the assumed 1 barg then the density of the gaseous hydrogen in the land tank will go up. This will again lead to higher energy demand as more electricity is needed to vaporize the LH2 to maintain the internal pressure. However, this process is fully powered by land-based electricity and the power consumption will not affect the energy usage of the Topeka vessel itself.

6.4.1.4 Pressure control in Topeka fuel tank

As the tank is a closed system under a given pressure with one part liquid and one part gas, the process of bunkering LH2 can lead to a pressure build-up. This occurs as the LH2 needs to displace the GH2 in the tank during the filling process. For LNG bunkering processes where the temperature and pressures in the tanks are similar, there are two connections between the tanks. One for LNG bunkering and one for vapor return to avoid pressure build-up in one tank and pressure drop in the other (ABS, 2015). Our case is more challenging as we use the pressure gradient between the tanks to power the bunkering. This implies that we cannot simply use the LNG set-up.

The volumetric flux out has to equate to the flux in. As have been determined, the bunkering speed is 1 kg LH2 per second. At the liquid density of 71.0 kg/m^3, this amounts to 0.014 m^3/s of cryogenic GH2 to be removed from the tank. Using the fuel tank pressure of 2 bara and a temperature of 22.8 kelvin, the respective boiling point (McCarty, 1981c), the density of the hydrogen is 2.50 kg/m^3. This implies that bunkering 10 tons of LH2 will demand the removal of 140.85 m^3 and 352.13 kg of hydrogen gas. The volume in itself is not an issue and had the gas been at the atmospheric temperature it would only amount to 11.37 kg which could possibly have been vented to the atmosphere, however, here it represents a technical challenge. Storage is also challenging as there would be a large pressure increase. A given volume of cryogenic GH2 would obtain a pressure of over 30 bar if allowed to reach 300 K confined in a constant volume.

The solution that has been chosen is reliquefication of the vapor instead of removal. When the tank is nearing its bunkering level, pressure rises. With a higher pressure, the saturation temperature goes up as well. It is now possible to have a two-phase mixture at a somewhat higher temperature. The LH2 being bunkered is supercooled to a temperature below the saturation temperature in the onboard tank. As mentioned, the filling takes place through nozzles at the top of the tank. This induces droplet formation of the LH2 forming a mist as it falls to the liquid surface in the tank. On its way down, it will reduce the temperature of the gas, effectively condensing it. This technique is called spray cooling. As more LH2 is filled, more gas is being condensed and the result is a stable or lower pressure in the tank, eliminating the issue.

6.4.1.5 LH2 tank

As an energy carrier, hydrogen has a supreme gravimetric density while the volumetric is less favorable. This imposes some challenges on the storage part as we want the energy density to be as high as possible. The Topeka project uses liquefaction to obtain this density as this is at the top of attainable hydrogen density without resorting to heavy and expensive metal hydrides. LH2 must be maintained at an extremely low temperature and well insulated from its surroundings to avoid heat ingress. Hydrogen can only exist in a liquid form at temperatures below its critical temperature of -239.9 °C. For critical temperature, a pressure of 13 bar is needed to maintain LH2 (Godula-Jopek, 2015). This implies that the tank system must have high thermal resistance. In this subchapter, we will provide a discussion on some of the main characteristics of the onboard cryogen storage vessel.

6.4.1.5.1 Tank type

There are mainly 3 types of tank concepts for maritime LH2 storage. IMO Type-C, Lattice Pressure Vessels (LPV) or ISO containers (Moss Maritime, 2018). The later of them has the advantage of being a commercialized technology with many producers. It is modular creating, certain flexibility to scale. However, they are limited by a small volume per unit and for a larger set-up like for the Topeka vessel, this is a disadvantage (Moss Maritime, 2018).

The LPV system does not have this disadvantage. It can be customarily designed to fit a wide variety of shapes and volumes. In many ways, this makes it ideal for ships as it is possible to utilize the hull space to accommodate as much fuel as possible. The core concept is having an inner insulated barrier. Outside, a layer of helium is circulated to maintain cryogenic conditions. This is done behind a tight secondary barrier. The disadvantage behind this design is that it is an unproven technology when it comes to commercialization. There are also very few suppliers as of now (Moss Maritime, 2018). In the future, this has the potential to become a widespread technology for maritime usage.

The tanks that have been chosen for the Topeka project is the IMO Type-C. This is a very well-proven technology with its roots in the space programs in the 60s and 70s where NASA developed cryogenic vessels for LH2 used in rockets (NCE Maritime CleanTech, 2019). We will explore some of the theory behind the technology but the core concept is to have an inner barrier of a hydrogen proof stainless steel. This will contain the liquid and can be designed to withstand a certain amount of internal pressure. This inner tank is surrounded by a vacuum contained by a secondary steel barrier. Between the double-wall, multi-layered insulation (MLI) is used to reduce thermal radiation. The outer tank can also be supplemented by an additional layer of insulation (Moss Maritime, 2018).

According to representatives of Wilhelmsen, a set-up with 2 IMO Type-C, each with a volume of 100 m^3 has been chosen.

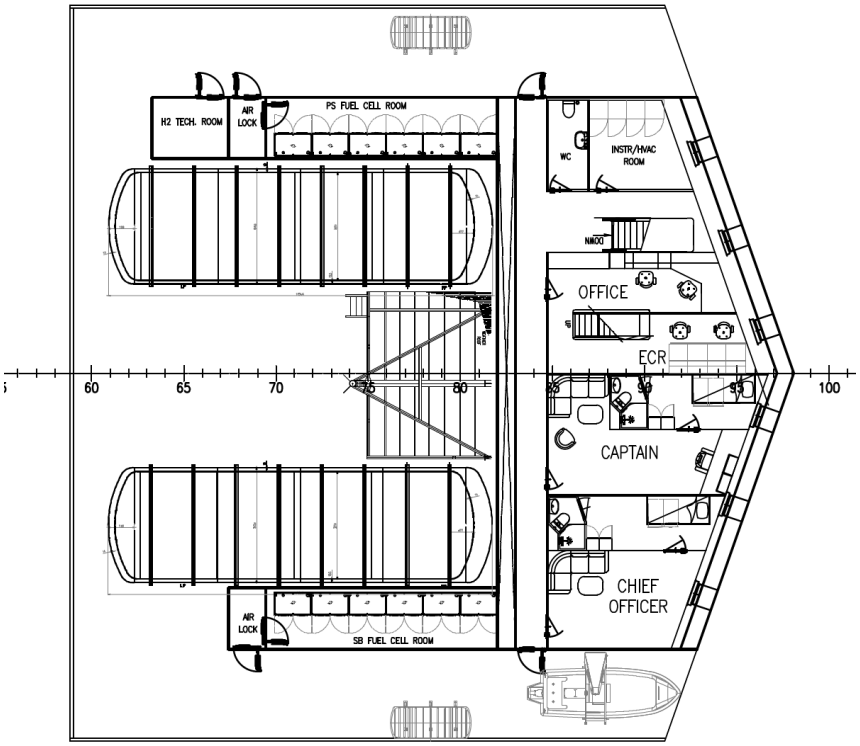

Figure 16 GA of top deck with crew accommodation and hydrogen storage from LMG

6.4.1.5.2 Insulation

In this segment, we will provide a brief explanation of the insulation concept the tanks are based on.

When heat moves from one place to another, it can happen in three ways. These transfer modes are conduction, convection and radiation. Conduction takes place through a medium as atomic and molecular activity without any bulk motion. Energy is transferred from the molecules with higher levels, to molecules with lower energy levels (Incropera, 2017f). For the LH2 tank, this is how heat goes through the first steel barrier, then the MLI and finally the outer tank and insulation.

Convection focuses on the transfer of energy in the form of fluid motion. Where conduction transfers energy from A to B by transferring energy from a molecule in location A to a different molecule in location B, convection describes when the molecule itself moves from A to B. As the fluid will contain energy, fluid motion result in energy movement. Convection describes the combined movement of both bulk fluid motion or advection, and the random motion in a gas or liquid (Incropera, 2017g).

This is how heat propagates from the ambient air and into the exterior of the tank. It is also partly how heat is being distributed within the LH2.

The final heat transfer mode is radiation. In contrast to the first two, radiation transfer requires no matter. As the vacuum is the main insulator, radiation is the most important energy-transfer type in our tank. All materials that have a temperature above zero kelvin will experience atomic and molecular motion. When the configuration of the electron changes, they emit electromagnetic waves, also referred to as photons. The radiation travels at the speed of light until it is intercepted by another substance (Incropera, 2017h). The vacuum does not emit, absorb or scatter any of the radiation and is referred to as a non-participating medium. The net thermal loss due to radiation from a surface enclosed by another surface with different temperature is given by the Stefan Boltzmann's law (Nave, 2016b).

$$q_{radiation} = \varepsilon E\left(T_{Surface}\right) - \alpha G\left(T_{Suroundings}\right) = \varepsilon\sigma(T_{Surface}^4 - T_{Suroundings}^4)$$

Equation 41 Net radiation heat loss

$$\varepsilon = Emissivity$$

$$\alpha = Absorptivity$$

$$\sigma = Stefan\ Boltzmann\ constant = 5.67 * 10^{-8}\ W/m^2K^4$$

This equation is based on a gray surface which is defined as having an emissivity and absorptivity of equal values. These are properties of the surface and both material choice and finish are of importance. Metallic objects generally have lower values and the best electrical conducting materials like gold and silver have the lowest with emissivity down towards 0.02 (Incropera, 2017i).

The emissivity plays a very important role in the radiation shield located in the middle of the vacuum. the role of this is that when the warmer outer tank emits radiation inwards towards the internal tank it will first hit the shield. The material is based on having low emissivity and low absorptivity. This results in a reflection of as much radiation as possible. However, some of the energy will be absorbed and the layer will be heated. This heat will be conducted through the thin film and to the surface on the opposite side. Here it will be emitted as radiation in towards the inner tank. By designing the shield as a combination of many of these thin reflective layers it is possible to drastically reduce the radiative heat flow from the ambient and into the hydrogen. This design is called multi-layered insulation and is very much used in space applications as radiation is the most important heat transfer type in extraterrestrial applications (Smith, 2019). It is also important that these layers are in as little physical contact with another as possible as conduction between them can easily be of a much larger magnitude than radiation.

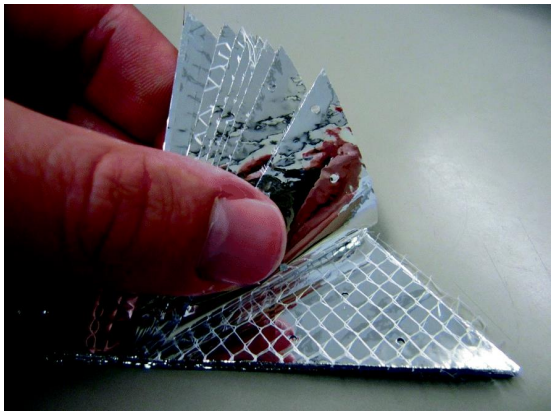

Figure 17 Typical MLI blanket (Walter, 2018)

We will now perform a simplified calculation describing how well an LH2 tank must be insulated compared to tanks containing LNG. The first factor to evaluate is the temperature delta. We assume an ambient temperature of 283 kelvin. As stated, hydrogen has a boiling point of 21 kelvin under a small overpressure. Depending on the composition, LNG has a boiling point at 111 kelvin (Basic Properties of LNG, 2009).

$$\Delta T_{LH2} = 283K - 21K = 262K$$

$$\Delta T_{LNG} = 283K - 111K = 172K$$

Based solely on this metric, an LH2 tank must be 52 % better insulated than an LNG tank, given the same heat ingress. A problem is that a similar heat ingress would not result in a similar boil-off volumetric rate. This will both be dependent on the latent heat of evaporation and the density.

We will discuss some of the physics of a phase change in more detail in the regasification chapter, but simplified it is the amount of heat needed to go from one phase to another at a constant temperature. This energy amount is 322.69 kJ/kg for hydrogen while LNG has a heat of vaporization of 509.27 kJ/kg. In this example, we assess the insulation need for similar tanks and geometries. This means that we must find the volumetric latent heat by multiplying by density. For hydrogen, this is 71 kg/m^3 and for LNG it is 450 kg/m^3 (Basic Properties of LNG, 2009). This implies:

$$h_{LH2}^{latent} = 322.96 \frac{kJ}{kg} * 71 \frac{kg}{m^3} = 22.9 \frac{MJ}{m^3}$$

$$h_{LNG}^{latent} = 509.27 \frac{kJ}{kg} * 450 \frac{kg}{m^3} = 229.2 \frac{MJ}{m^3}$$

This means that 1 unit of energy that can evaporate 1 unit-volume of LNG has the potential to evaporate roughly 10 unit-volumes of LH2.

Combining the temperature and latent potential, we end up with the factor of insulator capabilities. This amounts to 15.24, i.e. an LH2 tank need 15 times better insulation to obtain a similar boil-off rate in volume as an LNG tank. This highlights how important the tank properties on the Topeka vessel is.

The boil-off is only dependent on how much heat enters the tank. As this magnitude is given as the heat flux multiplied by the tank surface area, we note that the level in the tank will not affect the BO rate. In other words, a tank with a 1 m^3 per day BO will lose 1 m^3 per day regardless if it contains 100 or 3 m^3 of LH2.

The piping used to transport cryogenic hydrogen also requires very efficient insulation. The standard for liquid hydrogen pipes is vacuum jacketed piping where the same principle discussed for the tank applies (Vacuum Jacketed Piping, 2016). LMG has informed that vacuum insulated pipes are to be used on the Topeka vessel.

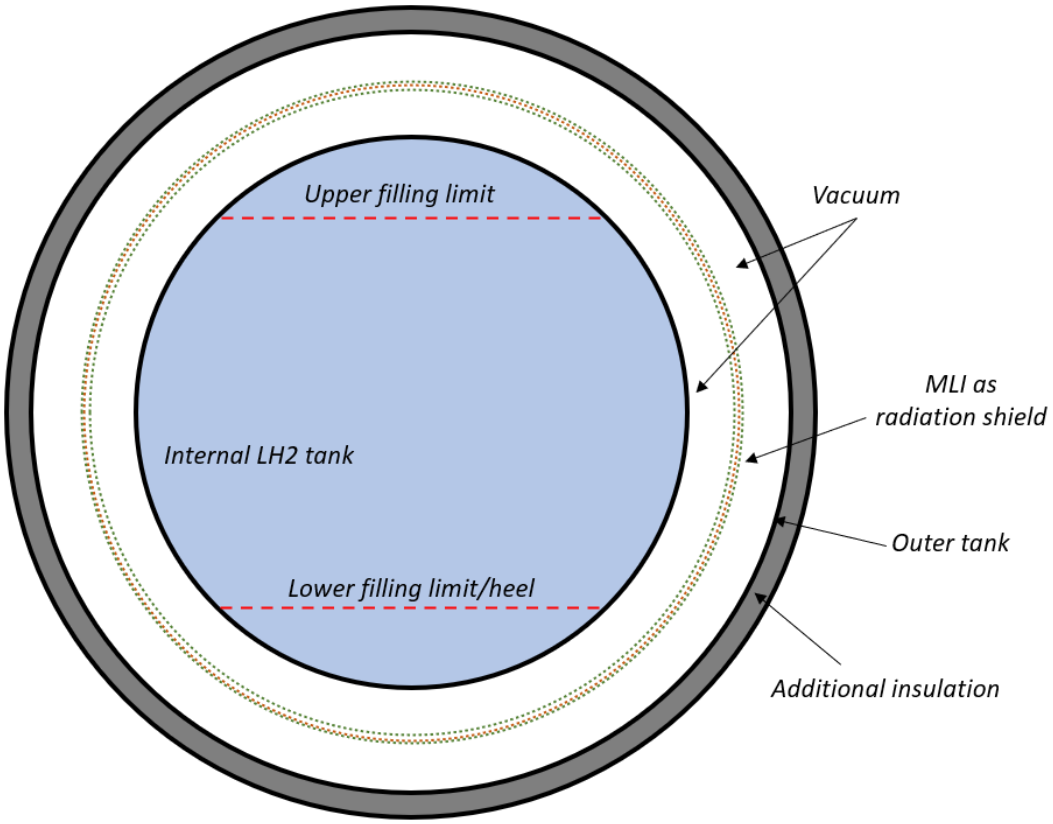

Figure 18 Illustration of insulation of IMO type-C cryogenic tank

6.4.1.5.3 Heel

The tank must be of the same cryogen temperature when it is to be filled. This implies that either it must be cooled down before bunkering commences or it must be kept at this temperature constantly. As the process of precooling is tedious and energy demanding, a better solution is to maintain a minimum amount of liquid hydrogen at the bottom of the tank at all times. This is referred to as a "heel" of hydrogen in the industry and often constitutes 5 – 10 % of the nominal holding capacity. (Nexant, 2018). Note that the LPV tanks do not necessarily need this as they have an external circulation of helium.

6.4.1.5.4 Pressure

Pressure plays an important role when considering the tank. As there are no perfect insulators there will be some BO. There are three possibilities when handling the BO issue. The first and simplest is to vent the vaporized hydrogen into the atmosphere. This induces a loss of fuel and requires a ventilation system that can dispense the gas out from the vessel in a safe manner. From a technical point of view, this is possible but the economical aspect of continuously dumping fuel is less favorable. The second one is to use at least as much hydrogen as the boil-off produces. If these amounts match, it can be an economical solution. However, this is not the case if the ship is idle or at the quay. Hence dumping of the fuel is still needed. The third solution is to let the BO accumulate as gas in the tank, building pressure. This reduces losses.

The last one is the solution chosen for the Topeka vessel, in combination with the two others, where a certain amount of pressure build-up is allowed for in the design. Over the continuous operation of the ship, fuel consumption will deplete the tanks and hence give room for more BO. Also, we have a safety vent where in case of adverse pressure levels, some gas will be vented to the atmosphere.

High pressure has some advantageous effects as it increases the density of the hydrogen gas, allowing for larger amounts stored. The disadvantage is that the technical requirements increase and the regulations are stricter for high pressure. The higher the initial pressure, the more pressure the system must withstand to be able to provide a certain time of ambient exposure before the safety valve kicks in.

Due to class rules for ships tending to be stricter for higher pressures, we assume the pressure in the tank to be 1 bar above the ambient i.e. 2 bara. The limits for what can be defined as dangerous cargo based on pressure may deviate from jurisdiction to jurisdiction but the cut-off point for the definition is typically 2 bar (Fry, 2013).

6.4.1.5.5 Safety

As mentioned, it is paramount that a well-functioning safety pressure release system is in place to account for adverse pressure rises. Another factor where pressure plays a role in the safety and reliability of the system is the potential inflow of ambient air. If a leak were to take place and air would enter the tank, it would immediately freeze and form a solid (Royal Society of Chemistry, 2020). This would impose negative consequences on the rest of the fuel system. As we want a certain amount of overpressure to avoid potentially harmful inflow, our assumption of 1 barg seems reasonable.

As the tank contains a large amount of energy and flammable fuel on a large moving vessel, the mechanical resilience of the tank should be mentioned. The chosen type-C tanks have been used for many years and many different cryogenic liquids (Kokarakis, 2015).

6.4.2 Pressurization of liquid hydrogen

Now that the hydrogen has been bunkered and safely stored in the main fuel tanks, we will describe the processes used for conditioning the fuel for usage in the FC stacks. The general set-up of the conditioning process has been described by engineers from LMG Marine in meetings and we have been shown some of the technical solutions to be used. However, these drawings are as of now deemed non-public information by the system design companies and due to this, we will utilize reproductions with a degree of simplifications in this thesis. We choose this solution to limit the need for confidentiality. The results will not be severely affected by this decision and this statement is relevant for both the regasification and the heating part of the process.

6.4.2.1 Pressurization system

The first step is that the LH2 will flow down to one of two conditioning tanks, CT. The CT's are smaller tanks that are installed at a level lower than the bottom of the fuel tank to allow for gravity to help with the transfer between the tanks. When the small tank has been filled to its desired limit the valves are shut and the tank is isolated from the rest of the system. Now an electric heating circuit in the tank adds heat to the LH2. This will induce a pressure build-up to 6 barg, our target pressure in

the CT. This is 2 bar above the inlet conditions of the FC. We need a certain overpressure to account for the drop over the HX and the following piping system.

When the conditioning has been performed the hydrogen is ready for the evaporator and heat exchanger and the valves between the components are opened. The concept with two CT's is chosen as this support continuous operation. When one tank is in operation and fuels the FC's, the other one is being conditioned and will be ready when the first has been emptied. When the empty tank is to be refilled, first the vapor line at the top of the CT is opened, allowing the GH2 at 6 barg in the tank to be vented to the top of the large fuel tank. The CT's are small compared to the fuel tank and the pressure drops back to 1 barg. Now the line between the liquid phase of the tanks is opened allowing the filling to commence. While this is happening the gas-line is still open providing the release of the vapor and give room for the liquid. When the limit is reached the valves are shut and the process starts over again.

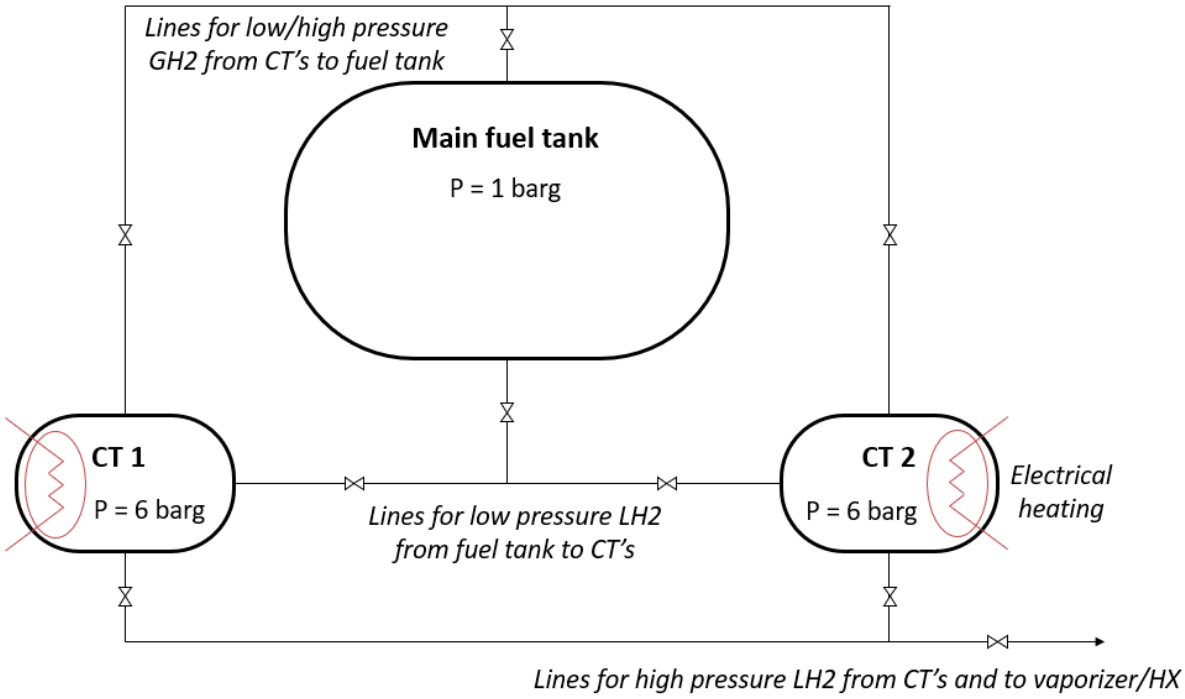

Figure 19 Concept flow sheet of hydrogen conditioning tanks

6.4.2.2 Power consumption

Now that the process part has been stated, we finalize the hydrogen compression part by calculating the specific energy needed for the process. This calculation is of importance as the heat ingress is performed by the use of electricity produced by the fuel cells.

The general thermodynamic process taking place is that incompressible liquid hydrogen experiences an increase in energy that changes the pressure from 2 to 7 bara under constant volume. We assume the temperature to increase from the saturation point of 2 bar and to that of 7 bar. From the tables in *Selected properties of hydrogen,* we find the change in energy to be 95.4 kJ/kg (McCarty, 1981c). This assumes a perfect system without inefficiencies. An accurate estimation of the true efficiency of this heater should be provided by its manufacturer but this discussion is deemed outside the scope

of this paper. To include the factor, we assume an efficiency of 95 %. This leads to an electricity demand of 187.06 kJ/kg hydrogen.

$$Energy_{Compression} = 187.06\ kJ/kg$$

One of the principles of our set-up is to have continuous fuel conditioning and flow to the FC's. When the power need is above production the battery will take the peak and when the power supply outweighs the demand the battery will store the excess. Due to this, we assume the average mass flow through the CT system to be of similar size as the reference fuel flow.

$$\dot{m}_{BoL}^{ref} = 121.50\ kgH_2/h \qquad \dot{m}_{EoL}^{ref} = 130.17\ kgH_2/h$$

Note that these mass flows take the conditioning itself into account as a constant estimated baseload was added. The losses in the fuel cell are also accounted for by using the hydrogen flow after FC inefficiencies. The power needed is:

$$Power\ CT_{BoL}^{ref} = 6.31\ kW \qquad Power\ CT_{EoL}^{ref} = 6.76\ kW$$

In this part, we assume 100 % of the heat ingress to be provided by the electric heater, i.e. an adiabatic pressure vessel. In reality, there will be a certain amount of heat leakage into the tank from its ambient surroundings. This will provide a slightly lower need for electricity but to calculate the true tank heat ingress we would need the specifics of the conditioning tank conductivity as well as its geometry. As this information is not readily available as of now, we use our calculations. This provides a conservative estimate as numbers for power demand will be slightly above the true power demand.

6.4.3 Regasification and heating of the fuel

After the high-pressure LH2 leaves the CT system it enters a heat exchanger where heat is added to first vaporize the hydrogen, before further heating to the necessary condition. In this part, we split the subchapter into first the theory behind the regasification and then for the heating before we describe the technical set up of this system component.

6.4.3.1 Vaporization

When a substance goes through a phase change, intermolecular energy is either added or removed. As gas molecules move at a higher velocity than those in a liquid state and the molecular bonds are broken, a change from liquid to gas requires the addition of heat (Bapat, 2019). Here, we will add energy to the liquid to induce boiling, effectively creating GH2.

$$H_2^{Liquid} + Energy \rightarrow H_2^{Gas}$$

Equation 42 Phase change of hydrogen

The energy required for the transition is known as latent heat of evaporation or enthalpy of vaporization and is the delta between the specific enthalpy of the gas and the specific enthalpy of the liquid. Under constant pressure, this is equal to the entropy of vaporization (Wakeham, 2011).

$$\Delta H_{L\rightarrow G} = T\Delta S_{L\rightarrow G} = T(S_G - S_L)$$

Equation 43 Latent heat of vaporization

Note that in the above formula H does not constitute hydrogen but rather an enthalpy which is denoted by the same letter in the literature. A table with values for the relevant pressure is presented below (McCarty, 1981c)

	7 bar
Entropy – liq kJ/kgK	12.55
Entropy – gas kJ/kgK	23.67
Temperature K	29.02
$T^*(S_G - S_L) = H_{L\rightarrow G}$ kJ/kg	322.70

Table 8 Latent heat of hydrogen at 7 bar

For hydrogen, this amounts to ΔH_{H2} = 322.70 kJ/kg. As hydrogens intermolecular forces are weak, this is not a relatively large amount. As a reference, the latent heat of vaporization of water is ΔH_{H2} = 40.80 kJ/mole = 2,260 kJ/kg (Datt, 2014). This is caused by the stronger hydrogen bonding observed between water molecules. From an energy-specific point of view, it can be more relevant to compare LH2 to liquid natural gas. LNG consists of a mixture of mainly methane and ethane but by exclusively assessing methane we find its heat of vaporization at 509.3 kJ/kg (NIST, 2018a). With a lower heating value of 50 MJ/kg (McAllister, 2011) this equates to 1.0 % of its LHV. For hydrogen with an LHV of 119.9 MJ/kg, the respective relationship is 0.3 %. It takes about three times as much of its energy to evaporate natural gas as it does with hydrogen.

Note that these numbers exclude the para-ortho conversion which will be discussed in a separate subchapter.

6.4.3.2 Heating

The fuel must be at a temperature between 273 and 353 kelvin before it can enter the FC and be consumed. To obtain this condition it must be heated. When the hydrogen has been evaporated into its gaseous form it will maintain a cryogenic temperature of a similar magnitude as the liquid hydrogen. This is because the initial energy flux into the LH2 is only used to break up the bonds between the molecules and change its state from liquid to gas. The gas itself has not been considerably heated afterward. This is analogous to the well-known action of boiling water. After the liquid starts boiling the temperature becomes constant while the stove continuously adds energy to it. This heat is used only to vaporize the water, not warm it beyond the boiling point of 100 °C. The same is the case with hydrogen. Due to this phenomenon, we assume the initial gas temperature to be equal to that of hydrogens boiling point at the pressure of 7 bara which is 29 K (McCarty, 1981c).

6.4.3.3 Specific heat of hydrogen

The temperature of a gas is a physical property describing the energy of its molecules. The specific heat of gas describes the energy needed to increase the temperature of the given substance. It is defined as the temperature derivative of the energy (Drake, 2020).

$$c_v = \left[\frac{\partial e}{\partial T}\right]_v$$

Equation 44 Definition of specific heat

The subscript denotes constant volume. Our case consists of a closed system for the fuel and we will use the constant volume definition of heat capacity when modeling our process. The energy of the gas is highly dependent on temperature, but as it does not scale linearly with temperature over the

whole temperature range in question, its derivative, the heat capacity will also be dependent on temperature. In this segment, we will utilize the kinetic theory of physical gas dynamics and basic quantum mechanics to establish a set of expressions to calculate the continuous necessary inflow of energy to heat our fuel, at different temperatures within our range. Except for where specifically mentioned, the theory behind the following segment is based on the book *Introduction to Physical Gas Dynamics* by Vincenti and Kruger (Vincenti & Kruger, 1965).

6.4.3.3.1 Statistical mechanics

Especially at low temperatures, the macroscopic behavior of gas is better described by statistical mechanics, than classical kinetic theory. A distinctive feature of quantum mechanics is the fact that for one molecule, a distinctive set of permissible energy states exists. Here we will use the statistical methods to model the phenomena as a continuous function. The relationship between the quantum levels of the particle and its energy is given.

$$e = RT^2 \frac{\partial}{\partial T} \ln (Q)$$

Equation 45 Energy level to the quantum number

Where Q is the partition function related to the number of energy states permissible. In other words, the function tells us how the particles are divided up between the different energy groups.

6.4.3.3.2 Total energy and its contributions

In this part, we will list the different contributions of molecular energy and discuss them separately to determine how and of what magnitude they will have a practical effect on our specific case regarding the Topeka vessel. We will assume that hydrogen gas consists of weakly interacting particles. Based on this we can separate the energy of a given molecule into translational e_{tr} and internal e_{int} energy. The translational energy ignores the molecular structure and describes the kinetic energy of the moving particle. The internal energy is the sum of several contributions, rotational energy e_{rot}, vibrational energy e_{vib}, energy from electronic excitation e_{el} and the contribution from the nuclear spin e_{nuc}. The total energy is the summation of these terms.

$$e = e_{tr} + e_{rot} + e_{vib} + e_{el} + e_{nuc}$$

Equation 46 Molecular energy contributions

Assessing these contributions independently is an approximation. There is some coupling between the elements e.g. when rotation induces a “stretch” in the molecular bonding which again will influence the vibrational element. In real gas problems, these effects are minor and can be neglected (Guenault, 1988).

6.4.3.3.3 Translational energy

The specific translational energy is:

$$e_{tr} = \frac{3}{2}RT$$

Equation 47 Specific translational energy

The specific gas constant of hydrogen is R = 4.124 kJ/kgK (Bakken, 2017). As observable, this relationship follows the temperature linearly. It then follows that the translational heat capacity is constant.

$$c_{v\,tr} = \left[\frac{\partial e_{tr}}{\partial T}\right]_v = \frac{3}{2}R$$

Equation 48 Specific translational heat

6.4.3.3.4 Electronic excitation energy

Electronic excitation plays a role in every substance consisting of atoms but it is of a small magnitude and more important for the evaluation of monoatomic gases as they lack molecular structures. For the case of hydrogen in its diatomic state, molecular vibration and rotational effects far surpass the electronic effect. As it does not have any practical implications for our case, we choose to exclude the assessment of it and assume e_{el}= 0, which again leads to $c_{v\,el}$ = 0.

6.4.3.3.5 Vibrational energy

An approximation that works well when assessing vibrational energy is to regard the molecules as harmonic oscillators with the frequency ν. Using this we define the characteristic temperature of vibration for hydrogen as:

$$\Theta_{vib} \equiv \frac{h\nu}{k}$$

Equation 49 Characteristic temperature of vibration

Here, h represents the Planck constant of 6.6261*10^{-34} m^{2}kg/s and k represent the Boltzmann constant of 1.3806*10^{-23} m^{2}kg/s^{2}K. We use this to describe the energy.

$$e_{vib} = \frac{R\Theta_{vib}}{e^{\Theta_{vib}/T} - 1}$$

Equation 50 Specific vibrational energy

Again, with a basis in (44) we find the specific energy contribution from vibration.

$$c_{v\,vib} = \left[\frac{\partial e_{vib}}{\partial T}\right]_v = R\left(\frac{\Theta_{vib}}{T}\right)^2 \frac{e^{\Theta_{vib}/T}}{(e^{\Theta_{vib}/T} - 1)^2}$$

Equation 51 Specific heat of vibrations

The characteristic temperature of hydrogen is Θ_{vib} = 6,320 K (Baierlein, 1999). Below we represent a plot of the specific heat to temperature for a large range.

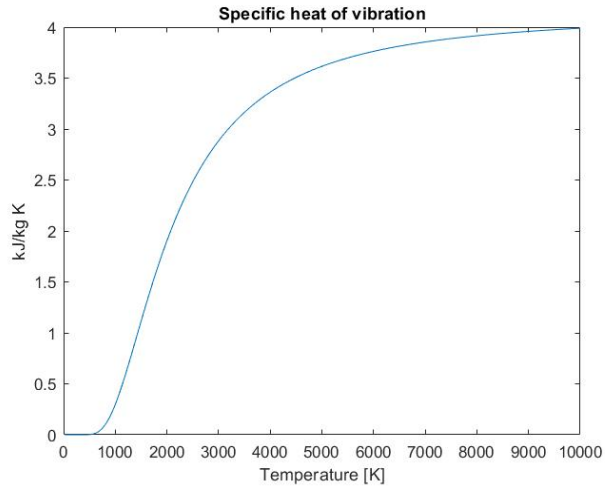

Figure 20 Plot of specific heat of vibrations

From this, it is apparent that for cryogenic and normal temperatures whereΘ_{vib}/T >> 1, the contribution from vibration goes toward zero. As our main focus is temperatures below 3-400 K, we choose to ignore this contribution in our further calculations. For temperatures in the higher regimes, we note that the specific heat capacity will go towards R, i.e. the same order of magnitude as the translational contribution.

6.4.3.3.6 Rotational energy

When assessing rotational energy of the diatomic hydrogen molecules we assume them to maintain the physical properties of a rigid dumbbell depicted by a constant moment of inertia, *I*. We will not go into the detailed steps of solving the Schrodinger equation for this contribution but the partition function resulting from it is given as a function of the relationship between the temperature and the characteristic temperature of rotation.

$$\Theta_{rot} \equiv \frac{h^2}{8\pi^2 Ik}$$

Equation 52 Characteristic temperature of rotation

$$Q_{rot} = \sum_{l=0}^{\infty}(2l+1)e^{-l(l+1)\Theta_{rot}/T}$$

Equation 53 Rotational partition function

The numerical value of this characteristic temperature must be found using spectroscopic analysis. For hydrogen it is Θ_{rot} = 87.5 K (Baierlein, 1999). As equation (53) cannot be summed explicitly for an arbitrary temperature, we will present approximations in two different temperature regimes.

For T >> Θ_{rot}

$$e_{rot} = RT$$

Equation 54 Rotational energy for T above the characteristic temperature

$$c_{v\,rot} = \left[\frac{\partial e_{rot}}{\partial T}\right]_v = R$$

Equation 55 Specific rotational energy

For T ≤ Θ_{rot} (Pauly, 2000)

$$e_{rot} = 6R\Theta_{rot}e^{-2\Theta_{rot}/T}$$

Equation 56 Rotational energy for T below the characteristic temperature

$$c_{v\,rot} = \left[\frac{\partial e_{rot}}{\partial T}\right]_v = 12R\left(\frac{\Theta_{rot}}{T}\right)^2 e^{-2\Theta_{rot}/T}$$

Equation 57 Specific rotational energy

(Guenault, 1988) states that at 200 kelvin the molecule is fully excited rotationally and energy then rises linearly as depicted in (54). Between this and the characteristic temperature, the formulas are inconclusive. To solve this issue, we assume that the specific heat of rotation goes from (57) to (55) as a weighted sum of the two contributions ranging from 100 % (57) to 100 % (55). The weight of the high-temperature specific heat is x = T/112.5 – 7/9. The low-temperature $c_{v\,rot}$ will have the weight 1 – x. The resulting plot of the specific heat due to rotation is presented below.

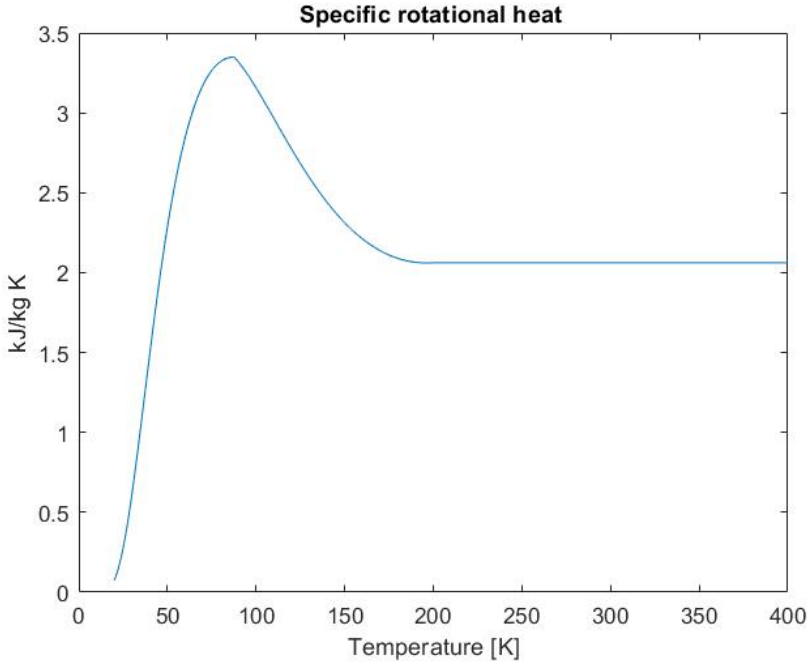

Figure 21 Plot of specific rotational energy

6.4.3.3.7 Nuclear spin energy

The contribution in energy from the nucleus, specifically its nuclear spin is for most chemical processes irrelevant. The exception for this is the case of hydrogen, particularly at low temperatures. Due to this, we will include a thorough discussion of it. We will no longer mainly use the book *Introduction to Physical Gas Dynamics* as our main source and the standard system of citations is therefore reinstated.

6.4.3.3.8 Para to ortho conversion

Hydrogen atoms go together in pairs and form diatomic molecules – these H_2 molecules are what is commonly referred to as hydrogen. Each of the nuclei, the core of the atom, will have a spin rotation (Leachman, 2009). It is this rotation that determines the state of the given molecule. If the spin of the two atoms is in the opposite direction it is defined as in the para-state. For a spin in the same direction, the definition of an ortho state is given.

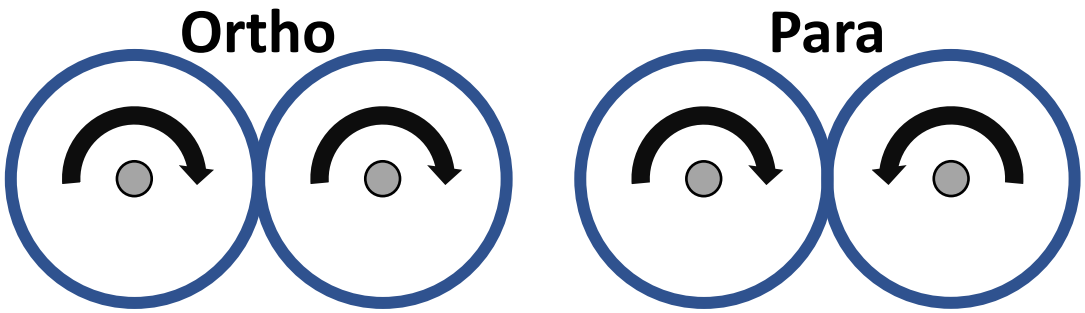

Figure 22 Illustration of hydrogen allotropic spin directions

These allotropes have different quantum energy levels and its equilibrium is the distribution between them, P/O.

The para-state has one single spin state, a singlet, while the ortho has three different spin states, a triplet. An energy level is defined as all of the states with an identical amount of energy and ortho hydrogen is therefore degenerate as it contains three states within one energy level (Vincenti & Kruger, 1965). The allocation between these are governed by the Boltzmann distribution defined as (Vincenti & Kruger, 1965):

$$\frac{N_j}{N} = \frac{C_j e^{-\varepsilon_j/kT}}{\sum_j C_j e^{-\varepsilon_j/kT}}$$

Equation 58 Boltzmann distribution of energy states

N denotes the total number of molecules while N_j denotes the number of one particular energy level. C_j and ε_j are constants dependent on the atoms and the energy states and k here is the Boltzmann constant. The only variable is the T for temperature and the P/O ratio is therefore dependent only on temperature. For our temperature range between 20 and 300 Kelvin we can use the relationship given in (Meagher, 2008) with the adjustment of using the reduced temperature instead of the direct temperature:

$$\chi_{Para\ H2}^{Equilibrium} = 0.1 * \left(e^{\frac{-5.313}{\tau}} + 0.1\right)^{-1} - 2.52 * 10^{-4} * \tau^3 + 3.71 * 10^{-3} * \tau^2 - 2.04 * 10^{-3} * \tau - 0.00227$$

Equation 59 Equilibrium composition P/O to temperature

$$\tau = \frac{T}{T_c}$$

Equation 60 Reduced temperature

Where T_c is the critical temperature of 32.938 K (Leachman, 2009). Note that this equation does not hold for high temperatures (Wilhelmsen, 2017).

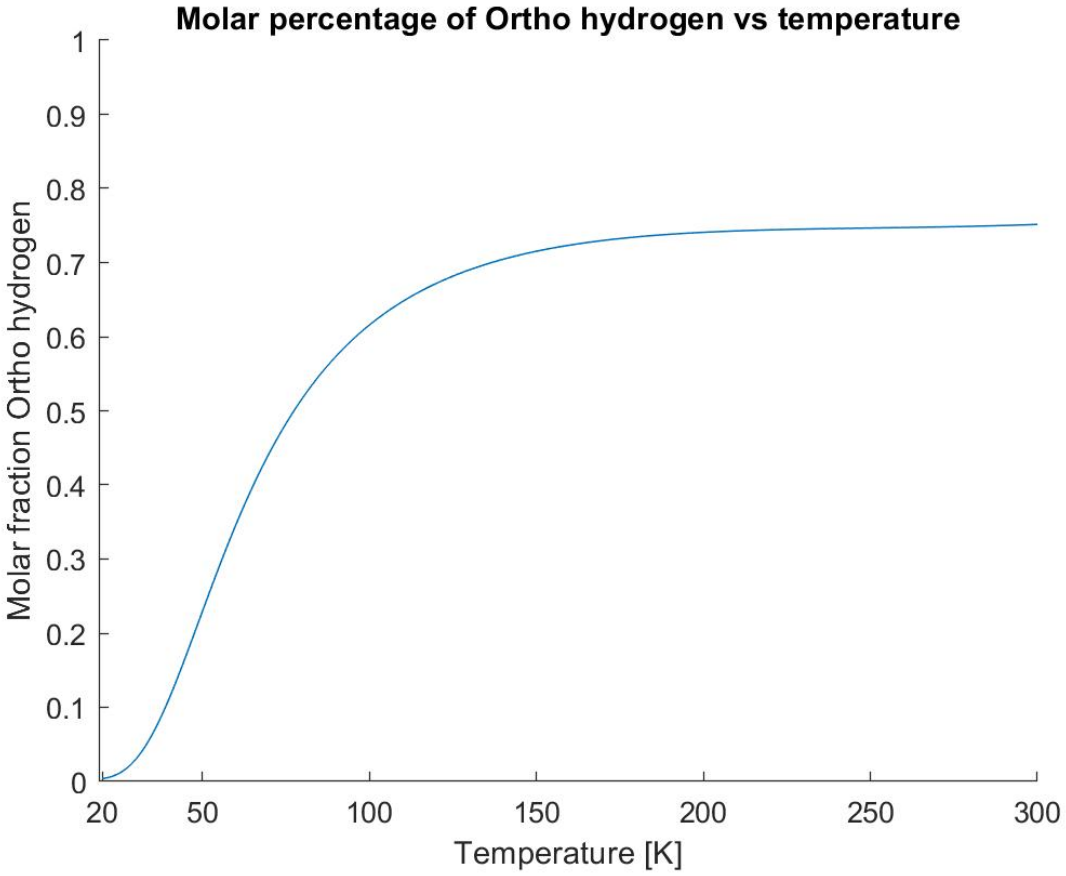

Figure 23 Plot of P/O ratio to temperature

When the temperature changes, the conversion will happen spontaneously but slow without a catalyst (Cardella, 2018).

$$Para\ Hydrogen \rightleftharpoons Ortho\ Hydrogen$$

Equation 61 Para Ortho reaction

The energy in the conversion of parahydrogen to orthohydrogen is $e_{P\rightarrow O}^{conversion}$ = 1.417 kJ/mol equating to 702.83 kJ/kg (Choi, 2004). As parahydrogen is more stable 99.75 % of the hydrogen at 19 K will be of this form. The equilibrium composition at 80 K is 50/50, while at normal room temperature 75 % of the molecules are in the ortho state. This 3:1 ratio at room temperature is commonly referred to as normal hydrogen (Leachman, 2009). For the conversion of liquid hydrogen to normal hydrogen, 74.94 % of the initial para molecules must increase its energy to obtain the P/O fraction. This implies that a total of 526.68 kJ must be added per kg of LH2 to acquire stable GH2 at room temperature.

The specific heat of conversion to equilibrium at a given temperature can be established.

$$c_{v\,nuc} = \left[\frac{\partial e_{nuc}}{\partial T}\right]_v = \left[\frac{\partial e_{P\to O}^{conversion}(1-\chi_{Para\,H2}^{Equilibrium})}{\partial T}\right]_v$$

Equation 62 Specific energy of nuclear spin

As we start by approximately 100 % para hydrogen and it is the change to ortho that consumes heat, we use the factor of $(1-\chi_{\text{Para H2}}^{\text{Equilibrium}})$ in the formula as the derivative of this will represent the change in ortho concentration.

$$c_{v\,nuc} = \frac{e_{P\to O}^{conversion}}{T_{crit}}\left(\frac{0.5313e^{-5.313/\tau}}{\tau^2\left(e^{-\frac{5.313}{\tau}}+0.1\right)^2} + 7.56*10^{-4}*\tau^2 - 7.42*10^{-3}*\tau + 2.04*10^{-3}\right)$$

Equation 63 Specific energy of nuclear spin to temperature

The division by T_{crit} is the result of using the chain rule on the formula (59). To test the credibility of this formula we used a numerical scheme to integrate it from 20 to 300 Kelvin. Comparing to the tabulated values presented by (Choi, 2004) and (Leachman, 2009), the disagreement amounts to 0.21 %.

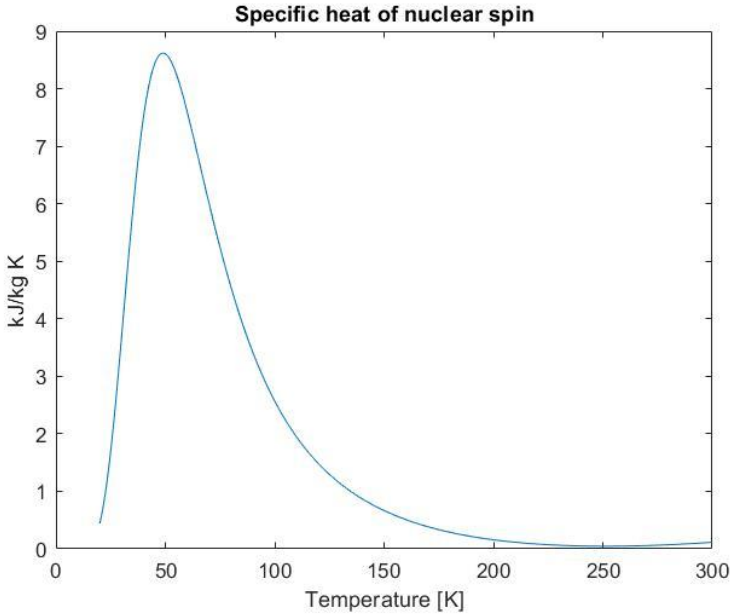

Figure 24 Plot of specific heat of nuclear spin

We have now determined that the magnitude of energy between different P/O stages is of a size that must be accounted for in our calculations if equilibrium will be obtained. As we will mainly store the hydrogen as LH2 and only briefly before consumption vaporize it, the speed of the reaction (59) is therefore of importance. The conversion between para and ortho hydrogen is very slow when not performed near a catalyst. This is because the change in spin requires a collision process changing the total spin. This again requires the presence of a 3-body force where the third body has the catalytic effect (Guenault, 1988). The conclusion of a very slow non-catalytic reaction is supported in papers regarding para hydrogen induced polarization (Wagner, 2014) and boil-off reduction in space stage fuel systems (Bliesner, 2013).

Based on this discussion, we will neglect the effect of P/O conversion. This can be additionally justified by the assumption that in the case of a hold up in the continuous flow of fuel and the onset of this reaction. The speed of reaction will most likely still be slower than the heat ingress from the surrounding environment of the system and counteract any notable and adverse effects.

6.4.3.3.9 Total specific heat

From the previous pages we see that for the practical case of the Topeka vessel, we have a specific heat consisting of the sum of the translational heat and the rotational heat. The electronic excitation is of less importance as we are dealing with diatomic molecules. The vibrational contribution is of neglectable importance for our range and we dismiss it. The magnitude of specific heat of nuclear spin for our temperature range is of great importance, however, the speed of reaction is minuscule given our environment and we choose to dismiss it. The resulting and relevant specific heat capacity is presented below.

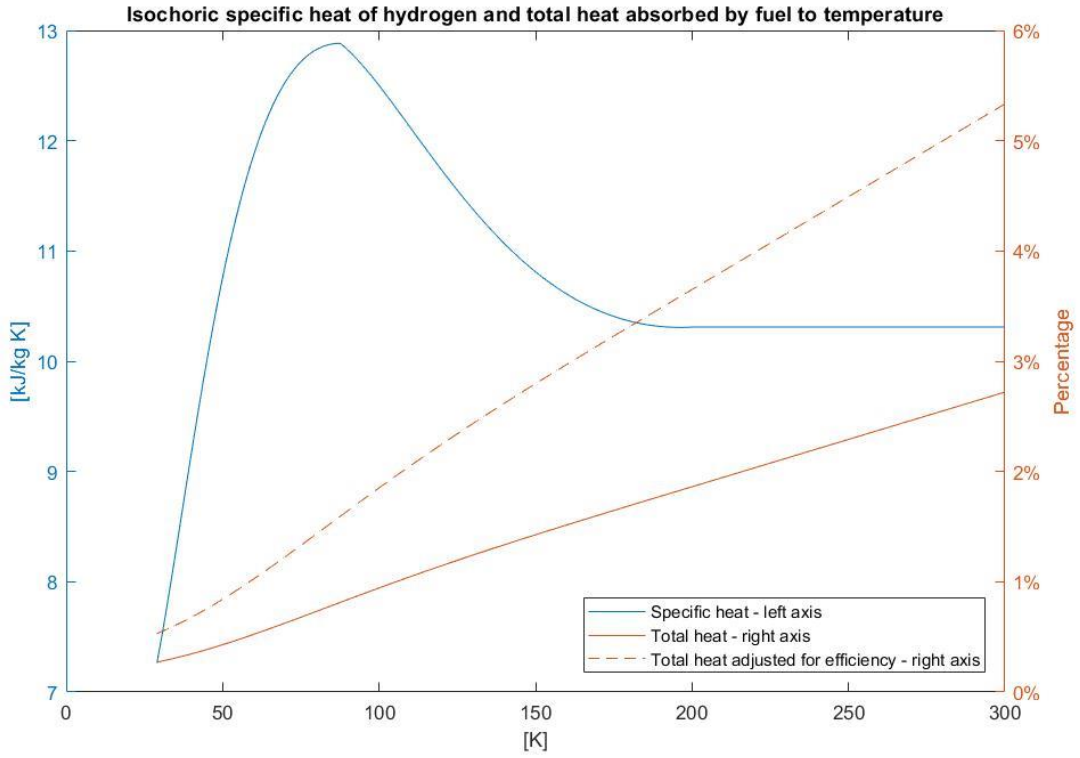

Figure 25 Specific heat of hydrogen and total heat absorbed to temperature

The latent heat of vaporization is included. The plot also includes the aggregated energy absorbed by the fuel as a percentage of the LHV with and without FC efficiency adjustments. In other words, the right-hand axis represents the amount of heat needed to go from liquid to gas with a certain temperature as a percentage of the energy in hydrogen. The adjusted and regular LHV percentage is included to show how much less efficient it is to use the produced electricity to heat the hydrogen.

6.4.3.4 Heat exchangers

With the foundation of the theory of heat in hydrogen established, we will discuss how the LH2 will be vaporized and heated. Referring back to the statement made in the preliminary part of pressurization, we again mention that due to non-public information the technical drawings and some specific solutions will not be included here. This will not negatively affect the calculations notably.

6.4.3.4.1 Fundamentals

A heat exchanger is a device, module or system where two or more fluids at different temperatures exchange energy through a solid. Many different designs exist and the main classifications are made based on its flow arrangement and construction type (Incropera, 2017a). These can include parallel-flow, counterflow, crossflow or finned/un-finned surfaces. Our issue at hand is to introduce energy into the liquid hydrogen and first, induce a phase change through boiling, and then, heat the gas to the correct temperature.

The technology that often is chosen for this process on land-based car fueling stations is ambient air vaporizer towers (Rong, 2017). As the name alludes, these use air as the heating fluid. Below is a schematic illustration of this concept for a hydrogen filling station.

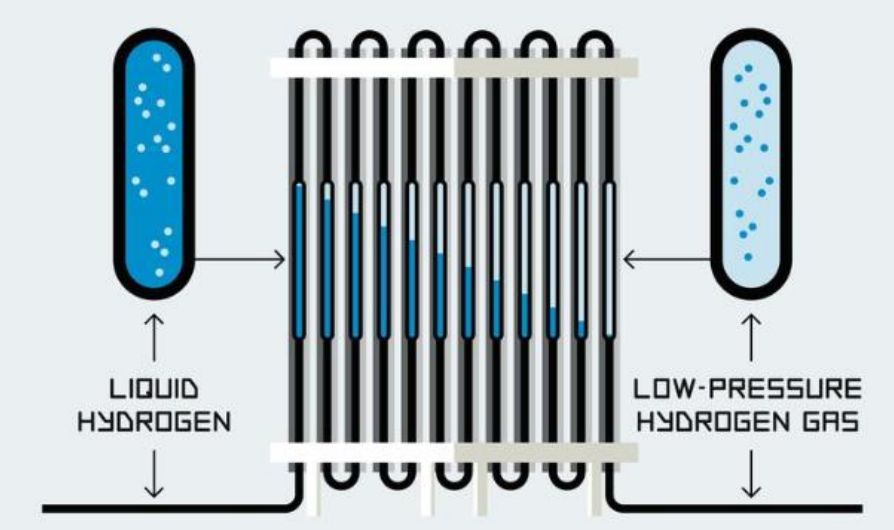

Figure 26 Illustration of air-based hydrogen vaporizer tower (Rong, 2017)

The hydrogen moves through the system powered by the resulting pressure gradient experienced when the density increases in a closed system. The heat exchange is due to free convection between the ambient air and the cold surface of the heating tubes. This works on regular filling stations but there are some issues regarding such an installation onboard a ship.

The air will naturally experience a dynamic where the hydrogen cools it down. This induces a density gradient in the air. As the gas is affected by gravity, this will produce a buoyancy force on the warmer air compared to the cold, and the gas close to the surface will flow downwards (Incropera, 2017b). A system like this will demand a large surface area and an unconfined space to allow for the airflow and to produce a load that can supply the ship. This is not optimal for a vessel on the ocean.

A different issue arises from the composition of air and its properties. Ambient air is mostly nitrogen and oxygen, which in itself can pose an issue regarding LH2's low-temperature regime. However, the

most common challenge with such a set-up is the moisture naturally present in the air. During normal operation, an ambient vaporizer will build up ice on its surface. This is negative from a performance point of view as the frost build-up will increase the thermal resistance and effectively decrease the heat transfer rate. Continuous flow demand shifting between vaporizer towers, requiring idle systems on stand-by (Cryoquip, 2014). This is not ideal on a ship both due to size, dependability and the naturally moist environment on the ocean.

Figure 27 Frost on air-based vaporizer tower (Cryoquip)

One of the most common HX's for general industrial applications is the shell and tube type. Over time this design has proven to be both robust and flexible, also, it can be supplied by many different producers (Fredheim & Solbraa, 2018). The general concept is having a bundle of tubes inside a larger shell. One fluid flows through the internal tubes while the other moves around them inside the shell. Below is an illustration of a standard shell and tube HX.

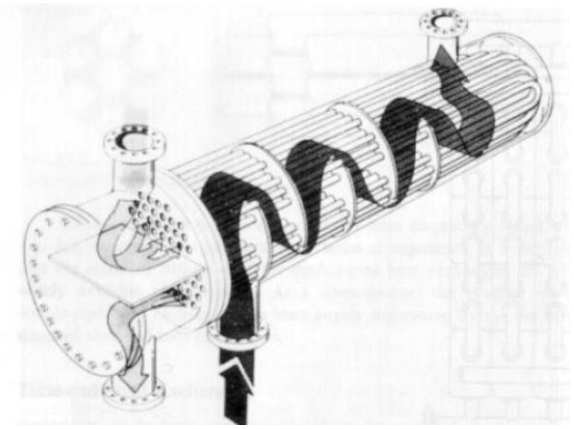

Figure 28 Shell and tube heat exchanger (Fredheim & Solbraa, 2018)

In our case, we have a gas that is under pressure as the fluid to be heated. We assume the heating fluid to be of lower pressure. Our initial assumption is that the hydrogen will flow through the internal tubes. This hypothesis has been supported by discussions with LMG Marine and their system provided, the technical detail around the HX has not been shared.

The heat exchanger and its energy dynamics can be simplified as an energy balance.

$$q_{Hydrogen} = q_{Working\ fluid}$$

Equation 64 Energy balance over the heat exchanger

Where the q represents the energy flow. To describe this flux, we use the simplified steady-flow thermal energy equation (Incropera, 2017c).

$$q = \dot{m}c(T_{in} - T_{out})$$

Equation 65 Heat flux through a heat exchanger

This states that the change in temperature through the system multiplied by its specific heat capacity and mass flux equates to the energy flow. This relationship will be correct regardless of the choice of HX type and arrangement. We have determined the mass flow, temperature range and specific heat of the hydrogen side of the equation. To identify these parameters on the other side we must first define our working fluid.

6.4.3.4.2 Working fluid

There are many factors to regard when deciding a working fluid in a heat exchanging process. Especially where the temperature range is as wide as ours ranging from the boiling point of hydrogen and up to 283 kelvin. The exchange can be through convection from a single-phase fluid or as boiling/condensation.

The use of phase change in heating/cooling processes are well known and is the core principle behind heating pumps where different pressure regimes result in different saturation temperatures (Moran, 2014). When the temperature range is particularly large, the use of several fluids with different boiling points can be used and these are referred to as mixed fluids. This is a complex process but it is widely used in the liquefaction plants producing LNG (Pettersen, 2016). Utilizing the nature of latent heat is of more importance when we try to impose a temperature change in the

opposite direction of the ambient temperature, i.e. cooling below ambient or heating above ambient temperature. In our case, we have a cold fluid where the goal is to obtain near ambient temperature. This supports the assumption of a single-phase liquid working fluid.

When designing a heat exchanger process the properties of the working fluids must be tuned to the pressure and temperature area of operation. As the temperature range in question goes from below -255 °C and up towards the operational temperature of the fuel cell of 10 °C, the heating media may be exposed to any temperature in this range. Free fluid flow is critical, i.e. it cannot freeze out in any part of the system and create blockages. We will evaluate elements that maintain a gaseous or liquid state in the cryogenic range. The physical properties of melting and boiling point are therefore of interest.

The points of phase change of substances are governed by its intermolecular forces mainly Van der Waals interactions (Clark, 2012). The weaker the forces, the lower the freezing and boiling points. Van der Waals forces are divided into two types, strong forces between two dipoles and weaker London Dispersion Forces. In the lower and more critical end of the temperature specter, we need molecules where we have the weaker forces to maintain a low freezing point. This means that the molecules must be non-polar and mainly the London forces are in play. These forces are explained by quantum mechanics as it involves the electron distribution around the atom (Rashe, 2019). As this distribution changes from moment to moment the polarization of the molecule also changes. Over time the positive and negative sides are aligned and it is non-polar, but at a given moment it will have a slight asymmetry. This time-dependent di-pol result in an attractive force (Encyclopedia Britannica, 2016). Below we present the substances with the lowest boiling and melting points.

Substance	Melting Point (°C)	Boiling Point (°C)
Helium	-272.20	-268.93
Hydrogen	-259.16	-252.88
Neon	-248.59	-246.05
Fluorine	-219.67	-188.11
Nitrogen	-210.00	-195.80
Oxygen	-218.79	-182.96
Argon	-189.34	-185.85
Methane	-182.50	-162.00
Carbon Dioxide	-78.46 (Sublimates)	

Table 9 Properties of selected substances (Royal Society of Chemistry, 2020) (Encyclopedia Britannica, 2018) (United States Geological Survey)

From this table, we see that if the heating fluid were to be in direct contact with an environment at the temperature of liquid hydrogen, only hydrogen and Helium would maintain a non-solid form.

In a perfect heat exchanger with a counterflow configuration, the cold temperature of the heating fluid going out will go towards the temperature of the hydrogen going in as the length goes towards infinity. As this is unlikely under normal operating conditions, we dismiss the idea of working fluid acquiring temperatures in the very coldest region. LMG has provided the chosen working fluid for the set-up, an industrial chemical under the brand name of Freezium.

Freezium is a heat transfer fluid produced by Eastman Chemical Company (Arteco, 2020). The working fluid consist of a base of potassium formate, HCOOK.

It is a stable chemical with low corrosive abilities for most materials. This excludes some metals, namely aluminum, zinc and galvanized steel can corrode in contact with the fluid and the producer advises against the usage of these metals (Arteco-coolants, 2018). The compound is non-toxic and is biodegradable (Arteco-coolants, 2018). The combination of low freezing point, low toxicity and biodegradability of potassium formate solutions is well established and it is also used as a de-icing agent used on airport runways (Potassium Formate for Runway Deicing, 2020).

The respective melting point is determined by the concentration of the solution. As we see from the plot below gathered from the chemical company BASF, there exists a sharp minimum in the melting point at -60 °C (Potassium Formate for Runway Deicing, 2020). Eastman's mixture with this property has been named Freezium -60C and is the one chosen for our system. This chemical has a boiling point of 114 °C and an effective range of up to 85 °C (Fragol, 2016).

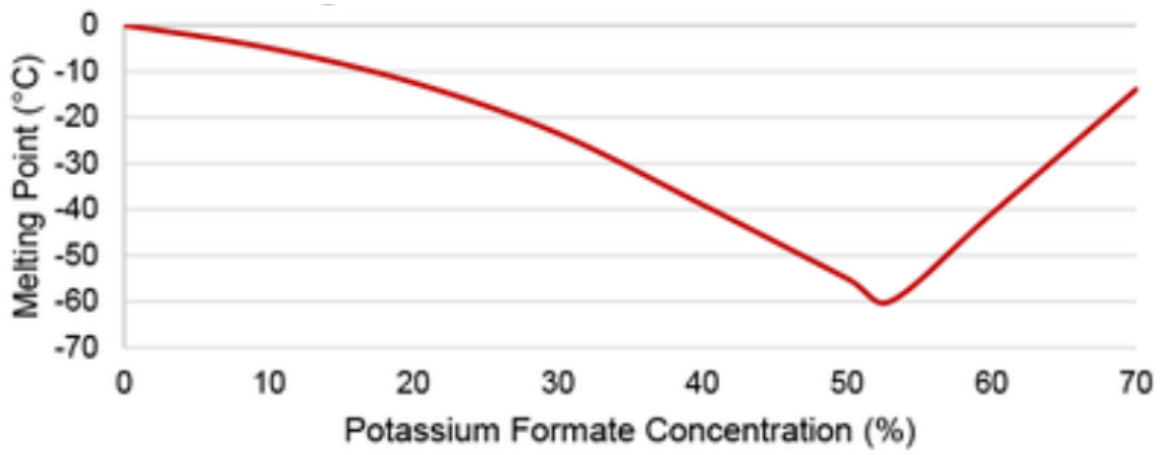

Figure 29 Freezium potassium concentration and melting point (Fragol, 2016)

The specific heat of our working fluid has been provided by a distributor (Fragol, 2016).

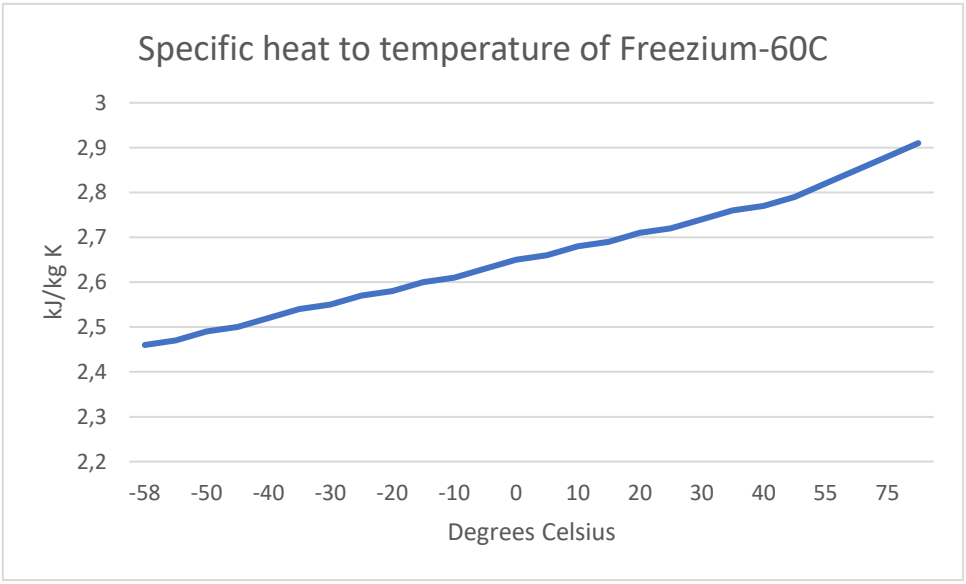

Figure 30 Plot of specific heat of Freezium to temperature

From this, we see that there is a temperature dependence of the specific heat. This makes it important to determine which temperature range we will operate in.

A different factor to consider regarding temperature is the viscosity of the fluid. For a continuous pumping process like ours, this will have a large effect on the necessary pumping power in the heating circuit. A good measure for this is the dimensionless quantity known as the Prandtl Number, Pr. The reason we choose to evaluate this is that it describes the relationship between the momentum transport capacity in the medium to the thermal transport capacity (Rapp, 2016).

$$Pr = \frac{{}^{\mu}/_{\rho}}{{}^{k}/_{\rho c_p}} = \frac{\nu}{\alpha} = \frac{momentum\ diffusivity}{thermal\ diffusivity}$$

Equation 66 Prandtl number

The alpha describes an often-used thermodynamic fluid property, the thermal diffusivity. This is defined as a material's ability to conduct thermal energy compared to its ability to store it (Incropera, 2017d). The lower the Prandtl number is, the better the fluid is as a heat-conducting liquid. In other words, we want Pr to be as low as possible. For Freezium the plot of Pr to temperature is presented below (Fragol, 2016).

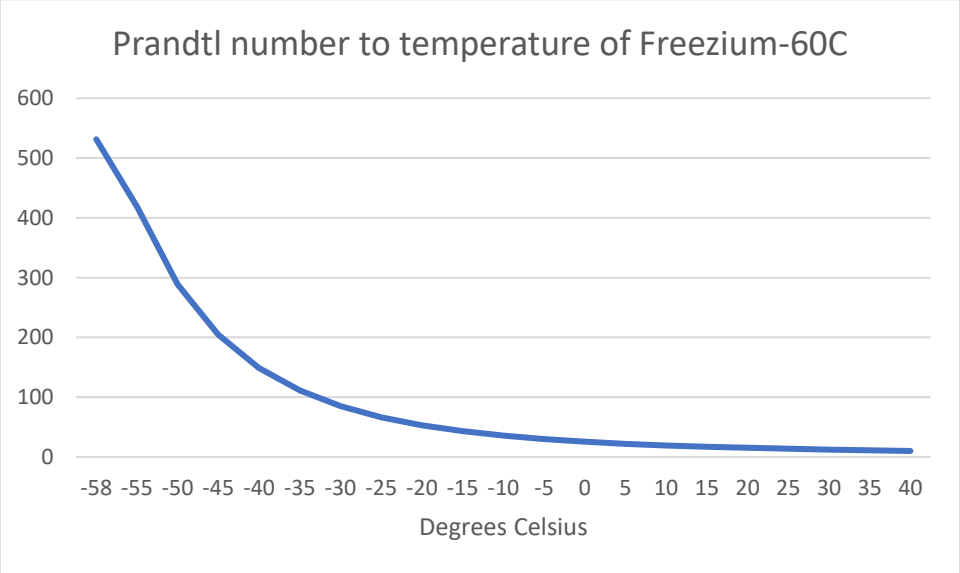

Figure 31 Prandtl number of Freezium to temperature

It becomes apparent that even though the fluid maintains a liquid state at temperatures towards -60 °C, it might not constitute a good heat transfer fluid in the lower end of the range.

6.4.3.4.3 Set up

In this part, we will describe the full set-up of our heating/cooling process. There are three different heat exchanging processes taking place onboard the ship simultaneously. One is to cool down the fuel cell stack, another is to use the heat generated from the FC to heat the hydrogen fuel and last we assume the fuel preparation to require less heat than the additional supplied from the FC, hence, we need to dispose of the excess heat production.

We want the efficiency of the complete fuel cell set-up to be as high as possible. The vessel will have a certain need for onboard heating and this should be provided by the FC. This is a factor that can be more important for vessels with a larger volume of accommodation space like ferries or cruise ships. Quantifying this is beyond the scope of this paper but we assume the magnitude to be lower than the other factors. This simplification is therefore assumed to be of a minor effect. Using as much of the waste heat as possible is good for efficiency and this is a factor that should be reviewed during the ship design process by the naval architects.

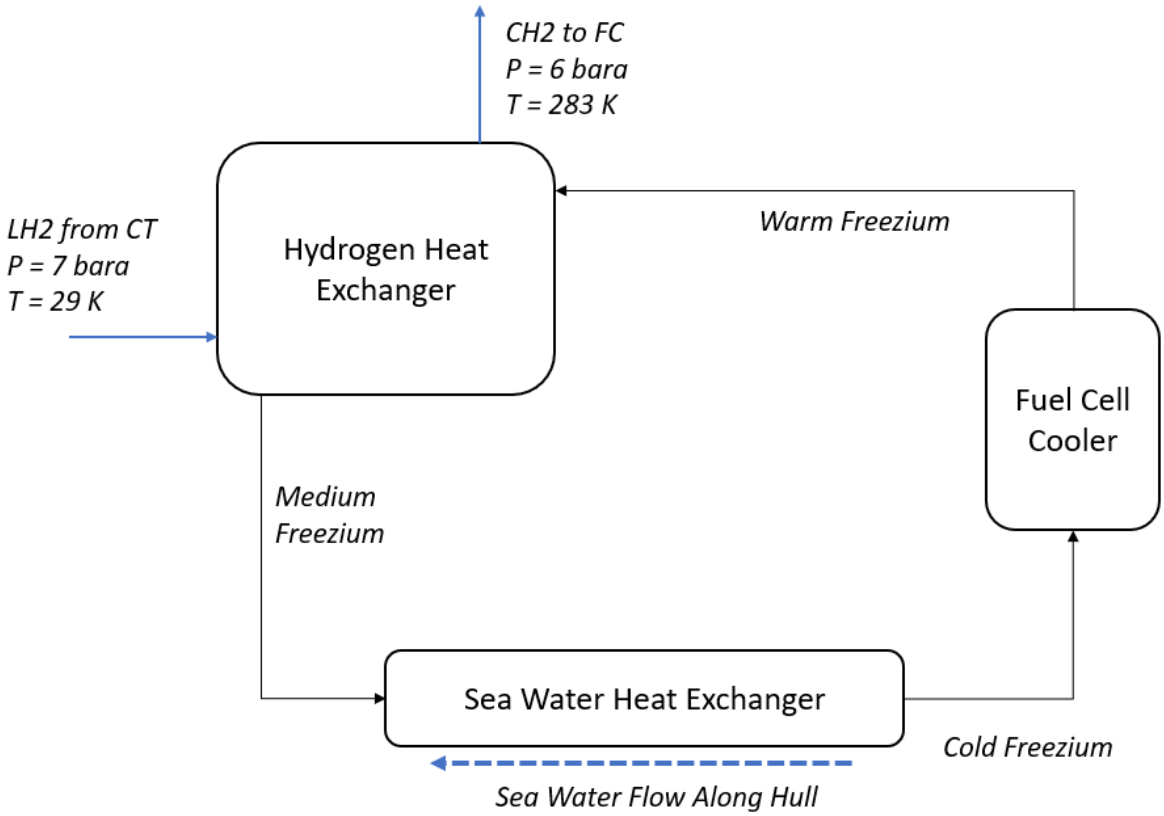

Figure 32 Simplified flow sheet of heat exchanger processes

Note that there is a pressure loss over the HX. This is to be expected and the drop of 1 bar has been assumed by LMG.

Now that the fluids have been chosen and the system has been defined, we use thermodynamics to calculate the loads on the different components of our system.

6.4.3.4.4 Thermodynamics

As stated, we have 3 different processes at hand. First, we will start by calculating the heat production from the fuel cell, then we will determine the heat needed for the hydrogen process and finally, we can find the excess heat that needs to be discharged to our could reservoir, namely the ocean.

FC heat production

In our calculations for heat production from the fuel cells, we will use an idealization based on its efficiency. The concept builds on the natural concept of conservation of energy. The chemical energy that can theoretically be released from the flow of hydrogen cannot disappear from the system. It will take the form of mainly electricity or heat. Vibrations (momentum), noise and light are other forms of energy that a process can produce but as discussed in the fuel cell section, this is not of significance here.

$$q_{FC} = LHV_{Hydrogen}\dot{m}(1 - \eta_{FC})$$

Equation 67 Heat produced by the fuel cell

This expression states that the heat produced from the FC will be the lower heating value of the fuel, multiplied by its mass flow multiplied by the ratio of non-electric energy production. The LHV is as stated previously 119.9 MJ/kg. In the FC chapter, we determined a reference efficiency as the mean between the extremes, for our reference power production. As we here will use the two mass flows, we also choose to use the two different efficiencies for BoL and EoL 52.8 and 49.1 %, respectively. The mass flows are as defined:

$$\dot{m}_{BoL}^{ref} = 121.50\ kgH_2/h \qquad \dot{m}_{EoL}^{ref} = 130.17\ kgH_2/h$$

$$q_{FC}^{BoL} = 1{,}909.7\ kW \qquad q_{FC}^{EoL} = 2{,}206.3\ kW$$

This will be the heat production from the stacks. We idealize the stacks as having three streams out. One electric stream, one with heat into the cooler and one as the heat stored in the water produced from the reaction. By examining the PEM cell reaction, it is apparent that the production of water follows the usage of hydrogen. According to LMG Marine, this liquid is to be directly discharged to the sea without any usage, intermediate storage or heat exchange. We must account for the heat released in this manner. We use (65). The mass of hydrogen molecules is 2 g/mole, for oxygen gas it is 32 g/mole and the resulting water is 18 g/mole. Based on the reaction equation of the PEM cell we calculate the mass flow of water to be of a magnitude of 9 times the mass flow of hydrogen, i.e. for every ton of fuel the ship consumes, it produces 9 tons of water. The mass flows are

$$\dot{m}_{BoL}^{ref} = 1{,}093.5\ kgH_2O/h \qquad \dot{m}_{EoL}^{ref} = 1{,}171.5\ kgH_2O/h$$

The specific heat of water is 4.186 kJ/kgK (Nave, 2000a). The temperature delta can be estimated based on a few assumptions. We will use the inlet temperature of hydrogen at 10 °C as our base temperature. Scientists from Sintef suggest the typical LT-PMFC internal temperature to be in the range of 60-80 °C. We choose to use the mean between them at 70 °C. This seems reasonable with our conclusion that the internal temperature must stay below the boiling point of water. The resulting temperature delta is then 60 °C.

$$q_{Water}^{BoL} = 76.3\ kW \qquad q_{Water}^{EoL} = 81.7\ kW$$

We observe that these represent 2 % of the respective heat production. By adjusting for them we end up with the final heat fluxes from the fuel cells.

$$q_{FC\,adj}^{BoL} = 1{,}833.4\ kW \qquad q_{FC\,adj}^{EoL} = 2{,}124.6\ kW$$

Hydrogen heating

When describing the system numerically, we will use the energy balance from (64) and (65).

$$\dot{m}(h_{evap} + c(T_{in} - T_{out})) = q_{Working\ fluid}$$

Equation 68 Heat flux in the hydrogen heat exchanger

Note that we have added the energy contribution from the latent heat as this also is provided by the HX. In our previous chapters, we have determined all the necessary variables on the left-hand side of this equation. The temperature is that of liquid hydrogen at 7 bar, 29 Kelvin. The temperature out is 283 Kelvin. The latent heat of evaporation is 322.69 kJ/kg and the mass flows are given as the extremes on the BoL – EoL range presented above.

The specific heat of hydrogen is dependent on temperature. As we have an expression for the whole range in question, we can use this to find an average value.

$$\bar{c} = \frac{1}{\Delta T}\int_{T_{in}}^{T_{out}} c(T)\, dT = 12.044\ kJ/kgK$$

Equation 69 Average specific heat

This is done numerically in Matlab.

$$h_{evap} + c(T_{in} - T_{out}) = \frac{322.70kJ}{kg} + \frac{12.04kJ}{kgK} * (283\ K - 29K) = 3{,}381.9\frac{kJ}{kg}$$

Equation 70 Specific energy over the hydrogen heat exchanger

Multiplying with the mass flows and changing from hours to seconds we obtain the loads.

$$q_{fuel}^{BoL} = 114.1\ kW \qquad q_{fuel}^{EoL} = 122.3\ kW$$

This is close to 3 % of the heat to be discharged from the FC's. We can conclude that the initial guess that there would be more heat in our system than necessary for fuel heating was correct. This leaves us with heat to remove from the system.

Sea Water Cooling

The load on the seawater heat exchanging cycle is the difference between the available heat from the fuel cells and the necessary heat from the fuel regasification and heating process. This results in:

$$q_{Sea}^{BoL} = 1{,}719.3\ kW \qquad q_{Sea}^{EoL} = 2{,}002.3\ kW$$

Many industrial plants close to a large body of water use this as a heat sink in thermodynamic processes. It has the attributes of being efficient and compact, compared to air cooling (Solbraa, 2019). Most water sources, and especially salt water provides some operational challenges, mainly due to fouling over time. This is the reason many LNG plants using seawater utilizes an indirect system with a closed-loop fresh-water cooling system (Solbraa, 2019). For us, this is not a concern as we can apply this technique by having the hull work as our solid separator between the closed-loop Freezium cycle and the ambient ocean or heat sink.

The specific heat of seawater is lower than for freshwater due to its salinity (UCSB Science Line, 2013). This is not of great importance for us as this situation is a special operating condition for heat

exchange where the mass flow multiplied by the heat capacity of one side is much larger than the other. This can be assumed as the mass flow of seawater along the hull is much larger than the flow of Freezium. The result is that the cold side of this heat exchanger will be at a near-constant temperature (Incropera, 2017e).

The water temperature of the surface layer of the Norwegian western coast is provided by the Norwegian Environment Agency. They collect temperature data regularly in several areas. The measurement we will use here is the annual average sea temperature on the voyage between Torungen and Stadt. Torungen is located about 60 km northeast from Kristiansand and Stadt is located in the northern part of Sogn og Fjordane. The stretch between them is a good fit four our case. The average water temperature for the years 2000 until 2016 is 10.0 °C (Albertsen, 2019). We will use this as our ambient water temperature.

Temperature

As we observed from the Pr curve of our fluid of choice, the temperature can be of great significance to our system. In this part, we will establish a reasonable temperature range for our cooling fluid to determine if adverse situations can be expected to occur.

When it comes to the temperature we have already defined if for the fuel cell interior, the hydrogen in and out of the HX and the ambient seawater temperature. The Freezium is supposed to remove heat from the fuel cells. As stated, we assume them to be of a temperature of 70 °C. From this, we can conclude that the Freezium out must be of temperature below 70 °C. This statement is based on Fourier's law stating the need for a temperature gradient for heat transfer to occur and also defines the heat to go from the hot medium and over to the cold medium (Incropera, 2017f). This is inherently intuitive.

$$T_{FC\ out}^{Coolant} < 70\ °C$$

When the Freezium leaves the HX, it has heated hydrogen from -244 °C. As the freezing point of the chosen solution is -59 °C, we know that we will not approach the coldest temperature regime, but this is still not enough to establish the lower value. From our calculations, we know that we must be able to remove energy from our coolant and out in the ocean. The temperature of the cold reservoir holds a relatively steady 10 °C, coincidently similar to the hot temperature of the GH2. Hence, the temperature both in and out of the seawater HX must be above this temperature. In addition to this, we know that the temperature out of the two heat exchangers is below the temperature going in. The opposite is true for the fuel cell cooling system. Combining these statements result in:

$$10\ °C < T_{Sea\ HX\ out}^{Coolant} < T_{H2\ HX\ out}^{Coolant} < T_{FC\ out}^{Coolant} < 70\ °C$$

Quantifying this range is of importance as this will determine the most important factors when designing the cooling/heating set-up, namely the mass flow of the working fluid and the respective viscosity. These two considerations will define the power consumption of the heat exchanger processes. From figure 31, we observe that the Prandtl number for our Freezium grade is in the favorable end of its range when we consider the presented temperature limits.

We have determined the heat fluxes over the units and the heat capacities of the fluids. with this, we can provide a discussion of the necessary mass flow of Freezium.

$$\dot{m}_{Coolant} = \frac{q_{HX}}{c_p \Delta T}$$

Equation 71 Mass flow of Freezium

Note that this temperature delta describes the change in temperature of one fluid over the HX and not the temperature difference between the two fluids exchanging energy.

To perform this assessment, we initially review the FC module where we know the temperature inside the fuel cell and we know the temperature of the seawater cooling the Freezium before entering the FC HX. We do not know the effectiveness of any of the heat exchangers so we also do not know the working fluid temperatures. Both the FC HX and the seawater HX can be idealized as one fluid stream and one reservoir with near-constant temperature. By doing this we can define the effectiveness of the HX as the delta between the working fluid exiting and the reservoir. A lower delta means that the exchanger has managed to impose a temperature of the fluid close to the theoretical optimum, i.e. the reservoir temperature. This delta will be used as our variable. Another assumption is that we use the same effect on both the FC and seawater HX.

The mass flow is constant over the whole system due to the incompressibility and conservation of mass. When it has been determined from the temperature delta over the FC HX, we use it to calculate the temperature delta over the other HX's. This gives us enough data to determine all the temperatures in the system. The result has been plotted in Matlab and is presented below.

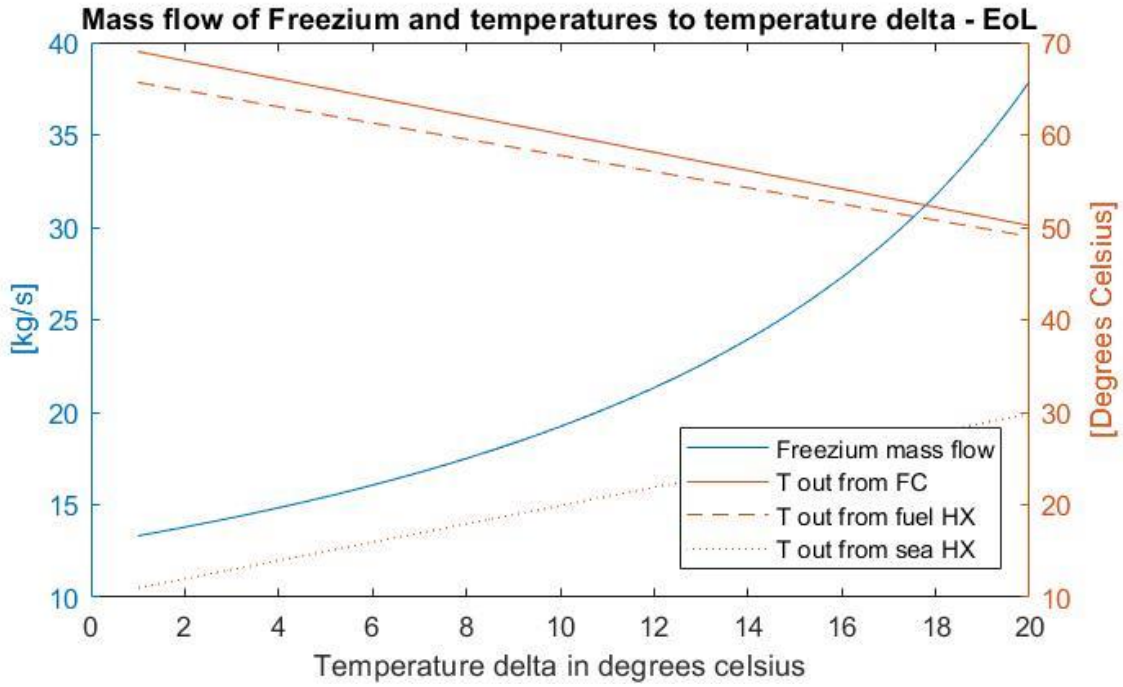

Figure 33 Mass flow of working fluid and temperature to HX efficiency

Note that we have used the numbers for End of Life FC conditions as this accounts for the highest load on the system over its lifetime. With the mass flow and temperatures established, we could calculate the viscosity from the temperature-dependent Prandtl number and find an expression for the pumping demand of the system. Albeit an interesting discussion, it would involve many assumptions making the result too unreliable to be of value. However, most of the necessary theory regarding continuous flow losses were discussed in the bunkering segment. The energy need has been accounted for in the power discussion as it is included in the provided data from LMG marine.

A challenge that becomes apparent here is that if the system is “self-heating”, it will not be able to obtain the correct CH2 temperature during start-up. The sea will be able to provide heat during this period but always below 10 °C. As the hydrogen is to be heated from -244 °C, the ocean can provide nearly all the heat up towards the FC design temperature. For small volumes, it could be possible to initiate the system based on this, but this can lead to a slow start-up before the FC can provide the necessary heat. A potential solution can be to install an electric heater connected to the CH2 pipe out from the HX to provide a final temperature boost. As there is always available power in the batteries, this can solve the issue.

6.4.3.4.5 Safety considerations

In cryogen and energy-producing processes, heat exchange is a very important component in the system. Here we will include a brief discussion on some of the risk factors.

A safety aspect to consider is how failures in the system will affect reliability. The most apparent risk is that the flow of Freezium fails. This loss in circulation can lead to much more extreme temperatures than what it is designed for. In the hydrogen HX, it can experience freeze out, making it impossible to regenerate circulation. An ice blockage would not be good but as we observe from the Pr number, a drop in temperature down from the design point can impose a drastic rise in flow resistance even without freezing.

In the FC, if heat is not expelled continuously, we could experience a temperature build-up resulting in system failure and mechanical damages to the stack. This must be avoided and a control system that quickly shuts down the FC in case of a cooling circulation drop must be imposed. Such a fail-safe will also solve the issue regarding the hydrogen HX as the volume of Freezium should be able to absorb the effect of the LH2/CH2 in the exchanger as long as the fuel flow is stopped.

As mentioned in the description of the working fluid, Freezium, no components in the heating circuit can be made out of aluminum, zinc or galvanized steel due to its corrosive effect. It this is not regarded in the design process; the reliability of the system can suffer.

6.4.3.4.6 Additional remarks

The electric engines will produce heat. This has not been accounted for here. As we have a surplus heat, we cannot use the electrical motor heat in a productive manner. A separate cooling cycle is assumed.

This paper mentioned the issue regarding cold start-up in the heat exchanger part, but only briefly. A thorough analysis of the start-up dynamics could potentially be an interesting subject for further research.

In the FC heat exchanger discussion, we adjusted for the heat loss through the water. However, we did not account for the heat from the gas exiting. It also excludes the heat added by the air from the compression process. These were assumed as isothermal processes, which is not the case.

6.4.4 Air compression

We have now performed a discussion regarding the flow of fuel from bunkering and into the cell. A subject that has so far only been mentioned briefly is the need for air in the reaction. Due to simple mechanics, the pressure on the airside of the cell must be close to the pressure on the hydrogen

side. The polymer separating the two can be damaged if there is a pressure delta resulting in mechanical strain. This implies the need for a compressor to provide an air stream of the correct temperature into the system. In this chapter, we will calculate the power consumption related to this process.

6.4.4.1 Composition

As presented in the FC segment, in addition to hydrogen we need oxygen. This oxygen comes from ambient air (Rashad, 2017). Air is a gas consisting of more than just oxygen. The main components are nitrogen, oxygen and argon and we idealize it as only consisting of these three with the respective molar ratio, 78 %, 21 % and 1 % (Mackenzie, 1995). Using the respective molar masses and this ratio, we obtain a molar mass of 28.97 g/mol (Evans, 2015).

6.4.4.2 Mass flow

The mass flow of air must follow the flow of hydrogen-based on the balance. This states that for every kg of hydrogen, we need 8 kg of oxygen. As only 21 % of the air is oxygen, the necessary minimum airflow is 38.1 kg per kg hydrogen. This assumes that all of the oxygen reacts. In reality, this is not the case and there is a need for an additional amount of oxygen. This magnitude is named oxygen excess ratio (OER) and describes the relationship between the supplied oxygen and the reacted (Guo, 2013). For state-of-the-art PEM fuel cells, this factor is often in the range of 2 (Svendsen, 2020). The implications of this is that the real inflow of air is 76.2 kg per kg hydrogen.

By using the hydrogen mass flows defined as the reference cases we can determine the airflow reference as well.

$$\dot{m}_{BoL}^{ref} = 9{,}257.2\ kgAir/h \qquad \dot{m}_{EoL}^{ref} = 9{,}917.8\ kgAir/h$$

This will be the amount of air that the compressors must be able to handle at the different points. The power consumption will be dependent on the mass flow but the installed capacity should be scaled to the EoL case as this is the highest.

6.4.4.3 Energy consumption of gas compression

By employing the method for polytropic compression presented in (Bakken, 2017) we can calculate the necessary energy demand for the compressions. The formulas used are:

$$H_p = \frac{n}{n-1} Z_1 R T_1 \left[\left(\frac{P_2}{P_1} \right)^{\frac{n-1}{n}} - 1 \right]$$

Equation 72 Polytropic head of gas compressions

$$\frac{n-1}{n} = \frac{k-1}{k\eta_p}$$

Equation 73 Polytropic exponent relationship to isentropic exponent

$$k = \frac{C_p}{C_v}$$

Equation 74 Specific heat ratio

The specific heat ratios are dependent on temperature and pressure and given as tabulated values.

$$Z = Compressibility\ factor$$

$$P = Pressure$$

$$T = Temperature$$

$$R = Specific\ gas\ constant$$

$$k = Isentropic\ exponent$$

$$\eta_p = Polytropic\ efficiency$$

$$\eta_{mechanical} = Mechanical\ efficiency$$

We use the polytropic specific head to calculate the total power.

$$Power = \frac{Mass\ flux * H_p}{\eta_p * \eta_{mechanical}}$$

Equation 75 Power consumption of the gas compressor

The subscripts denote if the condition in question is before or after the compression process. It should be mentioned that there is a distinction between isentropic volume exponent and isentropic temperature exponents. For near ambient conditions, real gases converge towards ideal gas behavior and we will for our calculations not distinguish between these exponents.

The general gas constant R_0 is equal to 8.3145 J/molK and the specific constant is established by dividing it by its molar mass (Helmenstine, 2019). This results in R = 287.03 J/kgK.

The polytropic exponent is dependent on the compressors pressure ratio and a lower ratio provides higher efficiency. As we have a pressure ratio of 5, we will assume a polytropic efficiency of 0.925 for the air compressor (Kotowicz, 2016). The other loss component is mechanical efficiency. This will vary with the size and ratio but an estimate often used in initial design estimations is 0.95 (Moshfeghian, 2015). The isentropic exponent is the relationship between the specific heat capacity at constant pressure to the one at constant volume (EngineeringToolBox, 2003). This value is dependent on temperature and pressure but for standard conditions, it amounts to 1.40 for air (EngineeringToolBox, 2003).

6.4.4.3.1 Compressibility factor

For ideal gases, the equation of state (EoS) is given as $Pv = RT$ as a combination of Boyle's and Charles laws (Hall, 2015). As gases are compressible, the volume change must be accounted for, especially at higher pressure or lower temperatures. The compressibility factor, Z, is a measure of the deviation between the real gas and the ideal gas behavior, i.e. for an ideal gas Z=1 (Properties of Cryogenic Fluids, 2010).

$$Z = \frac{Pv}{RT} = \frac{P}{\rho RT}$$

Equation 76 Compressibility factor

The gas constant R is by definition a constant and the pressure P and temperature T are given by the system. As we are dealing with air at ambient temperature and for a relatively low pressure range, we assume the compressibility factor for our compression to be 1.

6.4.4.4 Energy consumption

Based on this discussion, we can now calculate the polytropic head and the power consumption of the compression process. The process of bringing the gas from 1 bar to 5 bar has the following polytropic head:

$$H_p = 169.4\ kJ/kg$$

The true power need includes inefficiencies. The mass flow used are the reference cases, divided by 3600 to adjust to a per second basis.

$$Compressor\ power = \frac{H_p * mass\ flow}{\eta_p * \eta_{mechanical}}$$

Equation 77 Compressor power

$$Power\ Air\ Comp_{BoL}^{ref} = 495.7\ kW \qquad Power\ Air\ Comp_{EoL}^{ref} = 531.1\ kW$$

This power needs to be supplied as electricity.

As we observed from the calculations regarding air compression power need, this is a significant factor. As the power needed for pressurization scales directly with the pressure ratio, the possibility of using low-pressure FCs should be explored. The lower this magnitude is, the more of the produced electricity can be used as available power. The trade-off constitutes a potential loss in FC efficiency by lowering the incoming hydrogen pressure which would reduce the speed of reaction over the catalysts. This is a field where many companies do active research and fuel cell technology in the future can be expected to have improved characteristics. A more CAPEX intensive cell might improve the total economic feasibility of the project if it manages to reduce the compressor ratio by utilizing a lower internal pressure.

6.4.4.5 Air humidification

In addition to the pressure of the incoming air, the humidity has to be addressed as well. In PEM fuel cells, the membrane is at risk of drying if the air entering the cell is dry. Over time, this has the potential to deteriorate the cell and lead to system failure. To avoid this, a humidifier must be installed. Many vendors are supplying this component. By using the water production from the FC to saturate the gas, it does not increase the complexity of the set-up to a very large degree. As the component can be driven exclusively by the already flowing streams, it does not need additional power to run (Membrane Humidifiers). There will be a minor pressure drop over the component, so from a system definition, a small power consumption increase can be assumed. We assume the total effect on the energy consumption on the vessel to be negligible but as it is a vital component in a fuel cell power system, we deemed it necessary to mention.

6.5 Batteries

We have made references to batteries in many places throughout this paper and the electricity storage system will be of vital importance to our full power and propulsion system. The electric engines will demand power based on the velocity and situation of the vessel. This demand can be volatile and change faster than the supply from the fuel cells as the hydrogen fuel system has an inherently slower response. The ability to shave peak loads also works inversely. There will be situations where the stacks produce more power than the Topeka vessel consumes at that given time. As we do not want to waste energy, this can be stored in the batteries for future usage.

In addition to providing a smoother FC power and performance curves, the batteries also serve a critical safety purpose. They supply emergency power. A system for backup power is important for most vessels, and especially for ships serving the coastal regions of Western-Norway.

In this segment, we will briefly describe the general theory behind the power storage technology, assess the dynamics of the charging and usage cycles and then evaluate how these factors match up with the chosen battery capacity.

6.5.1 Theory

The vessel will have a lithium-based battery pack. Lithium-ion batteries (LIB) are the most used battery technology for consumer electronics and larger electric applications like electric cars (Shapley, 2012). This is the type of energy storage system used in ferries and vessels both in Norway and in other countries including the pioneering electrical ferry, Ampere (Stensvold, 2019).

The fundamental components bear some similarities to the fuel cells and a LIB contains an anode, a cathode, a separator, positive and negative current collectors and an electrolyte (How Does a Lithium-Ion Battery Work, 2017).

The Li-ion batteries are based on the principles of electrochemical potential, the tendency of metals to lose electrons. Lithium has the highest standard potential of the elements (Nave, 2016c). This can be explained as lithium has one electron in its valence shell (OpenStax, 2013). Nature always wants to move towards the stable outcome. For atoms, stability is increased when the outer shell is full (OpenStax, 2013). In the case of lithium, the outer shell can hold 8 electrons. This means that to obtain a stable electron structure, the element must either gain 7 electrons or lose one. For this reason, Li has a very high potential of losing its single electron. This makes lithium in its pure form a highly reactive metal and it is not found in nature (Lithium, 2020). To be stable, it has to be in a compound, bound to other elements.

When lithium is in a metal-oxide, it is stable compared to when it is on its own. A LIB works by having both a metal-oxide part and a part with atomic lithium. The component holding the atomic lithium is called the anode, while the metal-oxide component is referred to as the cathode (Arya, 2018). These two are separated by an electrolyte that is only permeable by lithium ions. The two parts are connected by an electrical conductor where the electrons can flow.

If we initially have a LIB without charge, the lithium will be in the stable metal-oxide structure having a net-zero charge. When we charge the battery, we add a voltage difference to the two sides by plugging it to the electrical grid or fuel cell production. The lithium in the oxide will be ionized by the power, effectively splitting it into an electron and a Li^+ ion. The electron moves through the conductor and into the anode. The anode will be negatively charged, effectively drawing the

positively charged Li^+ ions through the electrolyte. Here, they are reconnected with their electron, forming a net-zero charge in unstable lithium atoms. When the battery is fully charged, i.e. all the available lithium has gone from the cathode to the anode, the current is switched off. Now the lithium is "trapped" in the anode as it cannot move through the electrolyte in its non-ionized form. When the power is to be used, the conductor reconnects the two parts and the unstable atoms will lose the electrons and move through the electrolyte to regain its more stable situation. The electrons move through the conductor where we will utilize it as electrical power, driving the engines (Kempaiah, 2019).

The anodes role is to store the lithium without taking any active part in the chemical reaction. The most common material used as this storing medium today is graphite. This is due to its non-reactivity and its 2-dimensional structure where Li is stored between the carbon sheets (Lithium-Ion Battery, 2020). This storage capacity is one of the limiting factors when it comes to increasing the efficiency of lithium-based batteries. One of the more promising materials to replace graphite is silicon, with a theoretical capacity of 10 times that of carbon (Xiao, 2010). However, the issues regarding contraction and retraction in the material during cycles have yet to be solved on a commercial level (Xuefeng).

The cathode is the metal-oxide where the lithium is contained in its stable form. Li-ion batteries are mainly classified by their cathode materials and are referred to by the acronyms of their components like LCO, NMC or NCA (Zenith et al, 2019). The crystal structure is made out of a compound of $LiMO_2$ where the M represents either cobalt, nickel, aluminum, manganese or a combination of them. NCA and NMC are two technologies that have been used extensively. These refer to LIB with the composition of Li(**N**i**C**o**A**l)O_2 and Li(**N**i**M**n**C**o)O_2 respectively (Zenith et al, 2019). The relationship between the elements in the M group determines the characteristics of the battery like power density and energy density but the ratio of lithium to the group is always one to one, i.e. Li:M = 1:1 (Zenith et al, 2019). In this paper, the total battery capacity to the power supply and demand is in focus. The choice of battery material does not affect this directly but rather secondarily as cost and weight have an impact on the investment decision. To facilitate the discussion regarding this, we assume the battery to be of the NCA type, similar to those in Teslas.

The electrolyte separating these two is commonly an organic solution like ether (Lithium-Ion Battery, 2020).

6.5.2 Capacity

In this part, we will assess the necessary capacity of the installed battery capacity.

6.5.2.1 Safety

As stated, one of the most important roles the battery plays is to act as a safety measure in case of hydrogen power disruptions. When scaling the battery, the lowest safety demand must be an absolute minimum. In an emergency where the hydrogen cannot perform as the main fuel, the Topeka vessel must be able to get to the nearest port or calm and sheltered sea to drop anchor. We assume this demand to be of 1 hour of power but not at full speed. As observable from equation (8), the power demand goes up faster than the velocity, i.e. to increase energy efficiency with regards to the distance we should lower the velocity. Due to this, we assume a safety speed of 9.0 kts. The following power demand from this velocity is 1,023 kW. The energy demand for 1 hour of this power supply is close to 1 MWh. This must be the absolute lowest battery capacity, based on these assumptions.

Another liquid hydrogen ship project that has been assessed is the SF-Breeze in San Francisco. This is a concept involving a passenger fast ferry servicing the Bay Area. In the report, they discuss batteries as a safety measure. The conclusion they drew was that batteries shall be installed, but with a capacity only adequate for lighting and navigation purposes, not for propulsion (Pratt, 2016). There are two main differences between the SF-Breeze and the Topeka concepts. First, the SF was to operate with a top velocity of 35 knots. A vessel designed for such speeds must be as light as possible. The importance of the weight factor limits the potential size of a battery set-up as they are inherently heavy. The other disparity is the area of operation. While the Topeka vessels are to be operated along the Western Coast of Norway, the SF was to be operated within the San Francisco Bay. This is mostly a landlocked area with a relatively low probability of bad weather and wave conditions. It is also a highly trafficked area, making a potential rescue or support intervention swift. The requirement for extra battery capacity is higher for the Topeka project.

An alternative to having backup batteries of this capacity is by having a backup hydrogen supply. As we have a configuration of many stacks of fuel cells, it can be assumed that the hydrogen tank, compressor, vaporizer or heat exchanger present a larger risk of breakdown than all of the stacks. By having a buffer tank of compressed hydrogen, many of these risks are mitigated. The issue is size. As the conditions of the hydrogen gas supplied by the system are 6 bara and 283 Kelvin, it has a density of 0.51 kg/m^3. An hour of power at 9 kts will demand 54.0 – 58.3 kg of hydrogen, depending on the time of FC life. This implies a necessary compressed gas storage capacity of 105.9 – 114.4 m^3. One could argue that a tank of 350 bar or more could be situated onboard to be used only in such a situation, thereby reducing the volume drastically. However, the role of the battery is to be used as peak shaving and smoothing of the demand curve imposed on the FC's, in addition to safety. We can conclude that a hydrogen gas tank cannot replace the batteries.

$$E_{Battery}^{Safety\ minimum} = 1{,}000\ kWh$$

6.5.2.2 Efficiency improvement

Now that a minimum has been determined, we must assess how the batteries can contribute to increasing the overall efficiency of the vessel. The general idea is to have the battery act as a peak shaver. It will supply the additional demand not met by the fuel cells. Similarly, it will act as a reserve to store overshooting supply in situations where the demand reduces rapidly. These are important attributes but demand an accurate model of the system dynamics during the normal operational profile. Factors included are the response time for the fuel cell and hydrogen flow system, as well as the demand profile over the sailing operation. We deem it outside the scope of this paper to quantify this particular capacity requirement.

Using energy from the batteries is more efficient than using energy from the hydrogen as there are comparatively few losses from the battery to the engine vs from the LH2 and to the engine. This has two important implications. The first is that if avoidable, no charging of the batteries should be performed by the FC's. The only exception to this rule is in incidents where the safety margin of the capacity has been overextended. This situation can occur when the battery charge reaches a lower threshold than the minimum necessary available backup power. The other implication is that when there is an available supply of power from the battery, it should be used. This will save hydrogen from the fuel tank.

From these two statements, we can draw an important conclusion that affects the battery size. All charging of the batteries should take place in port from the national power grid. The vessel should

charge as much as possible each port call as the power supplied here is cheaper and more efficient than hydrogen. We assume that there is little to no chance that the cost of available energy from hydrogen is lower than that of Norwegian hydropower. The new limiting factor of the battery capacity is how much it is possible to charge while in port.

6.5.2.3 Land-based charging

When assessing the charging possibilities from the quay, we must address two factors. The first is to determine the amount of time in port, i.e. the available charging time. The next is to evaluate the accessible power supply from the port charging infrastructure.

6 ports are being served by the Topeka ro-ro vessel. The ship will load and unload cargo in each one of them and as it will follow a predetermined time-table, the time in quay will be relatively constant and predictable. Two of the calls will be for a longer duration than the 4 others. The first planned LH2 bunkering port is in Mongstad where the vessel will stay for a longer period than the other to allow for refueling. The other outlier is Risavika. To maintain a schedule well adapted to the needs of the customers located in the Risavika oil-base area, it will remain in quay there for an additional period to depart at 16:00. The 4 ports in between will be served in a similar time fashion.

Representatives from Wilhelmsen predict that the operational time in these 4 ports, i.e. the time where loading/unloading and charging can take place is 70 minutes. Both the calls in Mongstad and Risavika will be longer but oversizing the battery will harm the project's economic feasibility. We will discuss these factors later but due to this, we define 70 minutes as the available charging time.

$$t_{Port} = 70\ min$$

The next factor to assess is how the transfer of energy should take place and if there are any inefficiencies or losses regarding time or energy.

Norway is at the forefront of battery charging solutions for ships through the extensive focus on electric ferries. Some of these concepts are usable for the Topeka vessel as well. We can divide the charging into two categories, wireless and plug based.

Charging by a plug is the simplest solution and can be compared to the common electrical plugs in homes, obviously with a wider cross area. An advantage is that the losses from the connection are 0% (Jensen, 2019). When the connection itself is performed by a robot, the process can be very effective. This is the solution chosen for the World's first electric ferry, the Ampere (Cavotec, 2016).

Figure 34 Charging solution on MF Ampere. Screenshot (Cavotec, 2016)

Another solution is to use wireless charging. This is based on the induction principle and the ferry MF Folgefonn was the first to use this technology (Blich, 2017). The electromagnetic field eliminates the need for a physical connection and allows charging to commence at the very instance the vessel is positioned beside the key (Wartsila, 2018a). This is highly advantageous for routes where the time in port is very short, as is the case for ferries. As the charging time is short compared to the transit time, induction increases the available charging by up to 20 % (Wartsila, 2018b).

Figure 35 Induction charging solution for ferries *(Wartsila 2018b)*

In between these two main characteristics, we also have the concept of charging by physical connection using a pantograph. This is a solution where an arm with variable length is stretched out and physically connects with a conduction surface on the vessel (Jensen, 2019). A comparable

analogy is a technique used on some train systems where the power is supplied from the above through wires connected to the train by pantographs.

As the Topeka vessel will stay in port for longer periods than most ferries, we assume a plug-based solution to be favorable. This implies zero transfer losses but longer connection time. We estimate the time used to be 5 minutes for connection and disconnecting leaving us with 60 minutes available for power.

$$t_{Charging} = 60\ min$$

The next step is to determine the available power output. The battery ferry industry is moving rapidly and the charging effect has gone up from around 1,000 kW to 7,200 kW in the projects being planned today (Stensvold, 2017) (Siemens, 2019).

An issue with the fast charging of ships has been the available power output at the dock. As the time at the quay is short, a very high-power density is needed to adequately fill the batteries. A solution used in Norway is to have stationary battery packs located on land (Mossing, 2019). These installations continuously draw power from the available electrical grid. When the vessel docks, the energy is "dumped" over to the ship through its connection. This set-up manages to deliver the necessary electricity demand but as it involves additional and large batteries, it represents a high capital expenditure.

We will try to avoid this and focus on using the power from the grid. An advantage is that the ports are mostly located in industrial areas where the supply can be assumed better or more flexible than in cities and central areas. According to Equinor, the available power from the infrastructure on land at the Mongstad base is 840 kW. We assume this as the available port power for our route.

$$Power_{In\ port} = 840\ kW$$

As we now have both the available power and time, a multiplication of them yields the necessary battery capacity.

$$E_{Battery}^{Port\ charging} = 840\ kWh$$

The total battery capacity is the combination of the safety limit and the land power basis. The additional size from the hybrid usage implicates a size increase of 84 % from the minimum.

$$E_{Battery} = E_{Battery}^{Safety\ minimum} + E_{Battery}^{Port\ charging} = 1{,}840\ kWh$$

Equation 78 Battery capacity

Of this capacity, 45 % is available for hybrid usage.

This is close to the size LMG has presented as their preliminary base case of 1,600 kWh in total battery capacity.

6.5.2.4 Cost savings

As determined, the usage of batteries could reduce the need for hydrogen on some parts of the journey. Here, we will attempt to quantify the potential savings of hydrogen-based on the chosen battery capabilities.

There are 10 legs on a round trip for the Topeka vessel. Accounting for the safety margin, this implies 10 charge cycles of 840 kWh each, resulting in available energy of 8.4 MWh. The reference velocity of 12 kts and the reference power demand of 2,166 kW equates to the reference fuel cell consumptions:

$$C_{BoL}^{ref} = 56.85\ gH_2/kWh \qquad C_{EoL}^{ref} = 60.94\ gH_2/kWh$$

Multiplying the available battery energy with the necessary hydrogen demand per energy unit, we obtain the potential fuel savings.

$$\Delta Fuel_{BoL}^{ref} = 477.55 \frac{kgH_2}{round\ trip} \qquad \Delta Fuel_{EoL}^{ref} = 511.91 \frac{kgH_2}{round\ trip}$$

This represents a substantial potential for increasing the economic feasibility of the Topeka project, however, batteries do impose some negative effects as well.

6.5.2.5 Limiting factors

Minimum capacity is necessary but increasing the size above this threshold will have some adverse effects on the project. These are mainly the cost associated with additional weight and capital. They are extensive factors and as the battery installation comprises many smaller stacks and modules, we assume the total to scale one-to-one with storage capacity. We have assumed the battery type to be of the NCA technology.

Weight

For the NCA batteries the energy density can be regarded as high and is in the range of 200 – 260 Wh/kg (Zenith et al. 2019). This implicates a total weight of between 9.2 and 7.1 tons. When adjusting for the necessary 1 MWh, the weight addition for hybrid propulsion is 4.2 – 3.2 tons. This will add less than 1 % weight to the gross tonnage of the ship. Weight is understandably an important factor regarding power requirement and energy usage, but we assume this additional margin to not interfere with the general propulsion set-up. For large ferries with fully battery-powered systems, the battery packs weight can reach up towards 100 tons (Stensvold, 2016).

CAPEX

LIBs are an expensive form of energy storage, compared to conventional methods but the price per kWh has dropped significantly over the last years. The average price in 2018 of lithium-ion battery cells was USD 176 per kWh (Goldie-Scot, 2019). This price is dropping further and it is expected that the price reaches 100 USD/kWh in 2020 (Venkatasamy, 2019). As this is an estimate and to maintain a conservative estimate, we will use a cost of 200 USD/kWh for the cells. As the real battery pack price must include cooling, and control systems, the cell price is multiplied by two. The total battery price ends up at USD 736,000. By using the 1-year average USDNOK currency conversion rate of 9.2 we end up with a cost of NOK 6.8m for the total battery (Oslo Børs, 2020). The hybrid cost is NOK 3.1 m.

In addition to the cost of the batteries, the charging infrastructure will demand an investment.

In this paper, we will not perform a cost/investment analysis as this is beyond the scope and the price of delivered hydrogen is highly uncertain and would lead to low accuracy of the estimate.

6.5.3 Risk factors

As with all storage systems, there are some risks associated with Li-ion batteries. In this section, we will briefly review the fire risk.

One of the worst-case scenarios for a ship is a large fire on board the vessel. These incidents are rare but have happened in the past. The batteries can provide an additional risk if this occurs. A large part of the fire safety precautions taken on ships is overhead water sprinkler systems. These are initially supplied by a freshwater pressurized tank but as this has limited capacity, the need for additional water rises quickly. This demand is met by using saltwater pumps from the ocean (Automatic sprinkler system, 2016). For most situations, this is advantageous as it reduces the need for large and heavy freshwater systems and most fires are put out just as quickly with seawater as with freshwater. This does not necessarily apply to electrical systems.

In 2019, there was a fire in the battery ferry MF "Ytterøyning". Fire fighting started quickly and the situation was controlled with a full evacuation performed without anyone being harmed. After a while, a powerful explosion struck the vessel. It has been determined afterward that the saltwater sprinkler system was to blame as it short-circuited the system (Lura, 2019). Evaluations of the fire safety systems should be performed and adjusted based on the attributes of the energy storage system

7 Conclusion/Summary

In this paper, we have presented the Topeka liquid hydrogen propelled short-sea cargo vessel. The build-up of the thesis has been to follow the hydrogen flow from the land and into the fuel cell, as a response to the power demand from the vessel.

The Topeka concept is a ro-ro vessel that will serve the oil-bases on the western coast of Norway with a predictable schedule, powered by clean liquid hydrogen as a first of its kind. We defined a reference velocity to be used in our calculations as the transit speed of 12 knots.

$$V^{ref} = 12\ kts$$

By including the force on the ship from the water and air and accounting for the non-propulsion power requirement, we concluded on a power demand to operate the vessel under reference conditions.

$$Power\ Ship^{ref} = 2{,}166\ kW$$

The power is supplied by PEM fuel cells, the most advantageous FC technology for marine mobility today. As the energy of hydrogen is given, the actual hydrogen fuel demand is dependent on the efficiency. The efficiency of the cells will drop from the beginning of life and to the end, resulting in two fuel flows at 12 kts.

$$\dot{m}_{BoL}^{ref} = 121.50\ kgH_2/h \qquad \dot{m}_{EoL}^{ref} = 130.17\ kgH_2/h$$

This hydrogen must be conditioned from the liquid cryogenic state in the tank and into a state that the fuel cells can utilize. We discussed the factors involved and determined the inlet conditions to be 10 °C and 4 barg.

Before the hydrogen can be supplied by the fuel tank, it must be bunkered onto the vessel from the land. We described the process as a pipe between two pressurized cryogenic tanks. A pressure build-

up in the land tank pushes LH2 out from the bottom, into the pipeline and through spray nozzles at the top of the fuel tank. The pressure delta between the tanks to propel the flow was estimated to 1.2 bar, depending on the pipe diameter. A continuous heat ingress of 17 kW must be added to maintain a phase transition in the land tank to sustain the pressure for the given flow velocity.

The tank itself is an IMO type-C vacuum-insulated pressure vessel. When the fuel is needed, it is extracted from the bottom of the tank. The first step is that it flows into one of two conditioning tank where a small heat ingress builds pressure to 6 barg. The power needed to induce the increase in the CT is electrical and amounts to:

$$Power\ CT_{BoL}^{ref} = 6.3\ kW \qquad Power\ CT_{EoL}^{ref} = 6.8\ kW$$

The next step is to let the high-pressure LH2 flow into the main heat exchanger. The first part evaporates the hydrogen into gas. The latent heat of vaporization at 7 bar is 322.7 kJ/kg and this heat is added from the working fluid. After the phase change has been induced, the gas needs to be heated to the final temperature of 10 °C. We determined the temperature-dependent specific heat of hydrogen and used this to perform heat exchanger calculations.

The HX that has been chosen is a shell and tube heat exchanger where the hydrogen flows through the internal tubes. The working fluid is Freezium, a potassium-based chemical with low freezing point and good thermal properties. The necessary energy flux into the hydrogen fuel HX was calculated.

$$q_{BoL}^{fuel} = 114.1\ kW \qquad q_{EoL}^{fuel} = 122.3\ kW$$

Heat is continuously being produced by the fuel cells and this is where we source the energy for the fuel HX. By using the waste heat and not the electricity, the total efficiency is increased. The magnitude of heat production is dependent on fuel flow and efficiency as most of the FC losses generate heat. By adjusting for the heat leaving with the water, we determined the energy to be removed from the stacks during reference operation conditions.

$$q_{BoL}^{FC\ adj} = 1{,}833.4\ kW \qquad q_{EoL}^{FC\ adj} = 2{,}124.6\ kW$$

With the demand for heat at around 6 % of the supply, the vessel must expel the surplus. This is done by including a seawater heat exchanger to the process, after the fuel HX but before the fuel cell. This must account for the delta between the two others.

$$q_{BoL}^{Sea} = 1{,}719.3\ kW \qquad q_{EoL}^{Sea} = 2{,}002.3\ kW$$

Hydrogen has an interesting attribute as it has different energy levels depending on the nuclear spin of its atoms. The composition is dependent on temperature and we determined that the energy difference is substantial. A slow reaction speed in a non-catalytic environment led to the conclusion of a very limited effect on our process.

The hydrogen to water and power reaction demands oxygen as well. This oxidizer is supplied in the form of air and we calculated the necessary airflow accounting for its composition and the OER.

$$\dot{m}_{BoL}^{ref} = 9{,}257.2\frac{kgAir}{h} \qquad \dot{m}_{EoL}^{ref} = 9{,}917.8\frac{kgAir}{h}$$

This air has to be compressed and humidified before entering the cell. The compressor is an electrically driven component demanding energy.

$$Power\ Air\ Comp_{BoL}^{ref} = 495.7\ kW \qquad Power\ Air\ Comp_{EoL}^{ref} = 531.1\ kW$$

This is the polytropic power demand and is a quantity that is highly dependent on the pressure into the stack. Higher pressure requires more power and a low pressure stack can reduce the power consumption.

The last segment of the paper discussed batteries and their role on the vessel. The technology to be used is lithium-ion batteries. They provide a safety margin to allow the ship to get to shore in the event of fuel cell failure. This factor demands a 1,000 kWh capacity. The other role it plays is to act as a buffer absorbing demand surges and drops faster than the hydrogen flow. Based on the 70 minutes of available charging time in each port and an 840 kW electric power supply from land, we calculated the maximum usable battery. From this, we find the total battery size.

$$E_{Battery} = E_{Battery}^{Safety\ minimum} + E_{Battery}^{Port\ charging} = 1{,}840\ kWh$$

The idea is that using a plug-in hybrid concept will reduce the hydrogen demand and improve the reliability of the ship. Our calculations resulted in this potential hydrogen saving per round trip.

$$\Delta Fuel_{BoL}^{ref} = 477.6 \frac{kgH_2}{round\ trip} \qquad \Delta Fuel_{EoL}^{ref} = 511.9 \frac{kgH_2}{round\ trip}$$

The Topeka vessel is a revolutionary take on the way we move goods between coastal areas. This paper illustrates that the complex problem of LH2 powered maritime transport has the potential to be solved with the available technology. At the time of writing, the solutions described is the current choices for the project. The concept is still in the development and design stage and it is expected that some of the final solutions might deviate or change from those described here.

8 References

95 millioner til utslippsfrie løsninger (2019) URL: https://presse.enova.no/pressreleases/95-millioner-til-utslippsfrie-loesninger-2953300 (Accessed 03.02.2019)

ABS (2015) *LNG Bunkering: Technical and Operational Advisory* URL: https://ww2.eagle.org/content/dam/eagle/advisories-and-debriefs/ABS_LNG_Bunkering_Advisory.pdf (Accessed 15.04.2020)

Absolute pipe roughness. (2011) URL: https://www.enggcyclopedia.com/2011/09/absolute-roughness/ (Accessed 31.02.2020)

Albertsen, J. (2019) *Sjøtemperaturer I Nordsjøen og Skagerrak.* URL: https://miljostatus.miljodirektoratet.no/sjotemperatur-i-Nordsjoen-og-Skagerrak (Accessed 25.03.2020)

Arteco. (2020) *Freezium.* URL: https://www.arteco-coolants.com/en/products/heat-transfer-fluids/product-range/freezium (Accessed 01.05.2020)

Arteco-Coolants. (2018) *Freezium.* Product information sheet. 10/2018-v08.1 URL: https://www.arteco-coolants.com/en/system/files/downloads/freezium_english_08.1_0.pdf (Accessed 01.05.2020)

Arya, A. (2018) *Polymer Nanocomposites: synthesis and characterization.* URL: https://www.researchgate.net/publication/326315792_Polymer_Nanocomposites_synthesis_and_characterization (Accessed 06.05.2020)

Automatic sprinkler systems. (2016) URL: http://generalcargoship.com/fire-protection-automatic-sprinkler-system.html (Accessed 08.05.2020)

Baierlein, R. (1999) *Thermal Physics*. Cambridge University Press. Cambridge. Page 253.

Bakken, L. E. (2017) *Thermodynamics Compression and Expansion Processes.* Page 8-14.

Bapat, N. (2019) *Heat of Vaporization.* URL: https://chem.libretexts.org/Bookshelves/Physical_and_Theoretical_Chemistry_Textbook_Maps/Supplemental_Modules_(Physical_and_Theoretical_Chemistry)/Thermodynamics/Energies_and_Potentials/Enthalpy/Heat_of_Vaporization (Accessed 13.03.2020)

Basic Properties of LNG. (2009) URL: http://www.kosancrisplant.com/media/5648/1-lng_basics_82809_final_hq.pdf (Accessed 05.05.2020)

BKK (2019) *Liquid hydrogen to decarbonize maritime transport in Norway.* Project description for PILOT-E ENOVA application. Page 1.

Blich, V. (2017) *MF Folgefonn lades og fortøyes trådløst.* URL: https://www.skipsrevyen.no/article/mf-folgefonn-lades-og-fortoeyes-traadloest (Accessed 07.05.2020)

Bliesner, R. M. (2013) *Parahydrogen-Orthohydrogen Conversion for Boil-Off Reduction from Space Stage Fuel Systems.* Master Thesis. Washington State University. URL: https://s3.wp.wsu.edu/uploads/sites/44/2014/08/Bliesner-Masters-Thesis-Final-P-O-heat-shielding.pdf Page 9. (Accessed 19.02.2020)

Brown, A. (2019) *Hydrogen Transport.* The Chemical Engineer. https://www.thechemicalengineer.com/features/hydrogen-transport/ (Accessed 16.04.2020)

Bruijn, F. (2011) *PEMFC lifetime and durability an overview.* URL: https://www.sintef.no/globalassets/upload/materialer_kjemi/energikonvertering-og-materialer/bilder/pemfc-overview-thessaloniki-fa-debruijn---f.pdf Page 28. (Accessed 19.03.2020)

Cadwallader, L. C. (1999) *Safety issues with hydrogen as a vehicle fuel.* URL: https://inldigitallibrary.inl.gov/sites/sti/sti/3318091.pdf (Accessed 17.03.2020)

Cardella, U. F. (2018) *Large-scale hydrogen liquefaction under the aspect of economic viability.* Ph.D. dissertation. The Technical University of Munich. URL: https://mediatum.ub.tum.de/doc/1442078/1442078.pdf Page 17. (Accessed 19.02.2020)

Cavotec. (2016) *Cavotec mooremaster/automatic plug-in system.* URL: http://press.cavotec.com/videos/cavotec-moormaster-slash-automatic-plug-in-system-25224 (Accessed 07.05.2020)

Cengal Y. and Cimbala J. (2010) *Fluid Mechanics Fundamentals and Applications* 2nd edition. New York. McGraw-Hill. P.590-591

Choi, J. (2004) *Liquid Hydrogen Properties.* URL: https://inis.iaea.org/collection/NCLCollectionStore/_Public/36/045/36045728.pdf (Accessed 19.02.2020)

Chubbock, S. (2016) *Comparative analysis of internal combustion engine and fuel cell range extender.* SAE Int. J. Alt. Power. 5 (1) Page 175-152. DOI/URL: https://doi.org/10.4271/2016-01-1188 (Accessed 17.03.2020)

Clark, J. (2012) *Molecular Structures.* URL: https://www.chemguide.co.uk/atoms/structures/molecular.html (Accessed 13.02.2020)

Conversion and Storage of Energy (2012). URL: https://www.uio.no/studier/emner/matnat/fys/MENA3200/h12/undervisningsmateriale/energymaterials-2010-ch09-excerpts.pdf Page 9.10 (Accessed 20.03.2020)

Cryoquip (2014) *Cryoquip INSTALLATION Tips and Considerations for Ambient Vaporizers.* https://cryoind.com/wp-content/uploads/2014/09/2014-WINTER-Cryoquip-Installation-Tips-and-Considerations-for-Ambient-Vaporizers.pdf (Accessed 30.04.2020)

Datt, P. (2014) *Latent heat of vaporization/Condensation.* DOI/URL: https://doi.org/10.1007/978-90-481-2642-2_327 (Accessed 13.03.2020)

Deegan, P. (2018) *304, 316 & L-Grade Stainless Steels: What are the differences?* URL: https://www.vortexglobal.com/304-316-l-grade-stainless-steels-what-are-differences/ (Accessed 16.04.2020)

Diesel-Electric Propulsion (2020) URL: https://www.wartsila.com/encyclopedia/term/diesel-electric-propulsion (Accessed 10.02.2020)

DNV GL (2019a) *Maritime Forecast to 2050.* P.37

Drake, G. (2020) *Thermodynamics.* URL: https://britannica.com/science/thermodynamics (Accessed 14.03.2020)

Ekin, J. W. (2006) *Experimental Techniques in Low Temperature Environments.* Oxford University Press. Figure 6.20. URL: http://www.researchmeasurements.com/figures/6-20.pdf (Accessed 16.04.2020)

Encyclopedia Britannica. (2016) *Van der Waals Forces.* URL: https://www.britannica.com/science/van-der-Waals-forces (Accessed 17.02.2020)

Encyclopedia Britannica. (2018) *Methane.* URL: https://www.britannica.com/science/methane (Accessed 13.02.2020)

Encyclopedia Britannica. (2020) *Newtons Laws of Motion* URL: https://www.britannica.com/science/Newtons-laws-of-motion (Accessed 10.02.2020)

EngineeringToolBox. (2003) *Ratios of Specific Heat of Gases.* URL: https://www.engineeringtoolbox.com/specific-heat-ratio-d_608.html (Accessed 17.02.2020)

Environmentally friendly sea transport (2019) URL: https://www.colorline.com/about-us/environmentally-friendly-sea-transport (Accessed 03.02.2020)

European Commission. (2019) *The European Green Deal.* Brussels. COM (2019) 640 final.

Evans, P. (2015) *Density of Gases*. URL: https://theengineeringmindset.com/density-of-gases/ (Accessed 03.05.2020)

Export of Oil and Gas (2019) URL:https://www.norskpetroleum.no/en/production-and-exports/exports-of-oil-and-gas/ (Accessed 03.02.2020)

Fragol. (2016) *Daten Frezzium -60.*

Fredheim, A and Solbraa, E. (2018) *Offshore gas processing for rich gas transport.* Compendium TEP 4185 – Natural Gas Technology

Fry, P (2013) *Key Facts to Know When Shipping Dangerous Goods*. URL: https://www.cacgas.com.au/blog/bid/361547/key-facts-to-know-when-shipping-dangerous-goods (Accessed 17.03.2020)

FuelCellToday. (2020a) *PEMFC.* Johnson Matthey Plc. URL: http://www.fuelcelltoday.com/technologies/pemfc (Accessed 16.03.2020)

FuelCellToday. (2020b) *AFC.* Johnson Matthey Plc. URL: http://www.fuelcelltoday.com/technologies/afc (Accessed 16.03.2020)

Godula-Jopek, A. (2015) *Hydrogen Production by Electrolysis*. First edition. Munich: Wiley-VCH

Goldie-Scot, L. (2019) *A Behind the Scenes Take on Lithium-ion Battery Price.* URL: https://about.bnef.com/blog/behind-scenes-take-lithium-ion-battery-prices/ (Accessed 08.05.2020)

Granavolden-plattformen (2019) *Politisk plattform for en regjering utgått av Høyre, Fremskrittspartiet, Venstre og Kristelig Folkeparti.* Statsministerens kontor. URL: https://www.regjeringen.no/no/dokumenter/politisk-plattform/id2626036/#klima (Accessed 11.03.2020)

Guarascio, F. (2019) *Explainer: What an EU carbon border tax might look like and who would be hit.* URL:https://www.reuters.com/article/us-climate-change-eu-carbontax-explainer/explainer-what-an-eu-carbon-border-tax-might-look-like-and-who-would-be-hit-idUSKBN1YE1C4 (Accessed 03.02.2020)

Guenault, A. M. (1988) *Statistical Physics*. Kluwer Academic Publisher. The Netherlands. URL: https://books.google.no/books?id=81aNUoAv4vMC&lpg=PA86&ots=Pn_Pe6Okmu&dq=%22characteristic%20temperature%20of%20vibration%22%20%22hydrogen%22&pg=PR4#v=onepage&q=%22characteristic%20temperature%20of%20vibration%22%20%22hydrogen%22&f=false Chapter 7. (Accessed 15.03.2020)

Guo, A. (2013) *Air flow control based on optimal oxygen excess ratio in fuel cells for vehicles.* Journal of Modern Transportation. 21, 79-85 (2013) URL: https://link.springer.com/article/10.1007/s40534-013-0009-8

Gupta, S. (2016) *Preventing wax formation in marine diesel fuels.* URL: https://www.wilhelmsen.com/marine-products/oil-solutions/preventing-wax-formations-in-marine-diesel-fuels/ (Accessed 17.03.2020)

Hall, N. (2015) *Equation of State (Ideal Gas).* URL: https://www.grc.nasa.gov/WWW/k-12/airplane/eqstat.html (Accessed 19.02.2020)

Havelock, T. H. (1909) *The Wave-making Resistance of Ships: a Theoretical and Practical Analysis.* DOI/URL: https://royalsocietypublishing.org/doi/pdf/10.1098/rspa.1909.0033 Page 277. (Accessed 11.02.2020)

Helmenstine, A. M. (2019) *Chemistry Definition of Gas Constant (R).* URL: https://www.thoughtco.com/definition-of-gas-constant-r-604477 (Accessed 05.03.2020).

Holtebekk, T. (2018) *Brenselcelle.* URL: https://snl.no/brenselcelle (Accessed 16.03.2020)

Incropera, F. (2017a) *Incropera's Principles of heat and mass transfer.* 8th edition. John Wiley & Sons Singapore Pte. Ltd. Page 654

Incropera, F. (2017b) *Incropera's Principles of heat and mass transfer.* 8th edition. John Wiley & Sons Singapore Pte. Ltd. Page 548.

Incropera, F. (2017c) *Incropera's Principles of heat and mass transfer.* 8th edition. John Wiley & Sons Singapore Pte. Ltd. Page 17.

Incropera, F. (2017d) *Incropera's Principles of heat and mass transfer.* 8th edition. John Wiley & Sons Singapore Pte. Ltd. Page 71.

Incropera, F. (2017e) *Incropera's Principles of heat and mass transfer.* 8th edition. John Wiley & Sons Singapore Pte. Ltd. Page 663.

Incropera, F. (2017f) *Incropera's Principles of heat and mass transfer.* 8th edition. John Wiley & Sons Singapore Pte. Ltd. Page 3.

Incropera, F. (2017g) *Incropera's Principles of heat and mass transfer.* 8th edition. John Wiley & Sons Singapore Pte. Ltd. Page 6.

Incropera, F. (2017h) *Incropera's Principles of heat and mass transfer.* 8th edition. John Wiley & Sons Singapore Pte. Ltd. Page 8.

Jensen, S. (2019) *Ladeløsninger for elektriske ferger.* URL: https://site.uit.no/ladeteknologi/2019/11/06/ladelosninger-for-elektriske-ferger/ (Accessed 07.05.2020)

Kempaiah, R. (2019) *Lithium-Ion battery, How does it work?.* URL: https://www.youtube.com/watch?v=VxMM4g2Sk8U&ab_channel=LearnEngineering (Accessed 06.05.2020)

Khan, M. Y. (2006) *Effects of Diesel Addition on Viscosity of Linseed Oil and Consequent Effects on Performance Characteristics of CI Engine.* National Conference on Recent Developments and Future Trends in Mechanical Engineering. NIT Hamirpur, 2006 URL: https://www.researchgate.net/publication/302991246_Effects_of_Diesel_Addition_on_Viscosity_of_Linseed_Oil_and_Consequent_Effects_on_Performance_Characteristics_of_CI_Engine (Accessed 02.04.2020)

Khotseng, L. (2019) *Fuel Cell Thermodynamics*. DOI: 10.5772/intechopen.90141. URL: https://www.intechopen.com/online-first/fuel-cell-thermodynamics Chapter 2.3 (Accessed 20.03.2020)

Kjerstad, N. (2020) *nautisk mil.* URL: https://snl.no/nautisk_mil (Accessed 12.03.2020)

Kokarakis, J. (2015) *Standards and Guidelines for Natural Gas Fueled Ship Projects.* URL: https://www.onthemosway.eu/wp-content/uploads/2015/06/Standards-and-Guidelines-for-Natural-Gas-Fuelled-Ship-Projects%E2%80%99.pdf (Accessed 05.05.2020)

Kotowicz, J. (2016) *The methodology of the gas turbine efficiency calculation*. DOI: 10.1515/aoter-2016-0025 URL: https://www.researchgate.net/publication/316337118_The_methodology_of_the_gas_turbine_efficiency_calculation (Accessed 04.05.2020)

Kraftproduksjon (2019) URL: https://energifaktanorge.no/norsk-energiforsyning/kraftforsyningen/ (Accessed 03.02.2020)

Latarche, M. (2017) *Explaining the types of fuel used on ships.* URL: https://shipinsight.com/articles/explaining-the-types-of-fuel-used-on-ships (Accessed 03.02.2020)

Leachman, J. (2019) *Cryogenic Hydrogen Embrittlement.* Washington State University. ME 406 Lecture 13. https://hydrogen.wsu.edu/2019/02/18/cryogenic-hydrogen-embrittlement/ (Accessed 16.04.2020)

Leachman, J. W. *et al.* (2009) *Fundamental Equations of State for Parahydrogen, Normal Hydrogen, and Orthohydrogen.* Journal of Physical and Chemical Reference. Data 38, 721 DOI/URL: https://doi.org/10.1063/1.3160306 (Accessed 17.02.2020)

Life Cycle of a Ship (2013) URL: http://www.shippipedia.com/life-cycle-of-a-ship/ (Accessed 01.02.2020)

Lithium-Ion Battery. (2020) Clean Energy Institute. URL: https://www.cei.washington.edu/education/science-of-solar/battery-technology/ (Accessed 06.05.2020)

Lithium. (2020) Royal Society of Chemistry. URL: https://www.rsc.org/periodic-table/element/3/lithium (Accessed 06.05.2020)

Location of Cities: it has a lot to do with water, resources, history and being on the northern hemisphere (2017) URL: https://www.thiscityknows.com/location-of-cities-it-has-a-lot-to-do-with-water-resources-history-and-being-in-the-northern-hemisphere/ (Accessed: 01.02.2020)

Lura, C. (2019) *Har funnet årsaka til brannen og eksplosjonen på MF "Ytterøyningen".* URL: https://www.nrk.no/vestland/har-funne-arsaka-til-brannen-pa-ferja-mf-_ytteroyningen_-i-kvinnherad-1.14817180 (Accessed 08.05.2020)

Mackenzie, F.T. (1995) *Our changing planet.* Prentice-Hall. New Jersey. URL: https://eesc.columbia.edu/courses/ees/slides/climate/table_1.html (Accessed 03.05.2020)

McAllister, S. (2011) *Fundamentals of Combustion Processes.* Springer Science + Business Media LLC. DOI 10.1007/978-1-4419-7943-8 URL: https://link.springer.com/content/pdf/bbm%3A978-1-4419-7943-8%2F1.pdf Page 244. (Accessed 13.03.2020)

McCarty R. D. *et al.* (1981a) *Selected Properties of Hydrogen (Engineering Design Data).* National Bureau of Standards. Washington. Table 8. P. 6-142

McCarty R. D. *et al.* (1981b) *Selected Properties of Hydrogen (Engineering Design Data).* National Bureau of Standards. Washington. Part 1.2.12 and 1.2.13

McCarty R. D. *et al.* (1981c) *Selected Properties of Hydrogen (Engineering Design Data).* National Bureau of Standards. Washington. Table 2.

Meagher, J. P. (2008) *Modeling hydrogen liquefiers with kinetic conversion of ortho to para hydrogen in plate-fin heat exchangers.* Master thesis. State University of New York.

Membrane Humidifiers. Fumatech. URL: https://www.fumatech.com/NR/rdonlyres/0B9A1C7F-5BA6-4409-A003-5C4E79CD61AB/0/FUMATECH_BWT_GmbHMembrane_Humidifiers.pdf (Accessed 11.05.2020)

Mer gods fra vei til sjø og bane (2017) URL: https://www.regjeringen.no/no/aktuelt/mer-gods-fra-vei-til-sjo-og-bane/id2575336/ (Accessed 04.02.2020)

Mohamed, W. A. N. (2016) *Hydrogen preheating through waste heat recovery of an open-cathode PEM fuel cell leading to power output improvement.* Energy Conversion and Management. 124 (2016) Page 543-555. DOI/URL: https://doi.org/10.1016/j.enconman.2016.07.046 (Accessed 17.03.2020)

Moran, M (2014) *Fundamentals of Engineering Thermodynamics* 8th edition. John Wiley & Sons, Inc. Hoboken, New Jersey Page 272

Moshfeghian, M. (2015) *How to estimate compressor efficiency.* URL: http://www.jmcampbell.com/tip-of-the-month/2015/07/how-to-estimate-compressor-efficiency/ (Accessed 04.05.2020)

Moss Maritime. (2018) *Ship transport solution for liquefied hydrogen (LH2 Bunker Vessel).* Summary Report.

Mossing, J. (2019) *Batterifergen MF "Ampere" sliter igjen.* URL: https://www.bt.no/nyheter/lokalt/i/mRW3vv/batterifergen-mf-ampere-sliter-igjen (Accessed 08.05.2020)

Muller, C. (1996) *World Railroad Records & Firsts.* URL: https://www.railserve.com/stats_records/railroad_firsts.html (Accessed 01.02.2020)

NASA (2014) *Mach number: Role in compressible gas*. URL: https://www.grc.nasa.gov/WWW/BGH/machrole.html (Accessed 10.02.2020)

Nave, R. (2000a) *Specific heat.*URL: http://hyperphysics.phy-astr.gsu.edu/hbase/thermo/spht.html (Accessed 01.05.2020)

Nave, R. (2016b) *Stefan-Boltzmann Law.* URL: http://hyperphysics.phy-astr.gsu.edu/hbase/thermo/stefan.html (Accessed 05.05.2020)

Nave, R. (2016c) *Electrochemical potential.* URL: http://hyperphysics.phy-astr.gsu.edu/hbase/Tables/electpot.html (Accessed 06.05.2020)

NCE Maritime CleanTech. (2019) *Norwegian future value chains for liquid hydrogen.* Norwegian Centers of Expertise Maritime CleanTech

Nexant. (2008) *H2A Hydrogen Delivery Infrastructure Analysis Models and Conventional Pathways Options Analysis Results.*

NIST (2018a) *Methane*. URL: https://webbook.nist.gov/cgi/cbook.cgi?ID=C74828&Mask=4#ref-14 (Accessed 13.03.2020)

NIST. (2018b) *Hydrogen.* NIST Chemistry WebBook, SRD 69. URL: https://webbook.nist.gov/cgi/cbook.cgi?ID=C1333740&Mask=4 (Accessed 25.03.2020)

Norled. (2019a) *Norled velger Westcon I Ølen for bygging av verdens første hydrogen-ferje.* URL: https://www.norled.no/nyheter/norled-velger-westcon-i-olen-for-bygging-av-verdens-forste-hydrogen-ferje/ (Accessed 18.02.2020)

Norled. (2019b) *The appearance of the hydrogen ferry begins to take shape. URL:* https://www.norled.no/en/news/the-appearance-of-the-hydrogen-ferry-begins-to-take-shape/ (Accessed 18.02.2020)

Norled. (2019c) *Norled to build the world's first hydrogen ferry.* URL: https://www.norled.no/en/news/norled-to-build-the-worlds-first-hydrogen-ferry/ (Accessed 18.02.2020)

OpenStax. (2013) *Biology*. Chapter 2.1 Atoms, Isotopes, Ions, and Molecules: The Building Blocks. ISBN-10 1938168097 URL: https://cnx.org/contents/GFy_h8cu@9.87:vogY0C26@12/Atoms-Isotopes-Ions-and-Molecules-The-Building-Blocks (Accessed 06.05.2020)

Oslo Børs. (2019) *US dollar*. URL: https://www.oslobors.no/markedsaktivitet/#/details/USD.NB/overview (Accessed 08.05.2020)

Pauly, H. (2000) *Atom, Molecule and Cluster Beams I.* Springer Verlag. Berlin. URL: https://books.google.no/books?id=S5vsCAAAQBAJ&printsec=frontcover&dq=inauthor:%22Hans+Pauly%22&hl=en&sa=X&ved=0ahUKEwiil4WcspzoAhXq_CoKHePNDeIQ6AEIKTAA#v=onepage&q&f=false (Accessed 15.02.2020)

Pettersen, J. (2016) *LNG Technology.* 3rd edition. Compendium TEP 4185 – Natural Gas Technology

PILOT-E (2019) *Utlysning 2019.* URL: https://www.enova.no/pilot-e/utlysning-2019/ (Accessed 11.03.2020)

Potassium Formate for Runway Deicing. (2020) BASF Aerospace. URL: https://aerospace.basf.com/potassium-formate-for-runway-deicing.html (Accessed 01.05.2020)

Pratt, J. and Klebanoff, L. (2016) *Feasibility of the SF_BREEZE: A Zero-Emission, Hydrogen Fuel Cell, High-Speed Passenger Ferry.* Sandia National Laboratories Albuquerque.

Pratt, J. W. & Klebanoff, L. E. (2016) *Feasibility of the SF-BREEZE: a Zero-Emission, Hydrogen Fuel Cell, High-Speed Passenger Ferry.* Sandia National Laboratory. SAND2016-9719.

Pritchard, D. K. (2010) *Hazards of liquid hydrogen*. URL: https://www.hse.gov.uk/research/rrpdf/rr769.pdf (Accessed 15.04.2020)

Properties of Cryogenic Fluids. (2010) USPAS Cryogenic Short Course. MIT. Boston URL: https://uspas.fnal.gov/materials/10MIT/Lecture_1.3.pdf (Accessed 19.02.2020)

Properties of Seawater (2005) Engineering Toolbox URL: https://www.engineeringtoolbox.com/sea-water-properties-d_840.html (accessed 11.02.2020)

Rapp, B. (2016) *Microfluids: Modeling, Mechanics and Mathematics.* 1st edition. Elsiver. ISBN: 9781455731411. Chapter 9.9.3.

Rashad, A. (2017) *Hydrogen in fuel cells: An overview of promotions and demotions.* DOI: 10.15761/IJC.1000119 URL: https://www.oatext.com/hydrogen-in-fuel-cells-an-overview-of-promotions-and-demotions.php#Article_Info (Accessed 03.05.2020)

Rashe, K. (2019) *Van der Waals Force.* URL: https://chem.libretexts.org/Bookshelves/Physical_and_Theoretical_Chemistry_Textbook_Maps/Supplemental_Modules_(Physical_and_Theoretical_Chemistry)/Physical_Properties_of_Matter/Atomic_and_Molecular_Properties/Intermolecular_Forces/Van_der_Waals_Forces (Accessed 13.02.2020)

Recycling PEM Fuel Cells (2017) Ballard. Technical note. URL: https://www.ballard.com/docs/default-source/web-pdf's/recycling-technical-note_final.pdf (Accessed 19.03.2020)

Resistance and Powering of Ships. EN400: Principles of Ship Performance. United States Navan Academy. URL:https://www.usna.edu/NAOE/academics/en400.php Chapter 7. (Accessed 11.02.2020)

Rong, B. (2017) *How a Hydrogen Filling Station Works.* URL: https://www.roadandtrack.com/car-culture/g6917/how-hydrogen-filling-stations-work/?slide=2 (Accessed 08.05.2020)

Rong, B. (2017) *How a hydrogen filling station works.* URL: https://www.roadandtrack.com/car-culture/g6917/how-hydrogen-filling-stations-work/?slide=2 (Accessed 30.04.2020)

Royal Society of Chemistry. (2020) *Periodic table.* URL: https://www.rsc.org/periodic-table/ (Accessed 13.02.2020)

Schlichting, H and Gersten, K. (2000) *Boundary-Layer Theory.* Springer-Verlag. Berlin. Chapter 15.

Schumm, B. (2018) *Fuel cell.* URL: https://www.britannica.com/technology/fuel-cell (Accessed 16.03.2020)

Shapley, P. (2012) *Common Battery Types.* URL: http://butane.chem.uiuc.edu/pshapley/GenChem2/C6/3.html (Accessed 06.05.2020)

Ship Noise (2020) International Maritime Organization. URL: http://www.imo.org/en/MediaCentre/HotTopics/Pages/Noise.aspx (Accessed 17.03.2020)

Shipping and World Trade (2020) URL: https://www.ics-shipping.org/shipping-facts/shipping-and-world-trade (Accessed 01.02.2020)

Shippipedia (2013) *Propulsion Layouts.* URL: http://www.shippipedia.com/ships/propulsion-layouts/ (accessed 08.05.2020)

Siemens. (2019) *Elektrifisering av norges viktigste fergestrekning med rekordrask lading.* URL: http://www.mynewsdesk.com/no/siemens-as/pressreleases/elektrifiserer-norges-viktigste-fergestrekning-med-rekordrask-lading-2877270 (Accessed 07.05.2020)

Smith, L. (2019) *The ABCs of multi-layer insulation for space crafts.* URL: https://www.designnews.com/materials-assembly/abcs-multi-layer-insulation-spacecraft/114721359260796 (Accessed 05.05.2020)

Solbraa, E. (2019) *Key design selections for LNG plants.* TEP 08 – Gas processing and LNG.

Song, X. *Recent Developments in Silicon Anode Materials for High Performance Lithium-Ion Batteries.* URL: https://www.sigmaaldrich.com/technical-documents/articles/materials-science/recent-developments-in-silicon-anode-materials.html (Accessed 06.05.2020)

Stensvold, T. (2016) *89-tonn batterier I verdens største el-ferge.* Teknisk Ukeblad. URL: https://www.tu.no/artikler/89-tonn-batterier-i-verdens-storste-el-ferge/348995 (Accessed 06.05.2020)

Stensvold, T. (2017) *De lader ferge med 1,2 mW effect uten fysisk kontakt med fartøyet.* URL: https://www.tu.no/artikler/de-lader-ferge-med-1-2-megawatt-effekt-uten-fysisk-kontakt-med-fartoyet/409255 (Accessed 07.05.2020)

Stensvold, T. (2017) *Q 2021 vil Norge ha 60 ferger med batterier. Nå må Vegdirektoratet finne en standardløsning for lading*. URL: https://www.tu.no/artikler/i-2021-vil-norge-ha-60-ferger-med-batterier-na-ma-vegdirektoratet-finne-en-standardlosning-for-lading/414997 (Accessed 03.02.2020)

Stensvold, T. (2018) *Norled bygger verdens første hydrogen-ferge.* URL: https://www.tu.no/artikler/norled-bygger-verdens-forste-hydrogen-ferge/452526 (Accessed 18.02.2020)

Stensvold, T. (2019) *Island får sin første batteriferge.* Teknisk Ukeblad. URL: https://www.tu.no/artikler/island-far-sin-forste-batteriferge/458422 (Accessed 06.05.2020)

Stilwell *et. al.* (2018) *Ship.* Encyclopedia Britannica. URL: https://www.britannica.com/technology/ship/History-of-ships (Accessed 01.02.2020)

Sustainable Development Goals (2015) URL: https://www.undp.org/content/undp/en/home/sustainable-development-goals.html (Accessed 01.02.2020)

Svendsen, T. M. (2020) *Liquid hydrogen to decarbonize maritime transport in Norway: State-of-the-art PEM fuel cells for maritime applications.* CMR Prototech. Page 19.

Third IMO GHG Study (2014) URL: http://www.imo.org/en/OurWork/Environment/PollutionPrevention/AirPollution/Pages/Greenhouse-Gas-Studies-2014.aspx (Accessed 01.02.2020)

Tronstad, T. (2017) *Study on the Use of Fuel Cells in Shipping.* Page 34-41. EMSA and DNV GL

UCSB Science Line. (2013) *Why does saltwater freeze faster than freshwater?* URL: http://scienceline.ucsb.edu/getkey.php?key=3887 (Accessed 01.05.2020)

UN body adopts climate change strategy for shipping (2018) URL: http://www.imo.org/en/MediaCentre/PressBriefings/Pages/06GHGinitialstrategy.aspx (Accessed 01.02.2020)

United States Geological Survey. *Frozen carbon dioxide (dry ice) sublimates directly into a vapor.* URL: https://www.usgs.gov/media/images/frozen-carbon-dioxide-dry-ice-sublimates-directly-a-vapor (Accessed 13.02.2020)

Vacuum Jacketed Piping (2016) URL: https://h2tools.org/bestpractices/vacuum-jacketed-piping (Accessed 08.05.2020)

Vance J. E. (2018) *Ships* URL: https://www.britannica.com/technology/ship/Commercial-steam-navigation (Accessed 10.02.2020)

Venkatasamy, J. (2019) *Lithium-Ion Batteries – Price Trend and Cost Structure.* URL: https://www.beroeinc.com/article/lithium-ion-batteries-price-trend-cost-structure/ (Accessed 08.05.2020)

Vincenti, W. G. and Kruger, C. H. (1965) *Introduction to Physical Gas Dynamics.* Robert E. Krieger Publishing Company, New York. Chapter 1 to 7.

Wagner, S. (20104) *Conversion rate of para-hydrogen to ortho-hydrogen by oxygen: implications for PHIP gas storage and utilization.* Magn Reason Mater Phy 27, Page 195-199. DOI/URL: https://doi.org/10.1007/s100334-013-0399-y (Accessed 19.02.2020)

Wakeham, W. A. (2011) *Latent heat of vaporization.* DOI:10.1615/AtoZ.l.latent_heat_of_vaporization URL: http://www.thermopedia.com/content/916/ (Accessed 13.03.2020)

Walter, U. (2018) *Astronautics.* Springer Nature. Switzerland. Page. 758 DOI: https://doi.org/10.1007/978-3-319-74373-8

Wartsila. (2018a) *Wireless charging.* URL: https://www.wartsila.com/docs/default-source/product-files/ps/wireless-charging-leaflet-2018.pdf (Accessed 07.05.2020)

Wartsila. (2018b) *Wireless Charging* URL: https://www.wartsila.com/marine/build/power-systems/shore-connections/wireless-charging (Accessed 07.05.2020)

Wilhelmsen, Ø. (2017) *Reducing the exergy destruction in the cryogenic heat exchangers for hydrogen liquefaction processes.* SINTEF. Int. Jour. of Hyd. Ener. 43 (2018) Page 5033-5047. DOI/URL: https://doi.org/10.1016/j.ijhydene.2018.01.094 (Accessed 15.03.2020)

Xiao, J. (2010) *Stabilization of Silicon Anode for Li-Ion Batteries.* Journal of The Electrochemical Society. DOI: 10.1149/1.3464767 URL: https://www.pnnl.gov/science/highlights/highlight.asp?id=829 (Accessed 06.05.2020)

Zenith, F. et al. (2019) *Analyse av alternative driftsformer for ikke-elektrifiserte baner.* Sintef Raport 2019:00997. ISBN: 978-82-14-06371-4 Page 18.

Zhang, Y. (2011) *Corrected Values for Boiling Points and Enthalpies of Vaporization of Elements in Handbooks.* Journal of Chemical & Engineering Data. Vol 56. Page 331. URL: https://www.researchgate.net/publication/231538496_Corrected_Values_for_Boiling_Points_and_Enthalpies_of_Vaporization_of_Elements_in_Handbooks/stats (Accessed 13.03.2020)

9 Appendix

9.1.1 Code 1: FC consumption and efficiency to load

```
%Plot of consumption and efficiencies to load

n = 100; %Number of datapoints/iterations
loads = linspace(0.05,0.99,n); %Creating the load parameter
LHV = 30.03003; %g/kWh of hydrogen
%Empty variables to be used
BoL_consumption = zeros(1,n);
EoL_consumption = zeros(1,n);
BoL_efficiency = zeros(1,n);
EoL_efficiency = zeros(1,n);
%For-loop that fills the variable with the respective H2 consumption
for i = 1:n
 BoL_consumption(i) = FC_consumption_BoL(loads(i));
 EoL_consumption(i) = FC_consumption_EoL(loads(i));
end
%Plot of H2 consumption
figure
plot(loads*100,BoL_consumption,loads*100,EoL_consumption)
title('H2 Consumption of FC');
xlabel('Load');
ylabel('g/kWh');
xtickformat('percentage')
legend({'Beginning of Life','End of Life'}, 'location', 'northwest');
%For-loop that fills the variable with the respective FC efficency
for i = 1:n
 BoL_efficiency(i) = 100*LHV/FC_consumption_BoL(loads(i));
 EoL_efficiency(i) = 100*LHV/FC_consumption_EoL(loads(i));
end
%Plot of efficiency to load
figure
plot(loads*100,BoL_efficiency,loads*100,EoL_efficiency)
title('Efficiency of FC');
xlabel('Load');
ylabel('Efficiency');
xtickformat('percentage')
ytickformat('percentage')
legend({'Beginning of Life','End of Life'}, 'location', 'southwest');

%Function calculating the FC consumption at BoL
function Consumption=FC_consumption_BoL(load)

x = load; %variable to be used
```

```
Constant = 57.214;
p1 = -60.215;
p2 = 236.83;
p3 = -310.55;
p4 = 140.83;
p5 = 0;
p6 = 0;
%Calculates consumption in gH2/kWh
Consumption = Constant + p1*x + p2*x^2 + p3*x^3 + p4*x^4 + p5*x^5 + p6*x^6;

end

%Function calculating the FC consumption at EoL
function Consumption=FC_consumption_EoL(load)

x = load; %variable to be used
Constant = 55.605;
p1 = 1.6879;
p2 = 14.862;
p3 = -3.8031;
p4 = 7.7771;
p5 = 0;
%Calculates consumption in gH2/kWh
Consumption = Constant + p1*x + p2*x^2 + p3*x^3 + p4*x^4 + p5*x^5;

end

%Function calculating the FC consumption from load and age
function Consumption=FC_consumption(load,beta)

x = load;
b = beta; %Age factor

C_BoL = FC_consumption_BoL(x);
C_EoL = FC_consumption_EoL(x);

Consumption = C_BoL + b*(C_EoL - C_BoL);

end
```

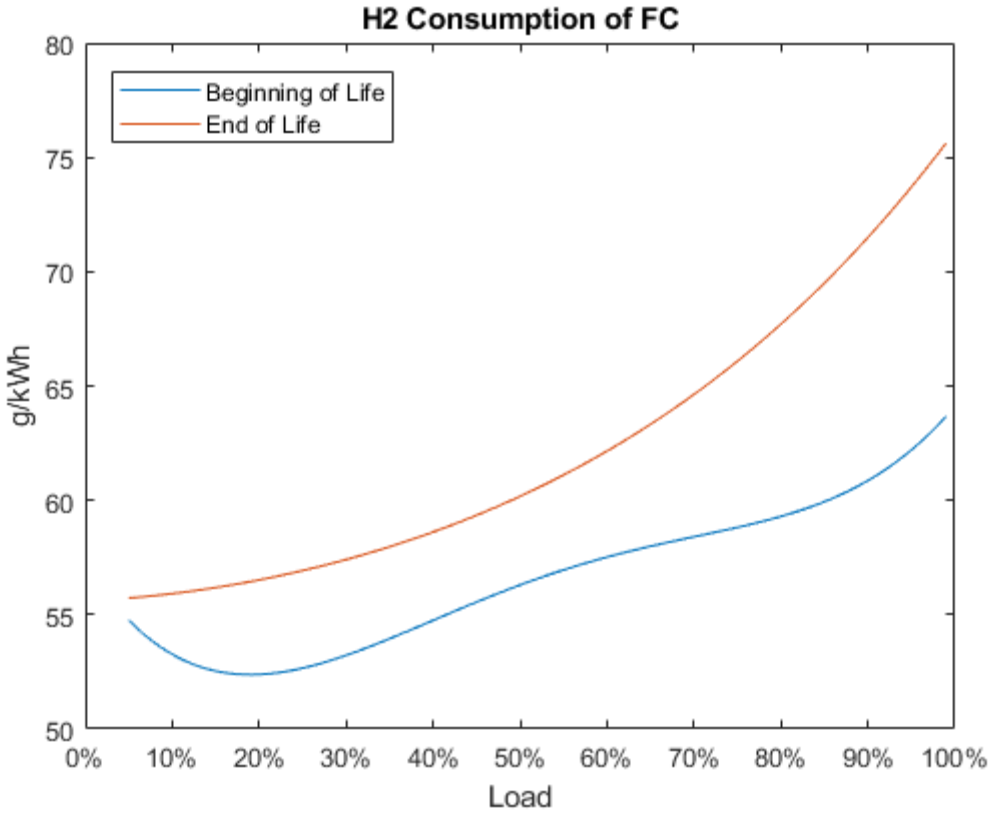

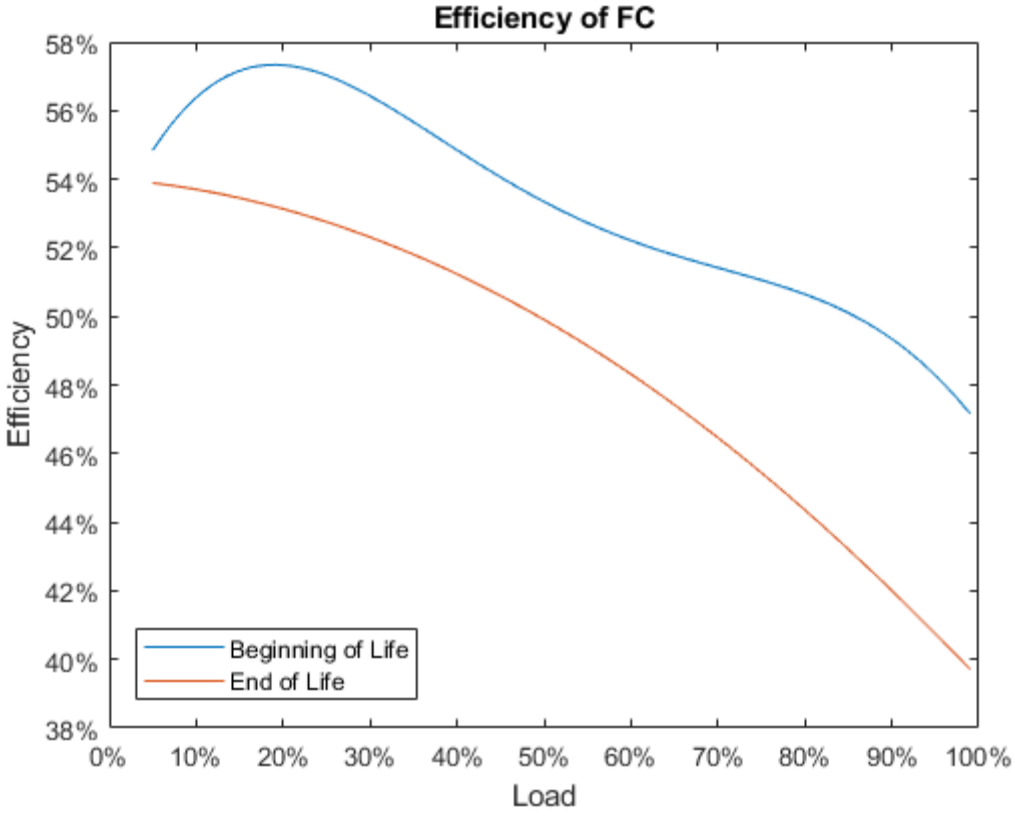

Published with MATLAB® R2017b

9.1.2 Code 2: Fuel mass flow calculations and plots

```
%mass flow plot
clc
%input
V_min_kts = 2; %minimum velocity in kts
V_max_kts = 14; %maximum velocity in kts
n = 1000; %Number of iterations
FC_tot = 4000; %Total FC capacity in kW

%Calculations
kts_to_mps = 0.51444; %Factor
V_min = V_min_kts*kts_to_mps; %Conversion to m/s
V_max = V_max_kts*kts_to_mps; %Conversion to m/s
dV = (V_max - V_min)/n; %Step size
%Creating empty variables
mass_flow_BoL = zeros(1,n);
mass_flow_EoL = zeros(1,n);
mass_distance_BoL = zeros(1,n);
mass_distance_EoL = zeros(1,n);

V = V_min; %Initial velocity
for i =1:n
    %Calculating the mass flow from velocity and total FC capacity
    [mass_flow_BoL(i), mass_flow_EoL(i)] = mass_flow(V,FC_tot); % kg/s
    %Conversion to mass per distance
    mass_distance_BoL(i) = mass_flow_BoL(i)/V; % kg/m
    mass_distance_EoL(i) = mass_flow_EoL(i)/V; % kg/m
    V = V + dV; %New velocity for next iteration
end

%Finds the lowest value in kg/s and the corresponding positin
[mass_flow_BoL_min,mass_flow_BoL_min_pos] = min(mass_flow_BoL);
%Converst the positin of lowest consumption to velocity
mass_flow_BoL_min_pos = mass_flow_BoL_min_pos*dV + V_min;
[mass_flow_EoL_min,mass_flow_EoL_min_pos] = min(mass_flow_EoL);
mass_flow_EoL_min_pos = mass_flow_EoL_min_pos*dV + V_min;

%Converts from kg/s to g/s
fprintf('The minimum mass flow is %.4f g/s at BoL and %.4f g/s at EoL
\n',mass_flow_BoL_min*1000,mass_flow_EoL_min*1000)
fprintf('These points are at %.4f m/s for BoL and %.4f m/s for EoL  \n
\n',mass_flow_BoL_min_pos, mass_flow_EoL_min_pos)

%Converts from kg/s to kg/h
fprintf('The minimum mass flow is %.4f kg/h at BoL and %.4f kg/h at EoL
\n',mass_flow_BoL_min*3600,mass_flow_EoL_min*3600)
%Coverts from m/s to kts
fprintf('These points are at %.4f kts for BoL and %.4f kts for EoL  \n
\n',mass_flow_BoL_min_pos/kts_to_mps, mass_flow_EoL_min_pos/kts_to_mps)

%Finds lowest value in kg/m and the corresponding position
[mass_distance_BoL_min,mass_distance_BoL_min_pos] = min(mass_distance_BoL);
[mass_distance_EoL_min,mass_distance_EoL_min_pos] = min(mass_distance_EoL);
%Converts the position of lowest consumption to velocity
```

```
mass_distance_BoL_min_pos = mass_distance_BoL_min_pos*dV + V_min;
mass_distance_EoL_min_pos = mass_distance_EoL_min_pos*dV + V_min;

%Converts from kg/m to g/m
fprintf('The minimum mass flow is %.4f g/m at BoL and %.4f g/m at EoL
\n',mass_distance_BoL_min*1000,mass_distance_EoL_min*1000)
fprintf('These points are at %.4f m/s for BoL and %.4f m/s for EoL  \n
\n',mass_distance_BoL_min_pos, mass_distance_EoL_min_pos)

%Converts from kg/m to kg/nm
fprintf('The minimum mass flow is %.4f kg/nm at BoL and %.4f kg/nm at EoL
\n',mass_flow_BoL_min*1852,mass_flow_EoL_min*1852)
%Converts from m/s to kts
fprintf('These points are at %.4f kts for BoL and %.4f kts for EoL  \n
\n',mass_distance_BoL_min_pos/kts_to_mps, mass_distance_EoL_min_pos/kts_to_mps)

%Plot of mass flow of hydrogen to speed in mps
figure
plot(linspace(V_min,V_max,n),mass_flow_BoL,linspace(V_min,V_max,n),mass_flow_EoL)
title('Mass flow of hydrogen to speed')
xlabel('m/s')
ylabel('kg/s')
legend('BoL','EoL','location','northwest')

%Plot of mass flow of hydrogen to speed in kts
figure
mass_flow_BoL = mass_flow_BoL*3600; %Converts to kg/h
mass_flow_EoL = mass_flow_EoL*3600;
plot(linspace(V_min_kts,V_max_kts,n),mass_flow_BoL,linspace(V_min_kts,V_max_kts,n),
mass_flow_EoL)
title('Mass flow of hydrogen to speed')
xlabel('knots')
ylabel('kg/h')
legend('BoL','EoL','location','northwest')

%Plot of mass flow of hydrogen to distance in mps
figure
plot(linspace(V_min,V_max,n),mass_distance_BoL*1000,linspace(V_min,V_max,n),mass_di
stance_EoL*1000)
title('Mass flow of hydrogen to distance')
xlabel('m/s')
ylabel('g/m')
legend('BoL','EoL','location','northwest')

%Plot of mass flow of hydrogen to distance in kts
figure
plot(linspace(V_min_kts,V_max_kts,n),mass_distance_BoL*1852,linspace(V_min_kts,V_ma
x_kts,n),mass_distance_EoL*1852)
title('Mass flow of hydrogen to distance')
xlabel('knots')
ylabel('kg/nm')
legend('BoL','EoL','location','northwest')

%Function calculating mass flow
function [mass_flow_BoL, mass_flow_EoL] = mass_flow(V,FC_total_capacity)
```

```
Power = Speed_to_Power(V); %Returns power in kW
x = Power/FC_total_capacity; %Calculates the ratio of power to capacity
C_BoL = FC_consumption_BoL(x); %Returns C in gH2/kWh
C_EoL = FC_consumption_EoL(x);
mass_flow_BoL = Power*C_BoL/(3600*1000); %Calculates mass flow in kg per second
mass_flow_EoL = Power*C_EoL/(3600*1000);

end

%Function calculating the FC consumption at BoL
function Consumption=FC_consumption_BoL(load)

x = load; %variable to be used
Constant = 57.214;
p1 = -60.215;
p2 = 236.83;
p3 = -310.55;
p4 = 140.83;
p5 = 0;
p6 = 0;
%Calculates consumption in gH2/kWh
Consumption = Constant + p1*x + p2*x^2 + p3*x^3 + p4*x^4 + p5*x^5 + p6*x^6;

end

%Function calculating the FC consumption at EoL
function Consumption=FC_consumption_EoL(load)

x = load; %variable to be used
Constant = 55.605;
p1 = 1.6879;
p2 = 14.862;
p3 = -3.8031;
p4 = 7.7771;
p5 = 0;
%Calculates consumption in gH2/kWh
Consumption = Constant + p1*x + p2*x^2 + p3*x^3 + p4*x^4 + p5*x^5;

end

function Power=Speed_to_Power(Velocity) %Takes in velocity in METERS PER SECOND.

V = Velocity;%variable to be used
Constant = 470.38 + 200; %the unctional constant pluss the base load
p1 = -445.25; %polynomial 1
p2 = 164.83;
p3 = -18.797;
p4 = 1.6244;

Power = Constant + p1*V + p2*V^2 + p3*V^3 + p4*V^4; %Calculates power in kW


end
```

```
The minimum mass flow is 4.6408 g/s at BoL and 4.8129 g/s at EoL

These points are at 1.7882 m/s for BoL and 1.7882 m/s for EoL


The minimum mass flow is 16.7069 kg/h at BoL and 17.3265 kg/h at EoL

These points are at 3.4760 kts for BoL and 3.4760 kts for EoL


The minimum mass flow is 2.1166 g/m at BoL and 2.2140 g/m at EoL

These points are at 2.6278 m/s for BoL and 2.5845 m/s for EoL


The minimum mass flow is 8.5948 kg/nm at BoL and 8.9135 kg/nm at EoL

These points are at 5.1080 kts for BoL and 5.0240 kts for EoL
```

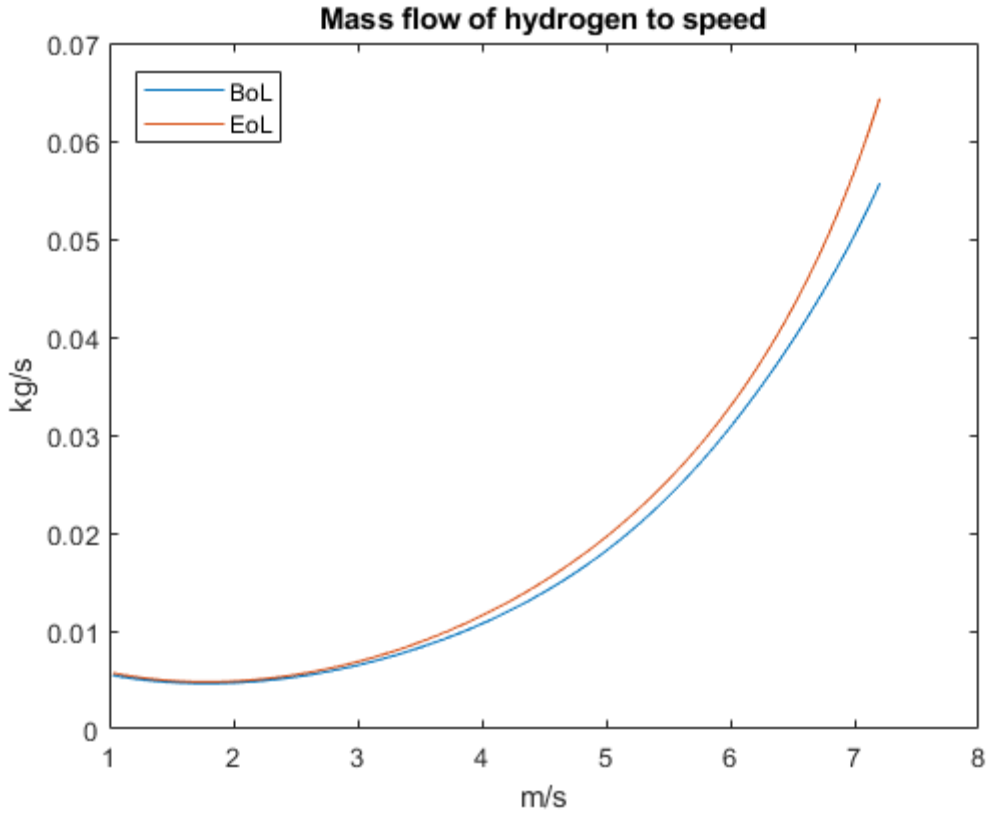
Mass flow of hydrogen to speed
BoL
EoL
kg/s
m/s
0.07
0.06
0.05
0.04
0.03
0.02
0.01
0
1
2
3
4
5
6
7
8

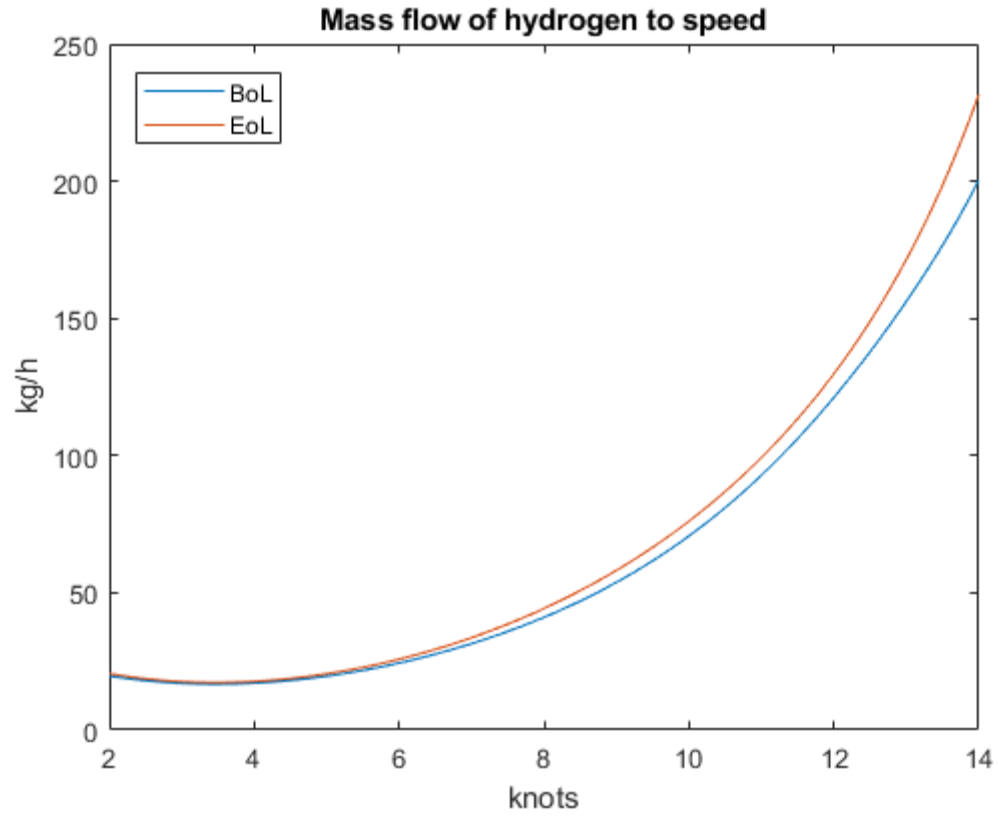
Mass flow of hydrogen to speed
BoL
EoL
kg/h
knots
250
200
150
100
50
0
2
4
6
8
10
12
14

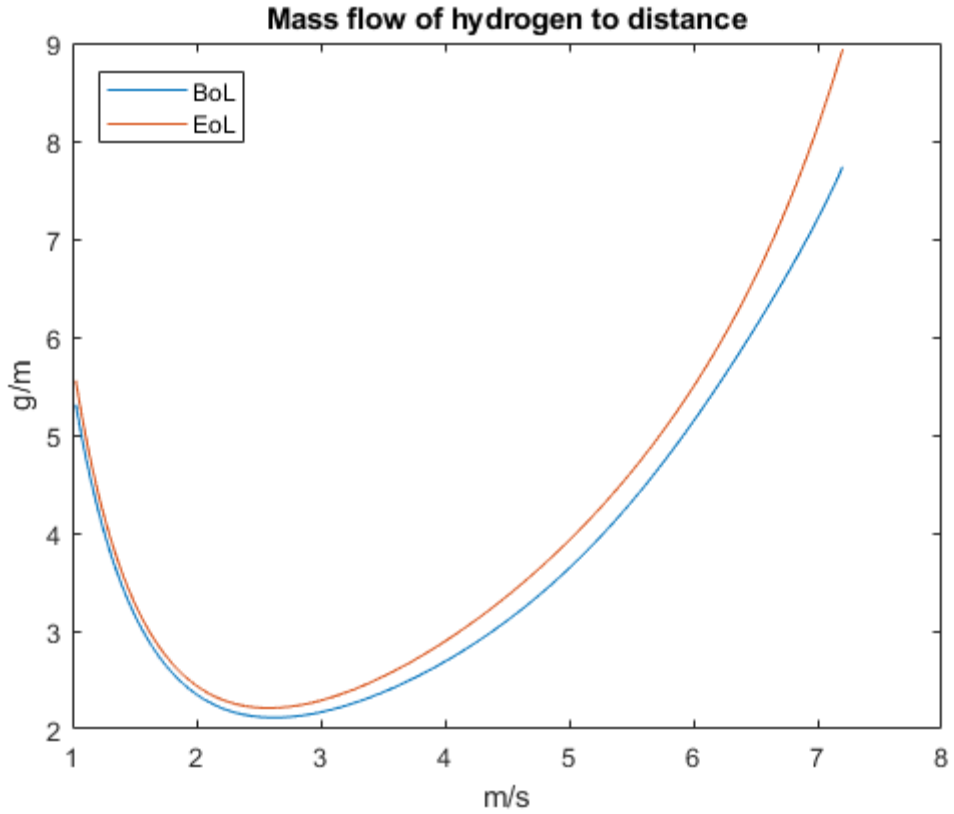

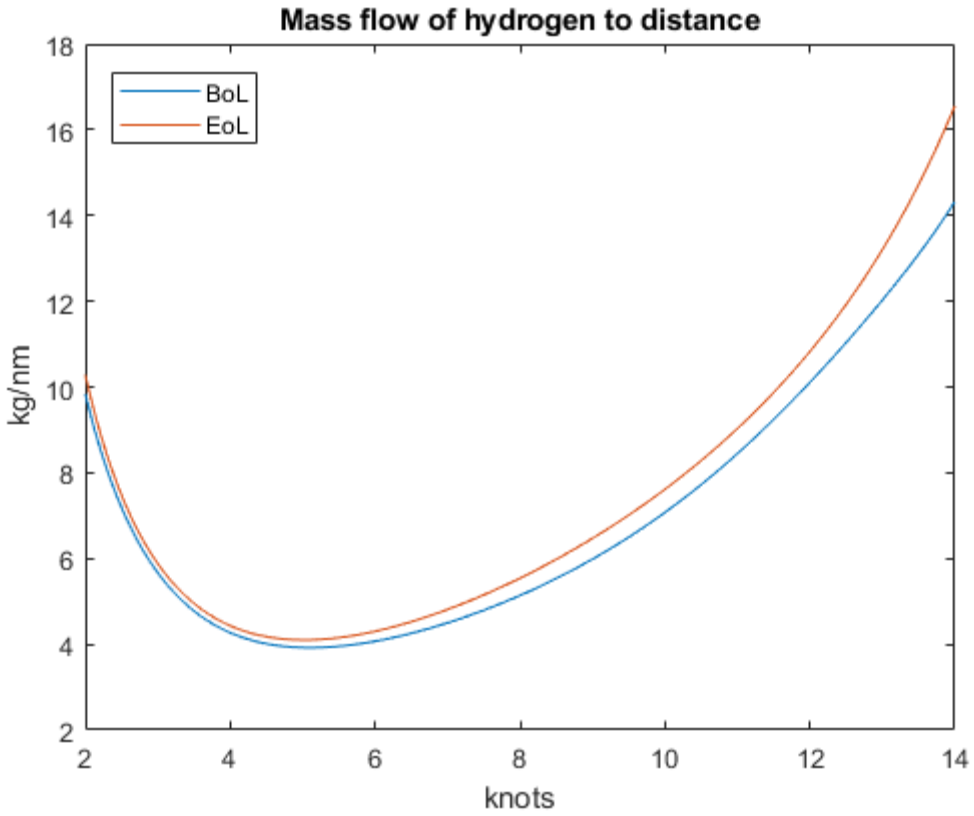

Published with MATLAB® R2017b

9.1.3 Code 3: Calculation on pressure to flow rate to ship

```
%Flow rate calculations

    %///////Inputs\\\\\\\\\\
    h = 13.8; %Height difference between tanks in meters
    L = 2*h; %Assumes that pipe is twice as long as height difference
    ro = 71; %Density of liquid hydrogen in kg/m^3
    my = 131.98*10^-7; %Viscosity of LH2 at T=20K -
https://www.bnl.gov/magnets/Staff/Gupta/cryogenic-data-handbook/Section3.pdf
    g = 9.81; %Gravity in m/s^2
    mass_flow = 60; %Hydrogen to be pumped in kg/min
    pipe_roughness = 0.000015;%Roughness of pipe, 0 for smooth 0.015mm for
stainless steel but given in meter https://www.enggcyclopedia.com/2011/09/absolute-
roughness/
    D_min = 0.035; %Smallest diameter in meters
    D_max = 0.085; %largest diameter in meters
    n = 1000; %Number of iterations
    P2 = 1.0; %Gauge pressure in tank on ship in barg
    K_L = 2.7; %Total coefficient of minor losses

    %Calculations
    mass_flow = mass_flow/60; %Conversion to kg/s
    dD = (D_max - D_min) / n; %Diameter differential
    D = D_min; %Initial diameter
    %Empty variable
    P = zeros(1,n);

    P_gravity = ro*g*h; %Gravity component
    %For-loop calculating the pressure in the land tank
    for i = 1:n

        P_velocity = 8*(mass_flow^2)/(ro*(pi^2)*D^4); %Velocity component
        relative_roughness = pipe_roughness/D;
        Re = 4*mass_flow*L/(my*pi*D^2); %Reynolds number
        f = Darcy(Re,relative_roughness); %Friction coefficient from darcy formula

        L_equiv = D*K_L/f; %Equivalent length of friction presser drop from minor
losses
        P_friction = f*8*(L + L_equiv)*(mass_flow^2)/(ro*(pi^2)*(D^5));

        P(i) = (P_velocity + P_gravity + P_friction)*10^-5 + P2;
        D = D + dD;

    end
    %Plot of the pressure to pipe diameter
    plot(linspace(D_min*1000,D_max*1000,n),P);
    title(sprintf('Pressure in tank on land to maintain %d kg/min flow rate to
diameter',mass_flow*60 ))
    xlabel('Diameter [mm]')
    ylabel('barg')

    %Numerical estimation of the darcy friction factor
    function friction = Darcy(Re,relative_roughness)
```

```
    F = - 1.8*log10(6.9/Re + (relative_roughness /3.7).^1.11); %http://snst-
hu.lzu.edu.cn/zhangyi/ndata/Haaland_equation.html
    f = [10, 1/F^2];
    while abs(f(2) - f(1)) > 10^-8
        F = -2*log10(relative_roughness/3.7 + 2.51/(Re*f(2)^2));
        f = [f(2),1/F^2];
    end
    friction = f(2);
    end
```

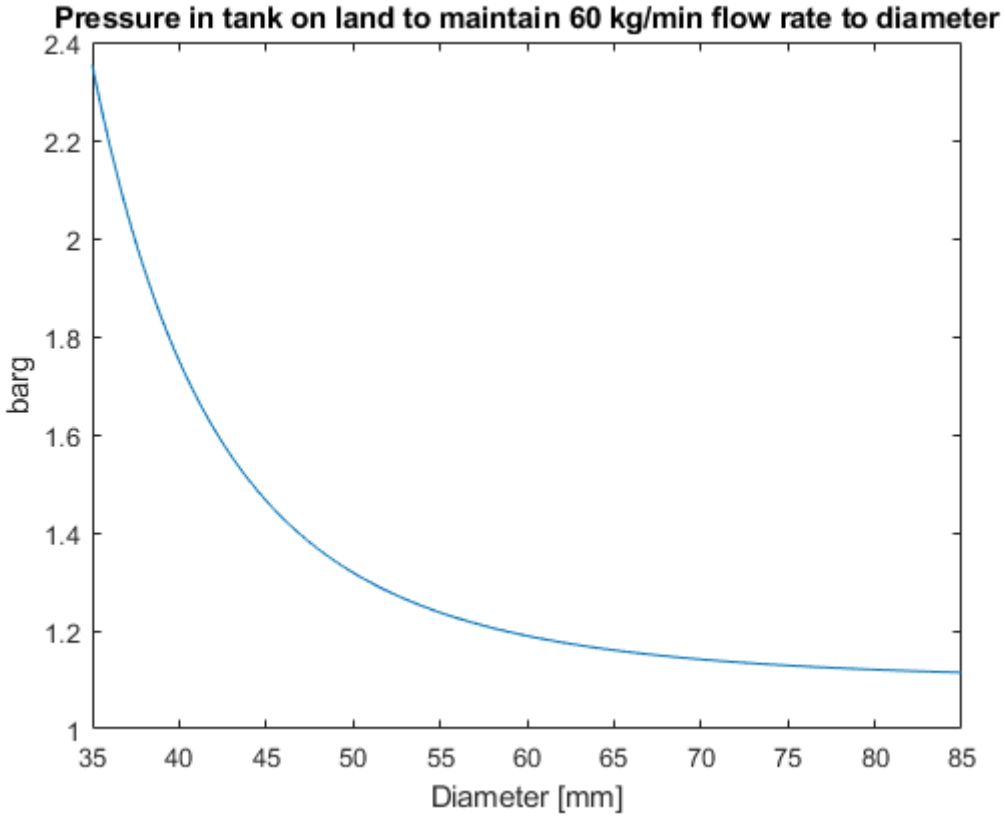

Published with MATLAB® R2017b

9.1.4 Code 4: Calculator and plot of hydrogen density to pressure and temperature

```
%Density plot

T_min = 40; %Minimum temperature in kelvin
T_max = 400; %Maximum temperature in kelvin
P_min = 1; %Minimum pressure in bar
P_max = 50; %MAximum pressure in bar

n = 300; %Number of iterations for temperture
m = 4;  %Number of pressure levels
dT = (T_max - T_min)/n; %Temperature differential
density = zeros(m,n); %Empty variable
%List over pressure levels
P = [1 2 3 4]; %Not dynamic
%For-loop for pressure levels
```

```
for j = 1:m
   T = T_min; %initial temperature
   %For-loop for temperatures for the respective pressure level
    for i = 1:n
    density(j,i) = Density(P(j),T);
    T = T +dT;
    end
end
%Plot of density to temperature
plot(linspace(T_min,T_max,n),density);
title('Density to temperture at different pressures')
xlabel('Temperature [K]');
ylabel('Density [kg/m^3]');
legend({'1 bar','2 bar','3 bar','4 bar'}, 'location', 'northeast');

%Density calculator
function ret = Density(P,T) % Takes in pressure in bar and temperature in kelvin

P = 0.986923*P; %Converting pressure from bar to atmospheres
R = 82.0597; %cm^3-atm/mol-K   General gas constant

if T <= 100 %Temperature below 100 K
    %Calculations of B
    b1 = 1.9397741*10^3;
    b2 = -1.9279522*10^5;
    b3 = -2.2890051*10^6;
    b4 = 1.1094088*10^7;

    B = (b1*T + b2 + b3/T + b4/(T^2))/(R*T);

    %Calculations of C
    if T <= 55 %Temperatures below 55 K

        if T < 32.957 %Temperatures below the critical temperature

            c1 = 1.0541776*10^5;
            c2 = -1.6597141*10^7;
            c3 = 1.0431411*10^9;
            c4 = -3.2538718*10^10;
            c5 = 5.1405848*10^11;
            c6 = -3.3123453*10^12;
        else %Temperatures between the critical point and 55 K

            c1 = 1.6971294*10^3;
            c2 = -5.0854223*10^5;
            c3 = 6.7284118*10^7;
            c4 = -3.8045171*10^9;
            c5 = 1.0789413*10^11;
            c6 = -1.1515642*10^12;

        end

        C = (c1*(T^2) + c2*T + c3 + c4/T + c5/(T^2) + c6/(T^3))/(R*T);

    else %Temperatures between 55 K and 100 K
```

```
        a1 = 388.682;
        a2 = 45.5;
        a3 = 0.6;
        a4 = 20;
        a5 = 4;
        C = a1*exp(a2/T)*(1 - exp(a3*(1 - (T/a4)*a5)));

    end

end

if T > 100; %temperatures above 100 K

    b = [42.464, -37.1172, -2.2982, 3.0484];
    x1 = 109.781/T;
    x2 = 20.615/T;
    c1 = 1310.5;
    c2 = 2.1486;
    B = 0;
    for i=1:4

        B = B + b(i)*(x1^((2*i-4)/4));
    end

    C = c1*sqrt(x2)*(1 + c2*(x2^3))*(1 - exp(1 - x2^(-3)));
end
syms ro
eqn = R*T*ro*(1 + B*ro + C*(ro^2)) - P == 0; %Equation for density in mol/cm3
ro1 = vpasolve( eqn, ro); %Solves the equation -> 3 solutions
ro2 = ro1(real(ro1)>0&imag(ro1)==0); %The solutions that are real and above zero
ro3 = ro2*2.016*10^3; % Converts the densities to kg/m^3
ret = ro3; %returns the solution
end
```

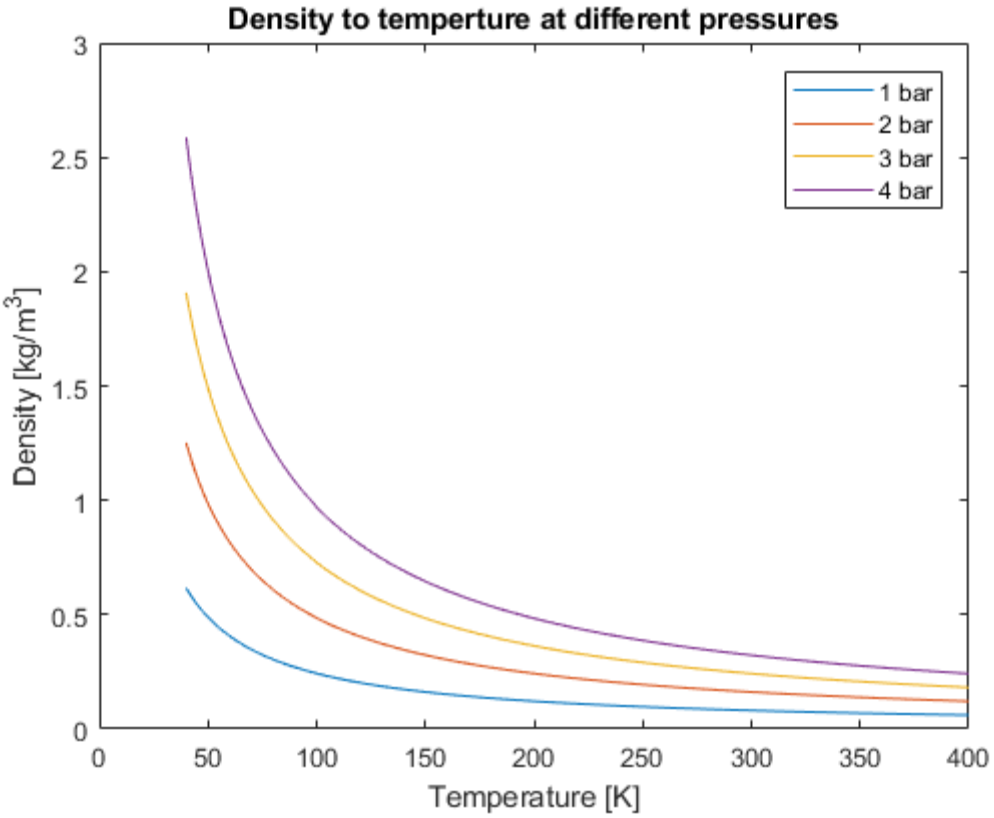

Published with MATLAB® R2017b

9.1.5 Code 5: Numeric calculator for pressure from density and temperature

```
%From density and temperature to pressure

density_target = min(Density(2.0,22.8))  %Finds the target density
Temperature = 300; %Temperature of target situation
P_min = 1; %Initial guess for lower pressure
P_max = 100; %Initial guess for upper pressure

density = Density(P_min,Temperature);

P_high = P_max;
P_low = P_min;
while abs(density - density_target) > 10^-4
    P = P_low + (P_high - P_low)/2; %Defines P as the mean between the limits
    density = Density(P,Temperature); %calculates the density with the mean

    if density > density_target %If the density is too high
        P_high = P_high - (P_high - P_low)/2; %Finds the new upper pressure

    elseif density < density_target %If the density is too low

        P_low = P; %Finds the new lower pressure
    end
```

```
end

density_target
density
P

%Density calculator
function ret = Density(P,T) % Takes in pressure in bar and temperature in kelvin

P = 0.986923*P; %Converting pressure from bar to atmospheres
R = 82.0597; %cm^3-atm/mol-K   General gas constant

if T <= 100 %Temperature below 100 K
    %Calculations of B
    b1 = 1.9397741*10^3;
    b2 = -1.9279522*10^5;
    b3 = -2.2890051*10^6;
    b4 = 1.1094088*10^7;

    B = (b1*T + b2 + b3/T + b4/(T^2))/(R*T);

    %Calculations of C
    if T <= 55 %Temperatures below 55 K

        if T < 32.957 %Temperatures below the critical temperature

            c1 = 1.0541776*10^5;
            c2 = -1.6597141*10^7;
            c3 = 1.0431411*10^9;
            c4 = -3.2538718*10^10;
            c5 = 5.1405848*10^11;
            c6 = -3.3123453*10^12;
        else %Temperatures between the critical point and 55 K

            c1 = 1.6971294*10^3;
            c2 = -5.0854223*10^5;
            c3 = 6.7284118*10^7;
            c4 = -3.8045171*10^9;
            c5 = 1.0789413*10^11;
            c6 = -1.1515642*10^12;

        end

        C = (c1*(T^2) + c2*T + c3 + c4/T + c5/(T^2) + c6/(T^3))/(R*T);

    else %Temperatures between 55 K and 100 K

        a1 = 388.682;
        a2 = 45.5;
        a3 = 0.6;
        a4 = 20;
        a5 = 4;
        C = a1*exp(a2/T)*(1 - exp(a3*(1 - (T/a4)*a5)));

    end
```

```
end

if T > 100; %temperatures above 100 K

    b = [42.464, -37.1172, -2.2982, 3.0484];
    x1 = 109.781/T;
    x2 = 20.615/T;
    c1 = 1310.5;
    c2 = 2.1486;
    B = 0;
    for i=1:4

        B = B + b(i)*(x1^((2*i-4)/4));
    end

    C = c1*sqrt(x2)*(1 + c2*(x2^3))*(1 - exp(1 - x2^(-3)));
end
syms ro
eqn = R*T*ro*(1 + B*ro + C*(ro^2)) - P == 0; %Equation for density in mol/cm3
ro1 = vpasolve( eqn, ro); %Solves the equation -> 3 solutions
ro2 = ro1(real(ro1)>0&imag(ro1)==0); %The solutions that are real and above zero
ro3 = ro2*2.016*10^3; % Converts the densities to kg/m^3
ret = ro3;
end
```

```
density_target =

2.500472105266869746508319210814 8

density_target =

 2.500472105266869746508319210814 8

density =

2.500376622253122339419525443141

P =

   32.2124
```

Published with MATLAB® R2017b

9.1.6 Code 6: Para to ortho distribution

```
%Plot of para and ortho hydrogen distribution

%Inputs
T_low = 20.00; %Low temperature of plot in Kelvin
```

```
T_high = 300.00; %High temperature of the plot in Kelvin
n = 1000; %Resolution of plot

%Constants
Tc = 32.937; %Critical temperature of hydrogen in Kelvin
dT  = (T_high-T_low)/n; %Temperature delta
%dE = 1.4169; %Conversion energy from para to orthohydrogen in kJ/mol

X_p = zeros(1,n);
X_o = zeros(1,n);

T=T_low-dT;
for i=1:n
    T=T+dT;
    t=T/Tc;
    X_p(i)= 0.1*((exp(-5.313/t)+0.1)^-1)-2.52*(10^-4)*(t^3)+3.71*(10^-3)*(t^2)-
2.04*(10^-3)*t-0.00227;
    X_o(i)=1-X_p(i);
end
T=linspace(T_low,T_high,n);
hold on;

plot(T,X_o)
ylim([0,1]);
xlim([19,300])
xticks([20 50 100 150 200 250 300]);
title('Molar percentage of Ortho hydrogen vs temperature');
xlabel('Temperature [K]')
ylabel('Molar fraction Ortho hydrogen')

hold off;
```

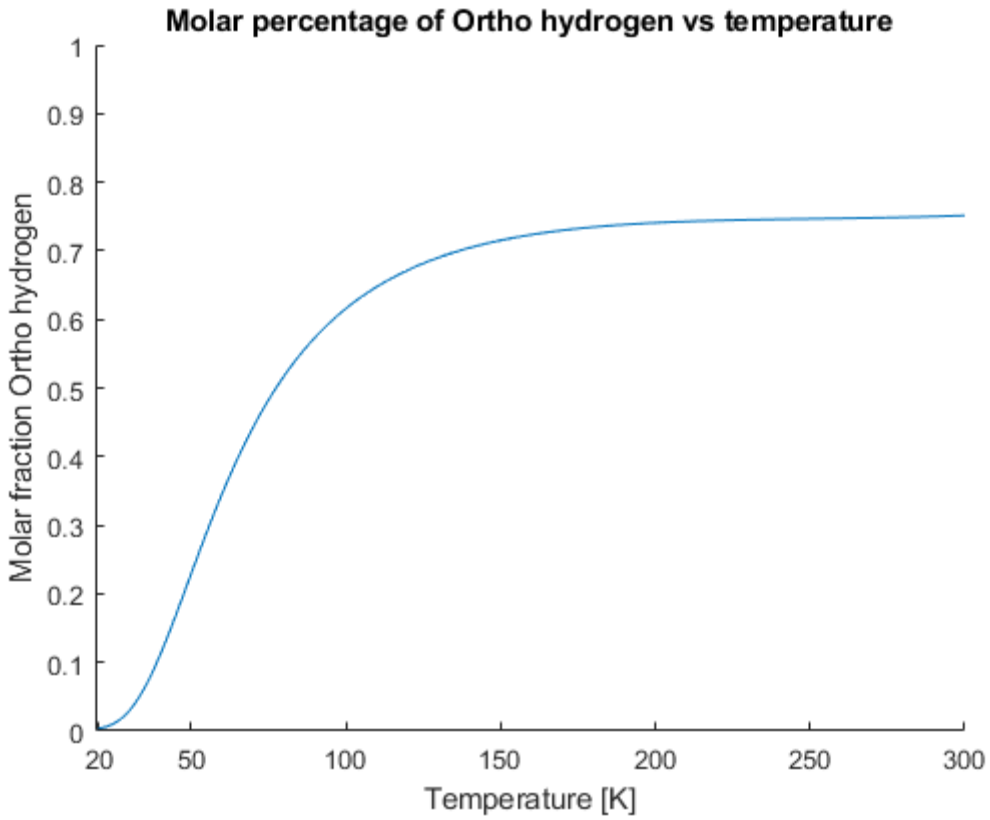

Published with MATLAB® R2017b

9.1.7 Code 7: Specific heat

```
%Specific heat plot and calculations

T_start = 29;  %Boiling point of hydrogen at 7 bara
T_end = 300;   %Ambient temperature
n = 1000;      %Number of iterations
R = 4.124;     %Hydrogen gas constant
LHV = 33.33;   %Lower heating value kWh/kg
H_vap = 322.691; %Latent heat of evaporation kJ/kg
Efficiency_ref = 0.51; %Efficiency of FC for referance case

dT = (T_end - T_start)/n; %Time differential
%Empty variables
Cv_tr = zeros(1,n);
Cv_rot = zeros(1,n);
Cv_nuc = zeros(1,n);
Cv_vib = zeros(1,n);
Cv = zeros(1,n);
Energy_ratio = zeros(1,n);
Energy_ratio_ref = zeros(1,n);

LHV = LHV*3600; %Conversion to kJ/kg
T = T_start;    %First temperature
Energy = H_vap; %Evaporation energy
```

```
for i = 1:n
    [Cv_tr(i), Cv_vib(i), Cv_rot(i),Cv_nuc(i)] = Specific_heat(T);
    T = T + dT;
    Cv(i) = Cv_tr(i) + Cv_rot(i);
    Energy = Energy + Cv(i)*dT;
    Energy_ratio(i) = Energy/LHV;
    Energy_ratio_ref(i) = Energy_ratio(i)/Efficiency_ref;
end
C_average = Energy/(T_end-T_start) %Calculation of average specific heat
%Plots
yyaxis left
plot(linspace(T_start,T_end,n),Cv)
title('Isochoric specific heat of hydrogen and total heat absorbed by fuel to
temperature');
xlabel('[K]')
ylabel('[kJ/kg K]')

yyaxis right
plot(linspace(T_start,T_end,n),Energy_ratio*100,linspace(T_start, ...
    T_end,n),Energy_ratio_ref*100)
ylabel('Percentage')
ytickformat('percentage')
legend('Specific heat - left axis','Total heat - right axis','Total heat adjusted
for efficiency - right axis','location','southeast')

function [Cv_tr, Cv_vib, Cv_rot, Cv_nuc] = Specific_heat(T) %takes in
                        %temperature and returns specific heat in kJ/kgK
%Constants
R = 4.124; %Specific gas constant of hydrogen in kJ/kgK.
sigma = 1; %symmetry factor

%Translational energy
Cv_tr = (3/2)*R; %Specific translational energy in kJ/kgK.

%Vibrational energy
T_char_vib = 6320; %Characteristic temperature of vibration in Kelvin
%Cv_vib = R * ((T_char_vib/2*T)/sinh(T_char_vib/2*T))^2;
Cv_vib = R * ((T_char_vib/T)^2)*exp(T_char_vib/T)/((exp(T_char_vib/T)-1)^2);

%Rotational energy
T_char_rot = 87.5; %Characteristic temperature of rotation in Kelvin.

if T <= T_char_rot
    Cv_rot = (12/sigma)*R*((T_char_rot/T)^2)*exp(-2*T_char_rot/T);
elseif T > 200
    Cv_rot = R/sigma;
else
    x_c = T/112.5 - 7/9;
    Cv_rot = (1 - x_c)*((12/sigma)*R*((T_char_rot/T)^2)*exp(-2*...
        T_char_rot/T)) + x_c*(R/sigma);
end
%Para/Ortho conversion
Conversion_energy = 702.83; %kJ/kg
T_crit = 32.938; %Kelvin
tau = T/T_crit;
```

```
A = 0.5313*exp(-5.313/tau)/(((tau^2)*(exp(-5.313/tau)+0.1)^2));
B = 7.56*(10^-4)*(tau^2) - 7.42*(10^-3)*tau + 2.04*(10^-3);
Cv_nuc = Conversion_energy*(A + B)/T_crit;
end
```

```
C_average =

   12.0437
```

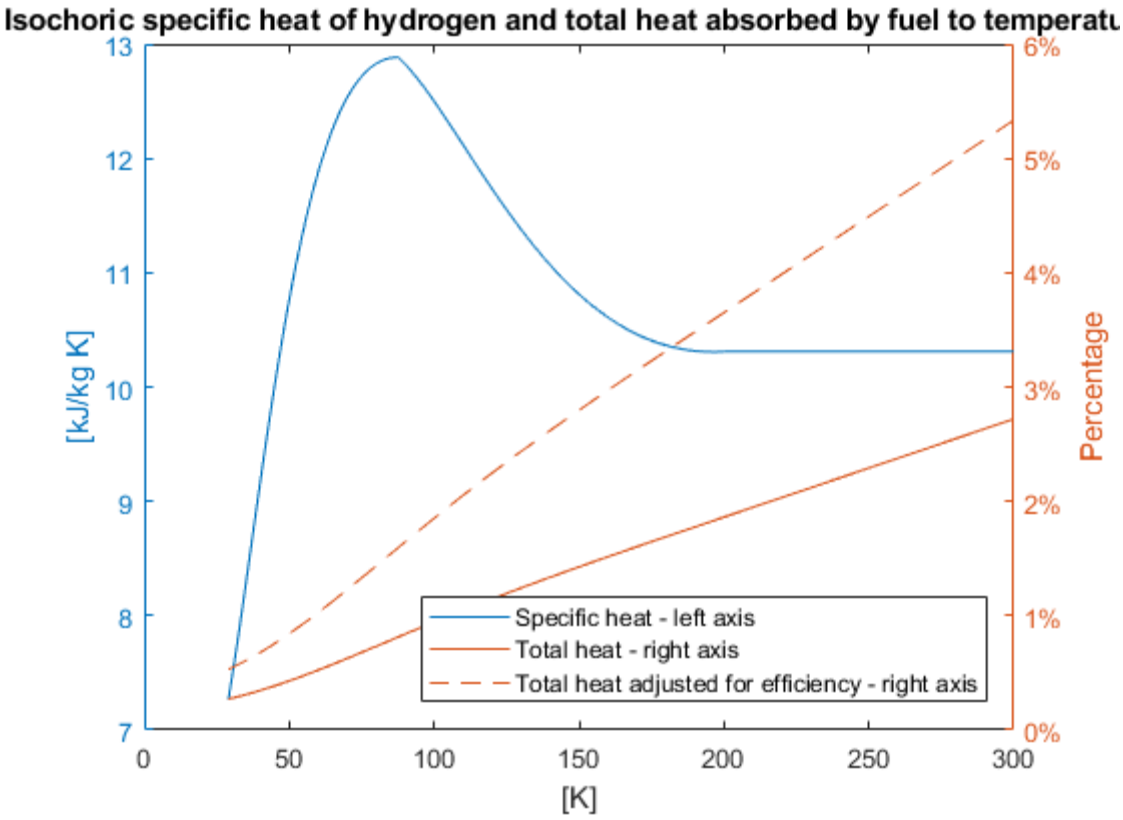

Published with MATLAB® R2017b

9.1.8 Code 8: Mass flow of Freezium

```
%Mass flow of Freezium for EoL conditions

%EoL
q_sea = 2002.33;  %Heat out to the sea
q_fuel = 122.28;  %Heat in to fuel
q_FC = 2124.61;    %Heat out from FC
Cp = 2.75;        %kJ/kgK of Freezium
T_FC_lim = 70;    %Limit for temp out of FC
T_sea_lim = 10;       %Limit for temp in to FC

%Assumes similar limits on both
dT_lim_low = 1;   %Lowest margin to limits
dT_lim_high = 20; %Higest margin to limits
n = 100;          %Number of iterations
DT = (dT_lim_high - dT_lim_low)/n; %Time differential
```

```
%Empty variables
mass_flow = zeros(1,n);
T_FC = zeros(1,n);
T_sea = zeros(1,n);
T_fuel = zeros(1,n);
dT = dT_lim_low;  %Initial limit
for i = 1:n
    T_FC(i) = T_FC_lim - dT;
    T_sea(i) = T_sea_lim + dT;
    dT_FC = T_FC(i) - T_sea(i); %Calculates the temperature
                                %delta over the FC

    mass_flow(i) = q_FC/(dT_FC * Cp);  %Using the temperature difference to
                                       %calculate the respective mass flow

    dT_fuel = q_fuel/(mass_flow(i) * Cp); %Using the mass flow to calculate
                                          %the other temperature deltas
    dT_sea = q_sea/(mass_flow(i) * Cp);

    T_fuel(i) = dT_sea + T_sea(i);  %Use the new temperature delta to
                                    %calculate the tmeperature out from
                                    %the fuel HX

    dT = dT + DT;                   %Finding the next temperature delta
end
%Plot mass flow of freezium
yyaxis left
plot(linspace(dT_lim_low,dT_lim_high,n),mass_flow)
title('Mass flow of Freezium and temperatures to temperature delta - EoL')
xlabel('Temperature delta in degrees celsius')
ylabel('[kg/s]')

yyaxis right
plot(linspace(dT_lim_low,dT_lim_high,n),T_FC,linspace(dT_lim_low,dT_lim_high,n),T_f
uel,linspace(dT_lim_low,dT_lim_high,n),T_sea)
ylabel('[Degrees Celsius]')
legend('Freezium mass flow','T out from FC','T out from fuel HX','T out from sea
HX','location','southeast')
```

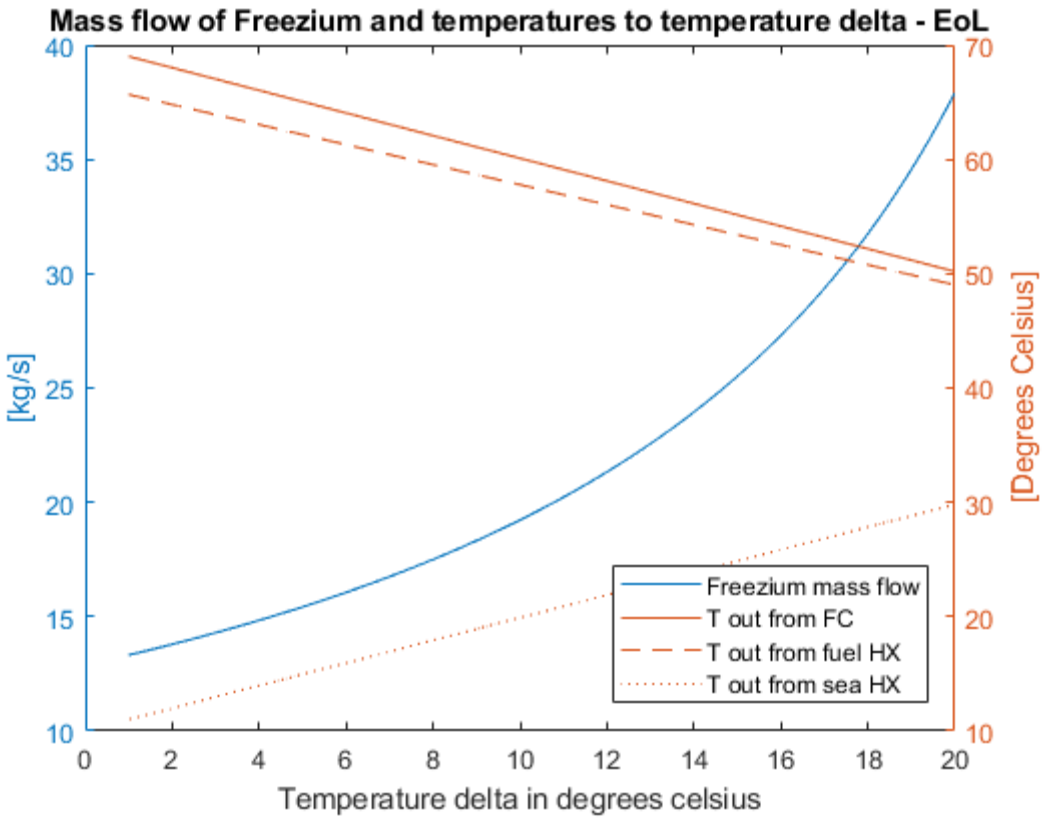

Published with MATLAB® R2017b

9.1.9 Code 9: Polytropic head and power from air compression

```
%Polytropic head of air compression

%Constants and input
T_1 = 283;    %Ambient temperature
P_1 = 1;      %Bar
P_2 = 5;
R = 0.28703; %kJ/kgK
nP = 0.925;     %Polytropic efficiency
nM = 0.95;    %Mechanical efficiency
k = 1.40;     %Specific heat ratio
mass_flow_BoL = 4628.57;     %kg/h
mass_flow_EoL = 4958.86;     %kg/h
Z = 1;        %Compressibility factor

%Calculations

mass_flow_BoL = mass_flow_BoL/3600; %Conversion to kg/s
mass_flow_EoL = mass_flow_EoL/3600;

n = 1/(1 - (k - 1)/(k*nP)); %Calculations of polytropic exponent

Hp = (n/(n - 1))*Z*R*T_1*((P_2/P_1)^((n - 1)/n) - 1)
%T_2 = T_1*((P_2/P_1)^((n-1)/n))
%cp_air = 1; %kJ/kgK
```

```
%Q = cp_air*(T_2 - T_1)*mass_flow_BoL
Power_BoL  = mass_flow_BoL*Hp/(nP*nM)
Power_EoL  = mass_flow_EoL*Hp/(nP*nM)
```

```
Hp =

  169.3557

Power_BoL =

  247.7872

Power_EoL =

  265.4690
```

Published with MATLAB® R2017b

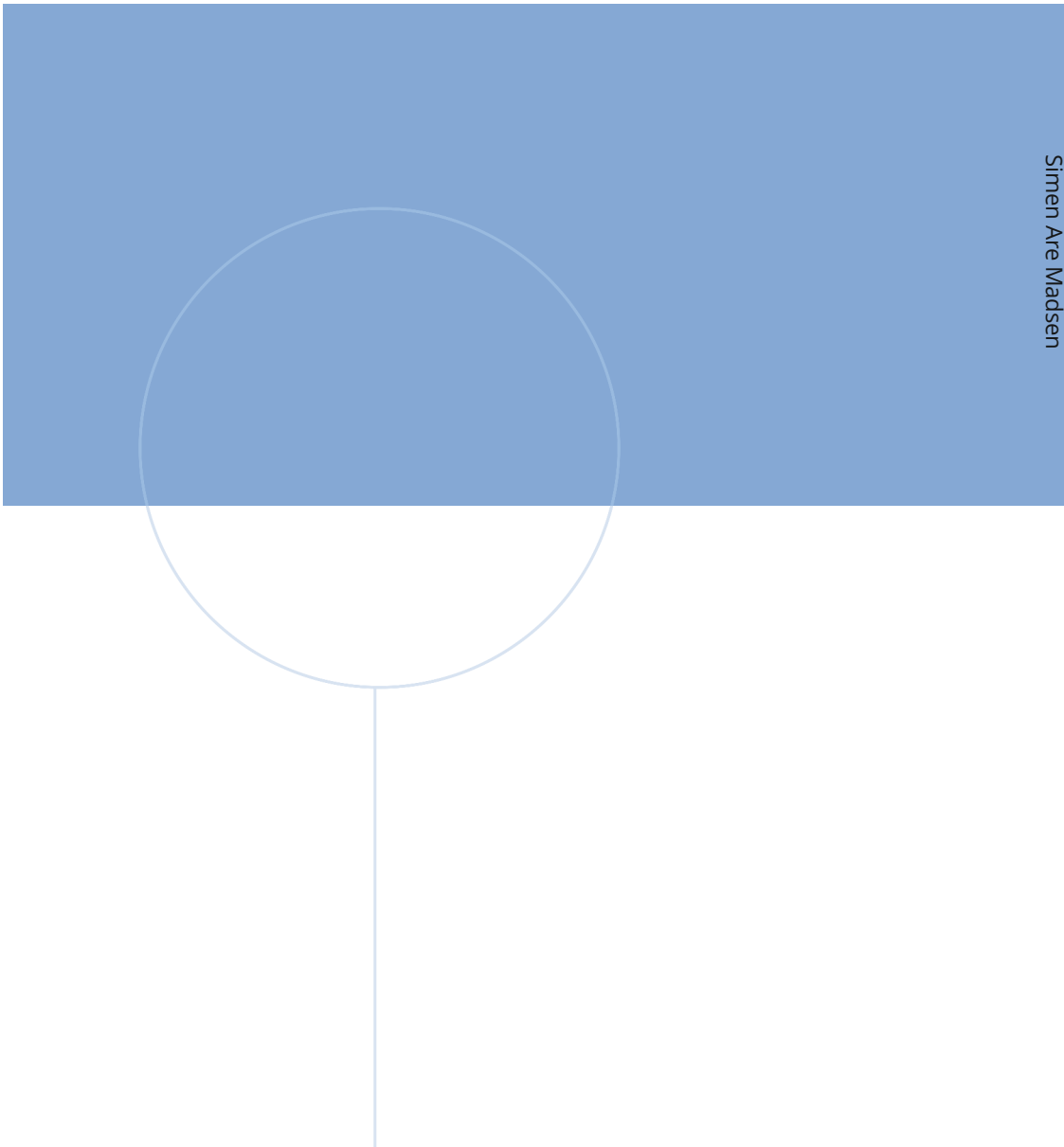

Simen Are Madsen

NTNU
Kunnskap for en bedre verden